POLITECHNIKA LUBELSKA

Dariusz Czerwiński

Modelling the critical parameters of high temperature superconductor devices in transient states

MONOGRAFIE

Lublin 2013

Modelling the critical parameters of high temperature superconductor devices in transient states

Monografie – Politechnika Lubelska

Politechnika Lubelska
Wydział Elektrotechniki i Informatyki
ul. Nadbystrzycka 38A
20-618 Lublin

Dariusz Czerwiński

Modelling the critical parameters of high temperature superconductor devices in transient states

Politechnika Lubelska
Lublin 2013

Recenzent:
dr hab. inż. Sławomir Kozak, prof. Instytutu Elektrotechniki

Skład i redakcja: Dariusz Czerwiński

Publikacja wydana za zgodą Rektora Politechniki Lubelskiej

ISBN: 978-83-63569-50-1

Wydawca: Politechnika Lubelska
ul. Nadbystrzycka 38D, 20-618 Lublin
Realizacja: Biblioteka Politechniki Lubelskiej
Ośrodek ds. Wydawnictw i Biblioteki Cyfrowej
ul. Nadbystrzycka 36A, 20-618 Lublin
tel. (81) 538-46-59, email: wydawca@pollub.pl
www.biblioteka.pollub.pl
Druk: TOP Agencja Reklamowa Agnieszka Łuczak
www.agencjatop.pl

Elektroniczna wersja książki dostępna w Bibliotece Cyfrowej PL www.bc.pollub.pl
Nakład: 100 egz.

Table of Contents

List of symbols

A – magnetic vector potential, Wb/m
a, b – random variables,
$c(T)$ – specific heat (temperature dependent), J/(kg·K)
c_p – specific heat, J/(kg·K),
E_c - value of critical electric field intensity, V/m,
F – heat flux density, W/m^2,
H_c – critical magnetic field strength, A/m,
H_{c1} – lower critical magnetic field strength, A/m,
H_{c2} – upper critical magnetic field strength, A/m,
I_c – critical current, A,
J – current density, A/m^2,
J_c – critical current density, A/m^2,
$J_c^{\bullet}$ – critical current density of HTS material in real scale model, A/m^2,
k_{ex} – exact solution,
k_o – solution with initial mesh step size,
k_p – solution with higher order mesh step size,
λ, κ – thermal conductivity, W/(m·K),
M – magnetization vector, A/m,
m – mass of an object, kg,
m_A – magnetic vector potential factor,
m_{cp} – specific heat capacity factor,
m_J – current density factor,
m_{qv} – volume heat source factor,
m_T – temperature factor,
m_t – time factor,
m_V – electric potential factor,
m_x – X dimension factor,
m_y – Y dimension factor,
m_z – Z dimension factor,
$m_{\lambda x}$ – thermal conductivity factor in X direction,
$m_{\lambda y}$ – thermal conductivity factor in Y direction,
$m_{\mu x}$ – magnetic permeability factor in X dimension,
$m_{\mu y}$ – magnetic permeability factor in Y dimension,
m_σ – electrical conductivity factor,
∇T – temperature gradient, K,
n – power factor in power law, which depends on the HTS material,
o – initial mesh step size,
p – higher order mesh step size,
$p(t)$ – instantaneous power, W,
Q – generated heat, J,

q – vector of heat flux, W/m^2,
q, q_v – volume heat generation, W/m^3,
r – order of error which depends on convergence,
r – Pearson correlation coefficient.
ρ_r – resistivity in resistive state, Ω·m,
ρ_s – resistivity in superconducting state, Ω·m,
$\rho^\bullet$ –electrical resistivity used in the simulations in real scale model, Ω·m,
T – actual temperature, K,
T_c – critical temperature, K,
T_s – time period, s,
V – volume, m^3,
μ − magnetic permeablility, H/m,
ρ – mass density, kg/m^3,
σ − electrical conductivity, S/m,
ω − angular frequency, rad/s,
. – decimal separator,

List of acronyms

1G – first generation,
2G – second generation,
AMSC – AMerican SuperConductor
BSCCO – Bismuth Strontium Calcium Copper Oxide superconductors family with following compounds: Bi-2201 – $Bi_2Sr_2CuO_6$, Bi-2212 – $Bi_2Sr_2CaCu_2O_8$, Bi-2223 – $Bi_2Sr_2Ca_2Cu_3O_{10}$,
CF – Current Flow,
CFRP – Carbon-Fibre-Reinforced Polymer,
CVD – Chemical Vapour Deposition,
HF – Heat Flow,
HTS – High Temperature Superconductor,
ITER – International Thermonuclear Experimental Reactor,
LSCO – $La_{2-x}Sr_xCuO_2$ lanthanum copper oxide superconductor family,
LTS – Low Temperature Superconductor,
MAGLEV – (derived from MAGnetic LEVitation) is a system of transportation that uses magnetic levitation to suspend, guide and propel vehicles with magnets,
MD – Magneto-Dynamics,
MOCVD – Metal Organic Chemical Vapour Deposition,
MOD – Metal Organic Deposition,
OLTC – On Load Tap Changer,
PIT – Powder In Tube technology,
PLD – Pulsed Laser Deposition,
PVD – Physical Vapour Deposition,
RCE – Reactive Co-Evaporation,
SFCL – Superconducting Fault Current Limiter,
SMES – Superconducting Magnetic Energy Storage,
SMS – Superconducting Magnetic Shield,
SQUID – Superconducting Quantum Interference Device,
YBCO –$YBa_2Cu_3O_7$ (Y123) superconductor,
MgB_2 – Magnesium Diboride,

1. Introduction

High temperature superconductors (HTS) were discovered in 1986 by two IBM scientists Karl Müller and Johannes Bednorz [7, 45]. This discovery led to rapid growth of research and development efforts in practical applications of high temperature superconducting devices. However, manufacturing problems with production of useful components out of HTS materials have significantly slowed the initial development. Many problems with the materials, such as flux-creep, weak-links, and poor mechanical properties should be overcame [52].

An electrical device can be termed as superconducting, if its design contains elements made of superconductor and these elements are working in the superconducting state. The device can contain a superconducting element, which may be the winding, current lead, track current, Josephson junction, pipe, cylinder, bifilar stack or other profiles [31, 124, 133, 140]. Primary typical uses of superconducting effect in power applications include [6, 22, 26-28, 69, 72, 88, 99, 115, 126, 137, 147]:

- Widespread use of superconductors to build strong superconducting magnets and electromagnets, in which an electric current is moving almost indefinitely. This implies a chance to produce very strong magnetic fields. The main practical application of this usage is focused on accelerators, or particle accelerators used by modern physics in order to conduct research on the structure of matter and to find new ones, predicted by the theory of building blocks of matter.
- Superconducting equipment used in nuclear technology.
- Strong magnetic fields allow for construction of the magnetic separators with very good efficiency level.
- Preparation of equipment used in electrolysis, which is an important process of chemical technology.
- Building strong electromagnets which allow for free lifting heavy objects (so-called magnetic levitation). MAGLEV is an example of this application.
- Superconducting energy storage device (SMES) used for storing energy in magnetic field.
- Construction of superconducting electrical machines and transformers.
- Superconducting fault current limiters SFCL, used for fault current limiting in electric power networks.
- Construction of cables and wires used for efficient current transport without loss.

Power applications are the most common applications of the superconducting phenomenon; however, additional applications can also be distinguished:

- Constructing high-performance analytical systems used in chemistry, biology and medicine (e.g. resonance mechanism),
- Construction of the magnetic field shields,
- Production of high-capacity computer and electronic memory for use in IT technology development,
- Use in electronics. A special role is played by the Josephson junction; tunnelling of electrons between two superconductors on the border of a superconductor – insulator – superconductor is the effect used.
- Josephson junction is also used for highly precise measurements of weak magnetic fields (medicine, cardiology), low voltage and frequency microwave thermometry noise, to determine the precise pattern of the electrical voltage. Other applications include acceleration signals in integrated electronic circuits.

Some metals and substances exhibit superconducting properties. A characteristic feature of superconductivity is almost zero resistivity and perfect diamagnetism (in the case of type I superconductors) of the material under certain conditions determined by the temperature, magnetic field, and electric current.

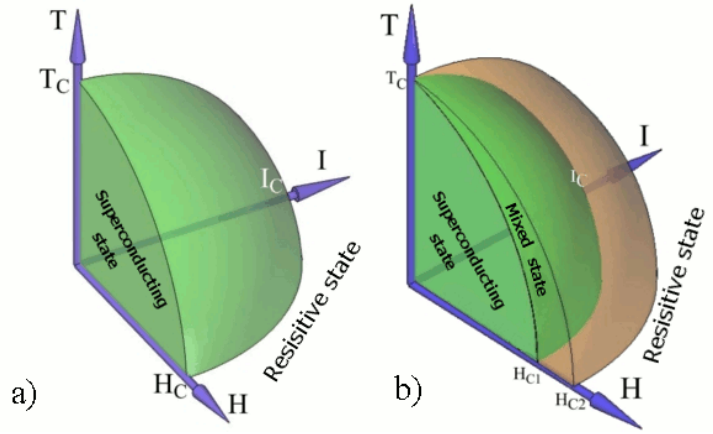

Fig. 1.1. Critical surfaces in superconductors: a) type I b) type II [81]

Superconducting materials are in the superconducting state when the point determined by the operating temperature, current density and magnetic field characteristic is below the surface of the material critical characteristics. Critical surface of superconductor is a function of three variables: temperature, current density and magnetic field intensity. The relationship between the intensity of the magnetic field and the critical current density (or vice versa) at a given temperature is a critical characteristic of a superconductor. When defining

critical parameters of superconductors magnetic field strength is often replaced by magnetic induction. During the transition of superconducting materials from the superconducting state to the resistive state, they change their electrical and magnetic properties rapidly. Each superconducting material can be designated with its critical parameters. These parameters are: critical temperature, critical current and critical magnetic field and are well defined in CENELEC standards [120]. Description of critical parameters is shown in Table 1.1.

Table 1.1 Definition of superconductors critical parameters according to PN-IEC 60050-815 [120]

Name	Symbol	Definition
critical temperature	T_c	temperature below which a superconductor exhibits superconductivity at zero magnetic field strength and zero electric current
critical (magnetic) field strength	H_c	magnetic field strength corresponding to the superconducting condensation energy at zero magnetic field strength
		Note – H_c is a function of temperature
lower critical (magnetic) field strength	H_{c1}	magnetic field strength at which a fluxon firstly penetrates a bulk type II superconductor deviating from the perfect diamagnetism when demagnetization factor is zero
		Note – H_{c1} is a function of temperature
upper critical (magnetic) field strength	H_{c2}	maximum magnetic field strength below which a type II superconductor is in the mixed state
		Note – H_{c2} is a function of temperature
critical current	I_c	maximum direct current that can be regarded as flowing without resistance
		Note – I_c is a function of temperature and magnetic field strength
critical current density	J_c	the electric current density at the critical current using either the cross-section of the whole conductor (overall) or of the non-stabilizer part of the conductor if there is a stabilizer

1.1. Superconducting materials

Disappearance of electrical resistance and Meissner effect (magnetic field inside the superconductor is screened by a lossless current flowing in the superconducting thin skin layer on the surface of the superconductor – the perfect diamagnetism) are the fundamental properties of superconductors. There is no precise criteria as to which metals can be superconductors. Matthias rule can be an approximate superconductive criterion; according to this criterion, a metal may be a superconductor if it satisfies the following conditions: the number of valence electrons is included in the range between 2 and 8, has

a certain atomic number and a specific crystallographic symmetry. Total number of metals exhibiting superconductivity properties stands at more than 20. Also alloys of metals which in their pure state are not superconducting exhibit superconducting properties. Superconductors were also searched for amongst low-dimensional organic compounds [53]. Organic superconductors of the so-called Bechgaard salts were discovered in the late seventies and eighties. Chosen metals, alloys and organic compounds which exhibit superconductivity are listed in the table below [24, 48, 77, 101, 124, 140, 160, 165, 167 – 169]:

Table 1.2 Chosen superconductors and their critical temperatures

Name	Type	T_c [K]
Be – beryllium	I, LTS	0.03
Ti – titanium	I, LTS	0.4
Cd – cadmium	I, LTS	0.5
Tl – thallium	I, LTS	2.4
In – indium	I, LTS	3.4
Sn – tin	I, LTS	3.7
La – lanthanum	I, LTS	4.8
V – vanadium	II, LTS	5.4
Pb – lead	I, LTS	7.2
Tc – technetium	I, LTS	8.2
Nb – niobium	II, LTS	9.3
NbTi	II, LTS, alloy	9.5
V_3Ga	II, LTS, A15	14.5
V_3Si	II, LTS, A15	15.7
Nb_3Al	II, LTS, A15	16.0
Nb_3Sn	II, LTS, A15	18.3
Nb_3Ge	II, LTS, A15	23.2
$(TMTSF)_2ClO_4$	II, LTS, organic	1.4
β-$(BEDT\text{-}TTF)_2I_3$	II, LTS, organic	8.1
$(BEDT\text{-}TTF)_2Cu(SCN)_2$	II, LTS, organic	10.4
MgB_2	II, HTS, ceramic	39-40
YBCO	II, HTS, ceramic	89
BSCCO, Bi-2212	II, HTS, ceramic	90-92
BSCCO, Bi-2223	II, HTS, ceramic	108
$HgBa_2Ca_2Cu_3O_8$	II, HTS, ceramic	135
$La[O1\text{-}_xF_x]FeAs$	II, HTS, iron based	56
$(Ba,K)Fe_2As_2$	II, HTS, iron based	38

High temperature superconductors are materials that behave as superconductors at high cryogenic temperatures i.e. theoretically 30 K and above. Recent development in the field of superconducting materials focused on high temperature superconductors, especially where the critical temperature is higher then 77 K (liquid nitrogen boiling temperature) because of cheap and easy cooling method that can be applied there [3, 7, 5, 47, 148, 157].

In the Meissner state, the superconductor can be treated as an ideal diamagnet, however high temperature superconductors possess another state – the so-called mixed state. In the mixed state (see Fig. 1.1) a sufficiently robust magnetic field applied will produce quantum vortices which might carry magnetic flux through the inside of the superconductor. The HTS superconductors and the matrices of the superconducting wires are partially penetrated by magnetic flux.

The tubes, through which the flux passes the superconductor, are 'pinned' to certain locations due to impurities in the crystal structure of the material. The transport current and external magnetic field are the determining factors of the tube movement. This phenomenon and the atomic structure determine the characteristics of the critical parameters of high temperature superconductors.

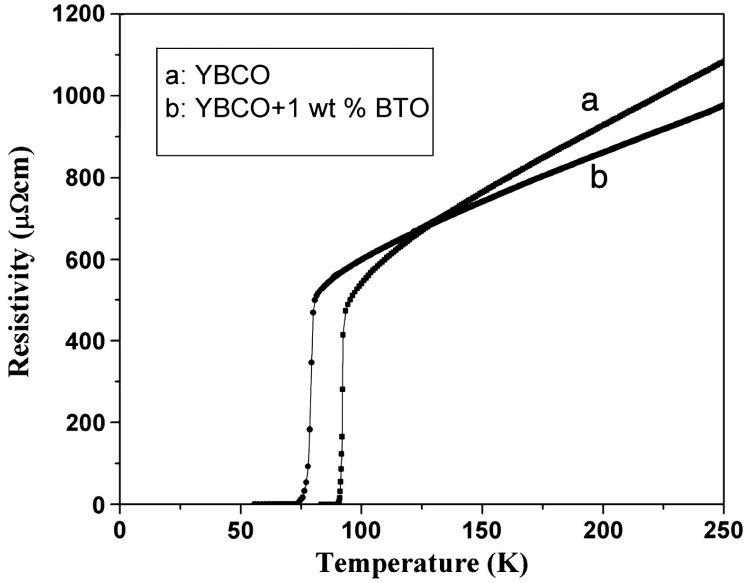

Fig. 1.2. Resistivity of thin YBCO film and its composite versus temperature [80]

In order to calculate the parameters of superconducting devices built of high temperature superconductors, it is necessary to know the characteristics of the material properties such as: resistivity, magnetic permeability or heat

conductivity. In the case of HTS superconductors, all these parameters are nonlinearly temperature dependent.

Resistivity in the function of temperature of YBCO thin films is shown in Fig. 1.2. Critical temperature and resistivity curve of YBCO strongly depend on material composition. Even a small amount of additives significantly changes properties of the superconducting material (Fig. 1.2). The critical temperature of the composite YBCO material is lower when compared to the critical temperature of the pure YBCO material; resistivity of pure YBCO tape is higher above the temperature of about 130 K.

Dependency of the critical current on the external magnetic field value and direction under the constant working temperature is another important aspect. The strongest dependency can be observed at the perpendicular magnetic field [90, 111, 129, 145]. Critical current versus magnetic field for YBCO coated conductor in lower temperatures is shown in Fig. 1.3. In higher temperatures, critical current as a function of field is shown in Fig. 1.4.

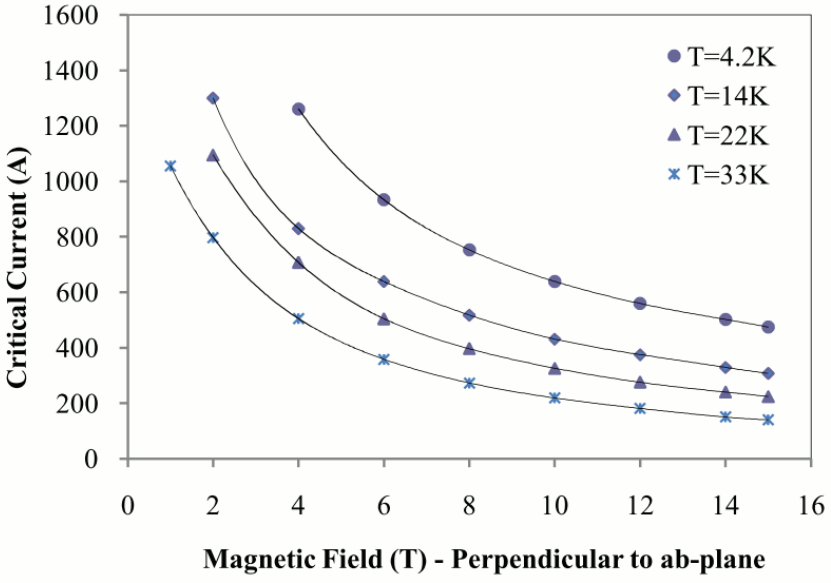

Fig. 1.3. The SCS12050 YBCO tape critical current as a function of field and temperature [90]

In the higher temperatures (above 50 K) the critical current value drops rapidly with magnetic flux density increment. For the field value of 1 T in the temperature equal 77 K, the critical current value is about 8 times smaller when compared to the self field value (Fig. 1.4).

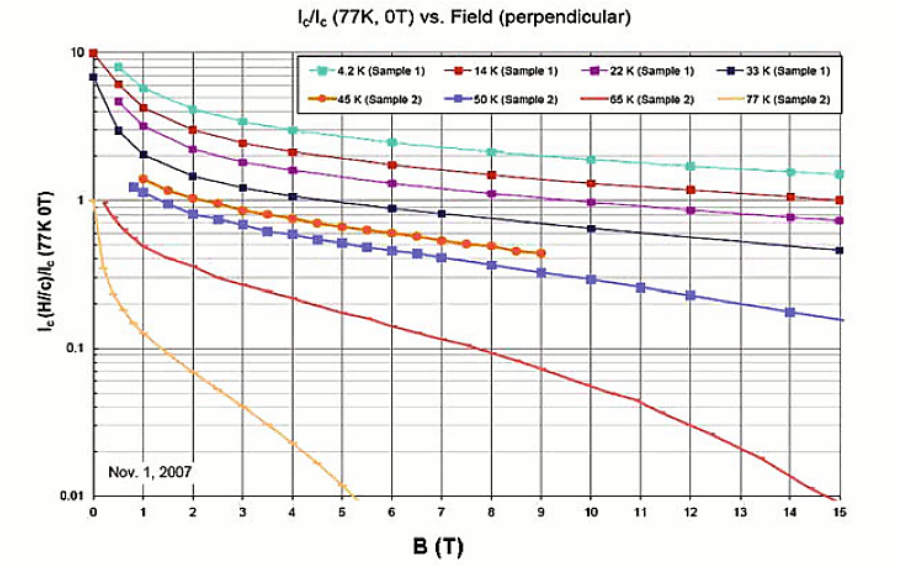

Fig. 1.4. SuperPower SCS4050 YBCO tape critical current as a function of field [145]

Nonlinear dependency of critical magnetic induction on the temperature for the chosen superconductors is shown in Fig. 1.5.

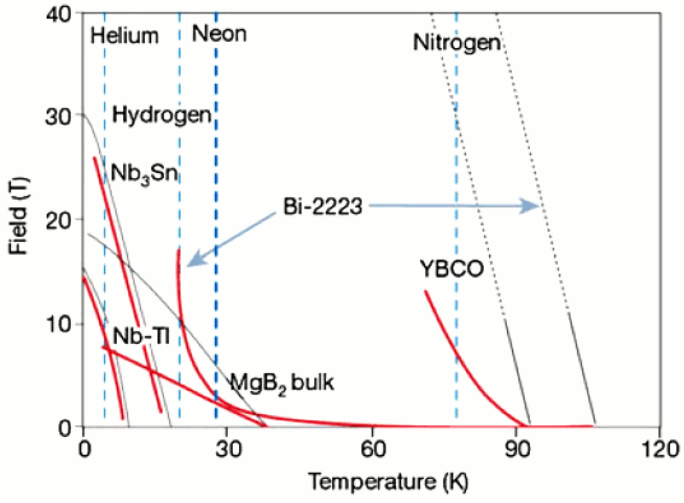

Fig. 1.5. Critical magnetic fields of different superconducting materials versus temperature. Black lines indicate the upper critical field, at which bulk superconductivity is destroyed. Red lines indicate their reversibility field, at which the bulk critical current density goes to zero [83]

For the superconducting devices cooled in liquid nitrogen bath and built of YBCO or BSCCO superconductor, the application range is defined with lower value of the irreversibility field. In the case of YBCO superconductors, the irreversible magnetic induction value is about 7 T, while for Bi-2223, it is about 0.3 T (Fig. 1.5).

One of the important properties of high temperature superconductors is their ability to conduct heat. There is a technological interest in how efficiently and by what means heat flows in these solids. The HTS superconductors' thermal conductivity temperature dependence has a big impact on a wide range of superconducting devices. Responsivity of radiation detectors depends on thin superconducting elements and their thermal conductivity. Thermal conduction additionally governs how quickly a local hot spot in a superconducting device spreads or is recovered; it is a very important factor in transient heat problems and stability of the device. In other words, thermal stability is very important to reliable operation of superconducting high temperature thin film structures [47].

Thermal conductivity of HTS superconductors also provides an important theoretical input. It gives the information on the phonons, charge carriers and the scattering process between them [47].

The thermal conductivity of YBCO and LSCO superconductors as a function of normalized temperature is shown in Fig. 1.6.

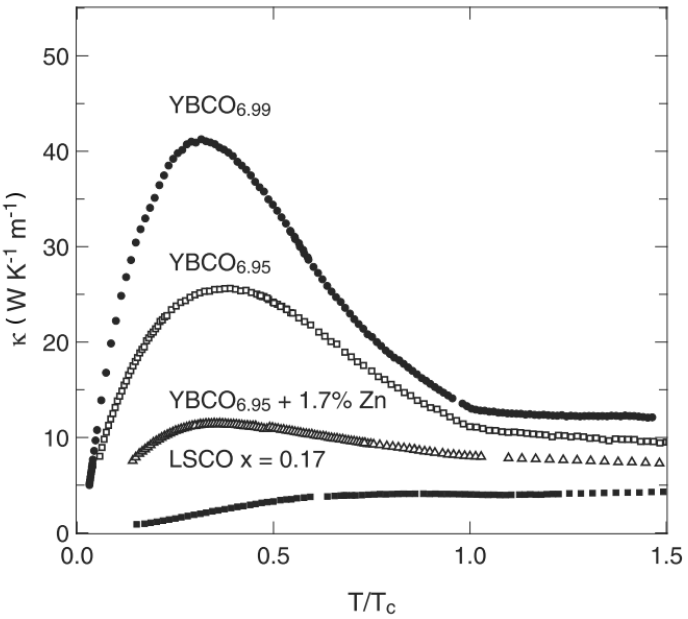

Fig. 1.6. Thermal conductivity of $YBa_2Cu_3O_y$ and $La_{2-x}Sr_xCuO_4$ versus temperature normalized at T_c [146]

In the temperature ranges up to T_c the thermal conductivity is strongly nonlinear, especially for YBCO high temperature superconductors.

Although it is a clear indicator of importance of the phonon-carrier interaction in normal state of the superconducting material, thermal conductivity growth below T_c is the result of a consolidation in the phonon mean-free path due to carrier condensation [47].

Important phenomenon, especially for AC superconducting application, is the magnetic hysteresis in bulk high temperature superconductors. Magnetic characteristics of high temperature superconductors are related to the form of penetration of magnetic flux into the superconductor. The flux goes through the high temperature superconductor in form of voritces [17, 25, 46, 50, 66, 122, 135, 170]. This can be observed as magnetic hysteresis loop, which has a different shape for various types of high temperature superconductors (Fig. 1.7).

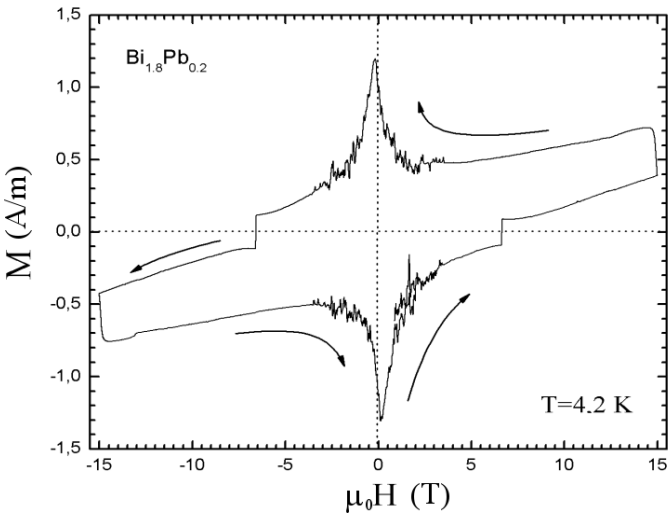

Fig. 1.7. Hysteresis loop of the magnetization curve in high magnetic field, of HTS superconductor $Bi_{1.8}Pb_{0.2}Sr_2Ca_2Cu_3O_{10}$ composition as a function of applied magnetic induction (arrows indicate the direction of variation of applied magnetic field) [135]

1.2. Aim and thesis

Knowledge of the behaviour of superconducting devices in transient states is very important to assess the stability of the unit. Disturbances of the superconducting state may be induced by mechanical, electromagnetic and heat reasons, but in effect, they finally reveal themselves as additional heat delivered to the superconducting element.

Due to the low heat capacity of materials at very low temperatures, even a small value of the energy input can cause a rapid rise in temperature over the local critical temperature of the superconductor and the formation of resistive zone. Resistive zone becomes an additional source of heat. That rise of the temperature in the superconducting element increases the heat generation.

Inhomogeneous transition of the device into the resistive state is presumed to result in an increased amount of heat dissipated in those components which are not in the superconducting state. Short-term current increase over the critical value is often dangerous for the device and can lead to physical damage. Awareness of the superconducting device response during transients allows for designing more robust applications.

Non-linear dependence of properties such as resistivity, magnetic permeability and thermal conductivity on temperature results in complicated numerical simulation of superconducting devices. During solution of the current flow and electrical circuit problems, it is important, from the viewpoint of final result, to introduce a non-linear resistivity on the temperature dependence. When solving alternating magnetic field problems, the parameters are non-linear characteristics of magnetic permeability and electrical conductivity. Non-linear dependence of heat conductivity on temperature is a significant issue in heat flow problem solution. In addition, the implementation of cooling (contact cooling or cryogenic liquid bath) is also very important.

The first objective of the dissertation is to improve the methods for calculating the critical parameters of high temperature superconductor devices in transient states and to verify the elaborated models with measurements. The second is to develop a non-contact system for detecting quick temperature changes in thin second generation HTS tapes.

Algorithms developed by the author and computer models of the devices with HTS bulk components as well as the second generation tapes have been used to achieve the first objective. The developed models can be used for numerical simulation of 2D and axisymmetrical geometries and are useful for such appliances as: superconducting fault current limiters, current leads and second generation HTS tapes.

Elaborated algorithms allow for combining three problems during simulations: current flow, magnetic field and heat transfer. The nonlinear superconductor temperature dependent characteristics of critical current, critical magnetic flux and thermal conductivity were taken into account. The models also includes the time and space variation in thermal power density, guiding the generation of heat in the superconducting element during the superconducting transition. Developed models were mostly verified with measurements.

In order to achieve the second objective, measurement system designed by the author has been used. The system uses infrared silicon photodiodes as sensors. The idea of the experiment is to measure temperature in a non-contact manner by an infrared photodiode placed in a bath of liquid nitrogen with the

HTS tape. The signal from the photodiode is amplified and converted to voltage signal registered by data acquisition computer system. Short response time (5 ns) photodiodes were used to obtain the changes of temperature at the appropriate time.

The assumption of the above objectives has lead to formatiation of the **thesis**:

Computer models of dynamic process changes of critical parameters of devices made from bulk HTS and 2G HTS wire combined with object programming in LUA allow to determine the impact of the pulse causing disruptions in superconducting stability on the parameters of superconducting elements.

1.3. Scope of work

Implementation of the set objectives is presented in subsequent chapters.

The second chapter is devoted to the description of the high temperature superconductors for power applications and first and second generation wires. Working conditions of superconductors are also described in high-current devices, the structure of these devices and their most important implementations.

Knowledge of superconducting device parameters is necessary for building a proper and functional model.

The third chapter describes the basic concepts and issues of transient state modelling in devices built of high temperature superconductors. The developed algorithms of hybrid modelling for contact cooling and cryogenic liquid cooling are described. The implementation of hybrid model was done by object programming in LUA language with the use of the FEM solver from the FEMM package. For discretization error estimation the comparison with the 2G tape model elaborated in COMSOL environment was made.

The transient states in second generation thin layer high temperature superconductor tape were analysed and compared with the results of measurements conducted. Inductive fault current limiter and current leads built of bulk HTS and 2G wire hybrid models were also proposed and analysed. Computational results of transients in the modelled superconducting devices allow to assess the changes in the critical parameters of the device. The problem of thin layer modelling and scale factor models is also described in this chapter.

Measurements of transient states in the second generation thin layer superconducting tape were described in the fourth chapter. The chapter contains description of the measurement system designed to record transients in the 2G tape. The measuring system consists of computer controlled supplying system; data acquisition system based on National Instruments DAQ board and LabView software, as well as a test stand with HTS tape and connected measuring probes. Recorded waveforms of instantaneous voltage and current allow to analyze the propagation of the quench zone, dynamic changes of temperature distribution

and generated heat. The designed and developed non-contact temperature measuring system to be performed in low temperatures with the use of IR photodiodes is described at the end of the chapter.

The final conclusions are presented in the summary. The conclusions confirm the aims of dissertation and realization of the postulated thesis pertaining to the study of transient states modelling in high temperature superconducting devices.

2. Devices built of High Temperature Superconductors

High temperature superconducting materials proved to be effective in many applications where low temperature superconductors were ineffective, especially in industrial applications. HTS wires working at liquid nitrogen temperature are used to build power cables, fault current limiters (FCL) and transformers for use in power networks. Numerous projects in these areas have been successfully designed and built [12, 18, 23, 75, 98-100, 138, 156, 159]. HTS superconductors are also used in construction of high-field excitation poles of direct current synchronous motors and generators.

The use of superconductors in place of conventional conductors can increase the average current density in the devices by a few orders of magnitude. Such large current densities allow for the generation of magnetic fields of the order of 30 T using low-temperature superconducting coils and the order of 60 T with the use of high temperature superconductors.

High value of the magnetic flux density and high current density generate enormous mechanical stresses caused by the Lorentz force. These stresses often exceed the mechanical strength of superconducting materials, and it is necessary to use additional structural reinforcements.

Superconducting magnets can produce high intensity magnetic fields. These magnets, with high magnetic field homogeneity, are essential part of the apparatus for nuclear magnetic resonance. Superconducting magnets are also used to test plasma in electron microscopes; magnetic lenses built of superconducting windings allow for greater resolution capabilities. Superconducting magnets are also used in particle accelerators. In power engineering, superconducting electromagnets called SMES may also be used for accumulation of energy (in the form of a magnetic field), which could be used in peak hours.

Magnetic bearing use superconducting magnetic levitation phenomenon (i.e Meissner effect). Such bearings have very good stability and low loss [116]. They are used in such devices as vacuum pumps, flywheels or electrical motors. Levitation phenomenon is also used in high speed rail.

Superconducting cables and power lines are used to transfer energy. In the summer of 2001, Pirelli have performed installation of about 130 m of HTS cables for Detroit Edison at the Frisbie Substation. The cables are able to deliver 100 million watts of power. It was the first time that commercial power was delivered to customers in the US through the superconducting cable [141].

Superconductors have also found numerous applications in measuring and computing:

- superconducting coil galvanometers with a sensitivity of 10^{-12} V voltage (classic apparatus sensitivity is 10^{-8} V)
- magnetometers (SQUIDs) to measure very weak magnetic field changes, such as superconducting quantum interferometer which allows detection of induction change of the order of 10^{-18} T ,
- bolometers used for detecting radiation,
- cryotrons and other superconducting memory elements of digital machines.

High temperature superconductors are widely used in the construction of energy devices and facilities. Table 2.1 presents chosen devices built of high temperature superconductors.

Table 2.1 Status of chosen high temperature superconducting devices [12, 23, 75, 82, 99, 100, 136, 141, 156, 159]

Application	HTS type	Company	Status
SCFL	Bi 2212 – bulk	ABB	6.4 MVA, tested
	YBCO – film	Siemens	1.2 MVA, tested
Cable	Bi 2223 – PIT	Pirelli	24 kV; 2.4 kA, 120 m
	Bi 2223 – PIT	SEI/TEPCO	66 kV; 1 kA, 100 m, tested
	Bi 2223 – PIT	Southwire	12.5 kV; 1.25 kA, 33 m, tested
	Bi 2223 – PIT	NKT	36 kV; 2 kA, 30 m, tested
Transformer	Bi 2223 – PIT	ABB	0.63 MVA, tested
	Bi 2223 – PIT	Siemens	1 MVA (traction), tested
Motor	Bi 2223 – PIT	ASC	3.7 MW, tested
Flywheel	YBCO-bulk	Mitsubishi	1.4 kWh, tested

2.1. Devices built of bulk high temperature superconductors

Fabrication of cable built of HTS ceramic superconducting materials has initially created some problems. Originally, uses of these superconductors, where the superconducting element is in a compact, rigid piece, were searched. High temperature superconductors in cylindrical form are used in inductive

superconducting current limiters. Superconductors in tubular form are used in superconducting current leads and resistive current limiters. Superconductors with more complex shapes are used in electric motors and magnetic levitators [72]. Bulk high temperature superconductors used for current limiters, current leads, motors and magnetic levitators are: BSCCO 2212, BSCCO 2223 and YBCO [64].

The first resistive HTS fault current limiter used in a power system, was built in Germany under the CURL 10 project. The main parameters of the resistive SFCL are presented in Table 2.2 [78].

Table 2.2 Chosen parameters of resistive HTS fault limiter constructed under the CURL 10 project

Parameter	Value
Voltage	10 kV
Frequency	50 Hz
Normal current	600 A_{RMS}
Fault duration	60 ms
Maximum limited current	8.75 kA
Temperature	66 K
Superconductor	BSCCO

The device is a three-phase resistive high temperature superconducting fault current limiter (SFCL) designed for voltage of 10 kV and power of 10 MVA. The limiter construction is based on 90 bifilar coils built of MCP BSCCO 2212 bulk high temperature superconductor (Fig. 2.1).

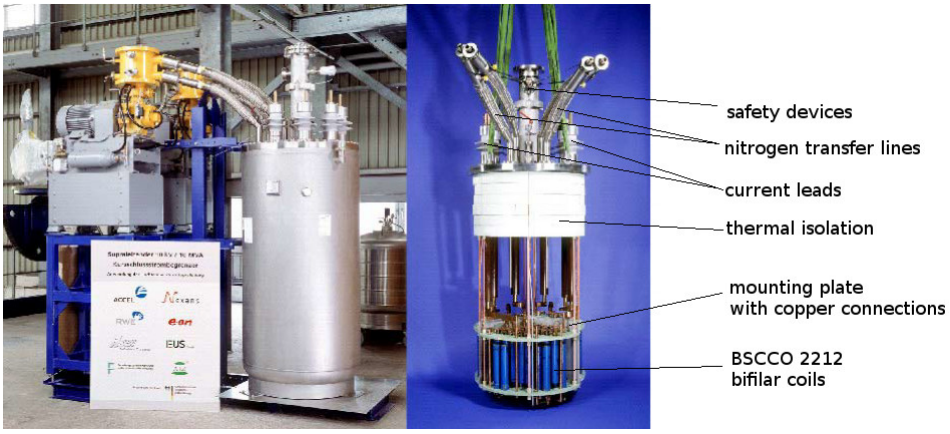

Fig. 2.1. 10 kV fault current limiter – CURL10 project [12,78]

The operating temperature (66 K) was achieved by cooling the liquid nitrogen using two Stirling cryocoolers. In 2005, it was the largest construction of HTS fault current limiter world wide. From April 2004 onwards, the device is installed and tested within the RWE utility network at Netphen near the city of Siegen in Germany [12,78].

Superconducting fault current limiters built of bulk HTS, have also been constructed by other centres. List of selected SFCL parameters and constructors is presented in the Table 2.3 [23, 75, 99, 156, 159].

Table 2.3 Chosen parameters of superconducting fault current limiters built of bulk HTS

Constructor	Country / Year	Characteristic	Superconductor	SFCL type
ABB	Switzerland / 2001	8 kV/800 A	BSCCO 2212	resistive
ACCEL	Germany / 2004	6.9 kV/600 A	BSCCO 2212	resistive
Nexans				
Nexans	Germany / 2004	63.5 kV/1.8 kA	BSCCO 2212	resistive and inductive
KEPRI	Korea / 2007	13.2 kV/630 A	BSCCO 2212	resistive
BYFAULT	France / 2002	1 kV / 100 A	YBCO	resistive
IEL	Poland / 2004	220 V / 5 A	BSCCO 2223	inductive

Bifilar BSCCO coil with parallel shunt resistor constructed by Baldan and others [4] was another device built of bulk high temperature superconductor. The coil was tested under fault current conditions using a 3 MVA single-phase transformer in a 220 V and 60 Hz line, achieving fault current peak of 8 kA. The fault current tests were performed from steady state peak current of 200 A by applying controlled short circuits increasing up to 8 kA.

The time period of short circuits was varying from one to six cycles. The test results show the function of the shunt resistor providing homogeneous quench behaviour of the HTS coil besides its intrinsic stabilizing role. The limiting current ratio achieves a factor of 4.2 during 5 cycles without any degradation of the BSCCO bulk coil [4].

CAN Superconductors Company specializes in fittings made of BSCCO 2223, it also has small elements made of YBCO [18]. Low contact resistance superconducting tubes made of BiPbSrCaCuO ceramics with silver-covered ends are suitable for current leads, effectively reducing heat leak into superconducting magnets. Table 2.4 presents chosen parameters of HTS tubes fabricated by CAN Superconductors [18].

Table 2.4 Chosen parameters of HTS tubes with silver contacts fabricated by CAN Superconductors [18]

Type	Dimensions			Critical current (A)	Conductive heat leak per pair between temperatures (W)
	Outer diameter (mm)	Length / Silver contact (mm)	Cross-section area (mm^2)	at 77 K	77 K - 4 K
CSL-7/70.2	6.6	70 / 10	14	100	0.08
CSL-7/120.2	6.6	120 /10	14	100	0.04
CSL-12/120.1	12.0	120 / 12	34	150	0.10
CSL-12/120.2	12.0	120 / 12	34	250	0.10
CSL-12/120.3	12.0	120 / 12	34	370	0.10
CSL-12/160.3	12.0	160 / 12	34	370	0.07
CSL-18/80.3	18.0	80 / 15	78	750	0.40
CSL-18/120.1	18.0	120 / 15	78	300	0.20
CSL-18/160.3	18.0	160 / 15	78	750	0.20
CSL-26/120.1	26.0	120 / 15	180	600	0.60
CSL-26/120.3	26.0	120 / 20	180	1500	0.60

Fig. 2.2. Superconducting magnetic shields (SMS) [18]

Superconducting magnetic shields, used to remove the background magnetic noise fields, are yet another type of devices built of BSCCO bulk high temperature superconductors. The signal-to-noise ratio is found to be boundless at specific points inside a superconducting cylinder and a superconducting cylinder with a central partition. Shielding factors of SMS are relevant to SQUID measurements of tiny dipole source fields in the presence of large background magnetic noise fields. Superconducting magnetic shields produced by CAN Superconductors are shown in Fig. 2.2.

Parameters of superconducting magnetic shields manufactured by CAN Superconductors are show in Table 2.5.

Table 2.5 Parameters of SMS manufactured by CAN Superconductors [18]

Parameter	Value
Material	Bi 2223 phase
Density	> 5.0 g/cm^3
Wall thickness	approx. 1.5 mm
Shielded magnetic flux density (77 K)	> 5 mT (typical value 10 mT)
Shielding factor (77 K, amplitude 2 mT, frequency 20 Hz – 10 kHz)	> 10^6
Shielding effectiveness (77 K, amplitude 2 mT, frequency 20 Hz – 10 kHz)	> 120 dB
Field noise at 1 Hz (cooled at 77 K in zero field)	< 50 fT/sqrt(Hz)
Critical temperature	108 K

Superconducting magnetic shields can be manufactured in form of tubes or vessels. Dimensions of superconducting magnetic shields manufactured by CAN are shown in Table 2.6.

Table 2.6 Superconducting Magnetic Shields product range (choise) [18]

Type	Inner diameter (mm)	Length (mm)
	Tubes	
CST-12/80	12	80
CST-15/80	15	80
CST-18/120	18	120
CST-21/120	21	120
CST-24/120	24	120
	Vessels	
CSV-12	12	42
CSV-24	24	84
CSV-32	32	128
CSV-50	50	200
CSV-66	66	264

The phenomenon of magnetic levitation is widely used for development of superconducting magnetic bearings and flywheel energy storage units [60, 83, 72, 100, 133]. First Flywheel Energy Storage unit developed world-wide was a 1 kWh unit developed by Chubu Electric Power and Mitsubishi Heavy

Industries. It was tested up to 20 000 rpm, thereby storing 1.4 kWh. In this unit, a thrust bearing based on a PrFeB ring-magnet levitates over a ring-arranged of 6 cm-sized MT-YBCO pellets of Dowa Mining (Fig. 2.3 a)) [100].

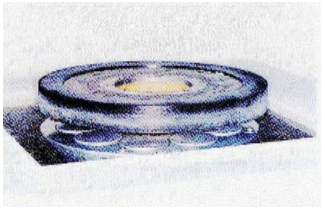

a)

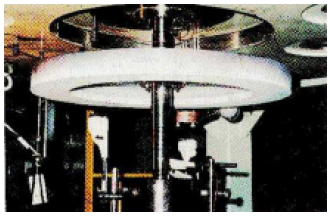

b)

Fig. 2.3. Flywheel elements: a) YBCO magnetic bearing, b) CFRP flying wheel [100]

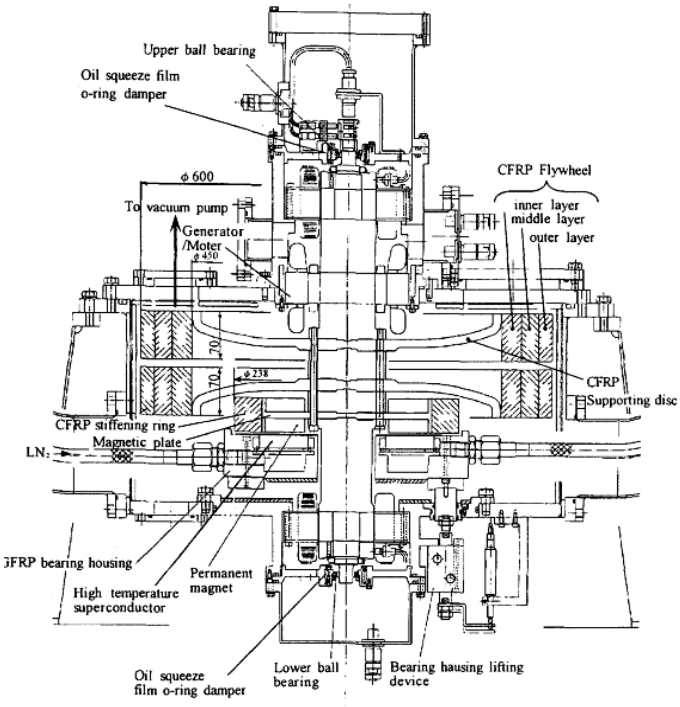

Fig. 2.4. Schematic of 1 kWh superconducting flywheel [100]

The magnetic bearing can operate up to 23 000 rpm and the levitation force of 1800 N is achieved at the gap distance of 2 mm. The two carbon-fibre-reinforced polymer (CFRP) flywheels are attached to the ring-magnet and integrated into the flywheel shaft (Fig. 2.3 b)) [100]. The schematic drawing of YBCO superconducting flywheel is shown in Fig. 2.4. The multi-ring

construction composed of three layers (inner, middle and outer) is used for decreasing of the radial stress. In test operation, the exchange of 1.05 kWh to and from the unit (unloading from 20 000 rpm down to 10 000 rpm) was successfully demonstrated several times [100].

The phenomenon of magnetic levitation is also used to build high-speed rail. Since the idea of MAGLEV was first devised in the early 1900s, the methods and implementations of the system have been explored and refined. The advances made in the field of high temperature superconductors have made application of this expertise a practical possibility and today there are full scale prototypes in Japan and the USA; there is even a high speed commercial maglev train in service in China [92, 103, 155]. The newest solution, which uses magnetic levitation, constructed by evico GmbH and IFW Dresden, is SupraTrans II. The test line commissioned in 2011 in Dresden is 80 m in length. Parameters of the SupraTrans II solution are shown in Table 2.7.

Table 2.7 Parameters of SupraTrans II [128]

Parameter	Value
Track length	80.84 m oval shape
NdFeB magnets	4.85 tons
Levitation force	8 ‑ 9 kN at 8 ‑ 10 mm
Superconductor	YBCO bulk
Speed	20 km/h
Vehicle mass	400 kg
Propulsion	Asynchronous short stator linear motor

Fig. 2.5. SupraTrans II vehicle and test track [128]

YBCO bulk superconductor is the high temperature superconductor used in the SupraTrans II vehicle. The vehicle and test track are shown in Fig. 2.5.

2.2. Devices built of first and second generation superconducting wires

Superconducting material is most commonly present in superconducting electrical devices in the form of wire. Type II superconductors have been used for construction of superconducting wires. Due to the need to ensure stable operation and minimize heat losses, superconducting wires have complex structure (Fig. 2.6). HTS wire is an essential element of high current superconducting devices, such as superconducting magnets, SMES and fault current limiters.

Superconductor is split into fibres with diameters ranging from a fraction of micrometer to several tens of micrometer, which are arranged in a matrix (stabilizer) built of material of good electrical and thermal conductivity properties. This type of wire is called 1G HTS wire (first generation high temperature superconducting wire).

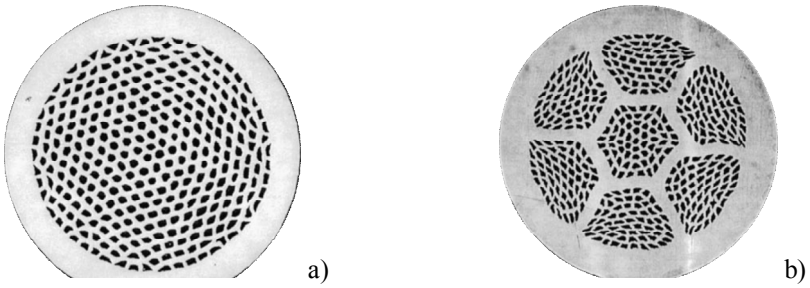

Fig. 2.6. BSCCO circular wire produced by Intermagnetics General Corporation: a) single stack, b) double stack [102]

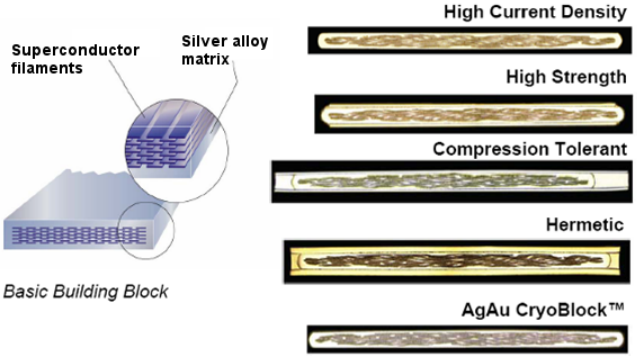

Fig. 2.7. BSCCO rectangular wire produced by American Superconductor Corporation [143]

The filaments are twisted in order to reduce the loss of external and internal magnetic field. The matrix of the HTS wire may be silver. Superconductor is therefore only a part of the total cross-section of the wire. The reason for this complex internal structure of superconducting wire is an attempt to minimize losses in transient states and AC losses. The 1G wire can also be produced in rectangular shapes, which are characterized by higher values of critical currents and used in construction of many superconducting devices [149].

First generation (1G) HTS wire is usually produced with technology called PID (powder in tube). First generation wire has been commercially available since late 1990s, however companies that produce 1G HTS wire are migrating to an improved solution of the second generation wire [132].

The second method of HTS wire manufacturing, allows production of superconducting coated conductors (also called the second generation (2G)). In this method, an appropriate layer of superconducting material is applied on the metal substrate (hastelloy) of suitable mechanical, thermal and electrical properties. After the heat treatment in an oxygen atmosphere, this material forms the thin superconducting film. Materials can be applied to a substrate in a chemical process (CVD – chemical vapour deposition) or physical process vacuum deposition (PVD – physical vapour deposition or PLD – Pulsed Laser Deposition), or in the process of organometallic deposition (MOD – metalorganic deposition). Other techniques of deposition in use are: MOCVD – metal organic chemical vapour deposition and RCE – reactive co-evaporation.

Second generation HTS wire consists of a few main layers of such materials like: high temperature superconductor (YBCO or REBCO), silver, substrate (usually Hastelloy C276) and copper – in the case of temperature stabilized wire. Second generation HTS wire has superior performance in a magnetic field and improved mechanical properties. The sample structure of SCS type wire is shown in Fig. 2.8.

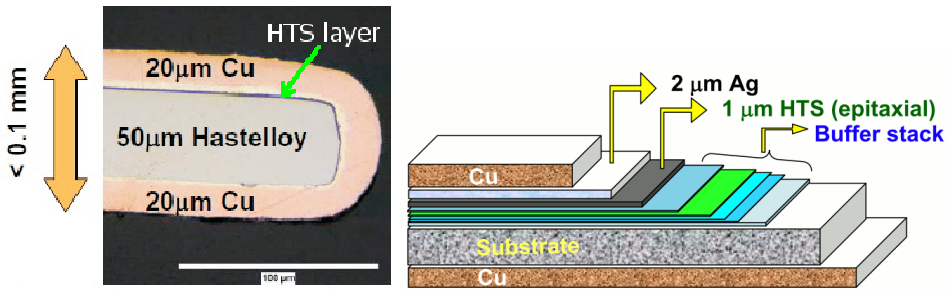

a) b)

Fig. 2.8. YBCO coated conductor wire produced by American Superconductor Corporation: a) SCS wire in magnification, b) structure of SCS wire [145]

The silver content in the case of 2G HTS wire is almost two orders of magnitude lower than the 1G HTS wire. From the technical perspective, the wire manufactured by AMSC can be customized at the last steps (slitting and lamination) for special application needs. The wire can be slit to different widths i.e.: 4 mm – for cables, 10 mm – for fault current limiter and windings in generators, 40 mm – full width strips used for developing strands in Roebel cable.

SuperPower 2G HTS Wire™ Specifications

SPEC	SCS 4050	SCS 12050	SF 12050	SF 12100	Unit	Comments
	SCS = Surround Copper Stabilizer SF = Stabilizer Free					
Width	4	12	12	12	mm	
Thickness	0.095	0.095	0.055	0.105	mm	
Silver Overlayer Thickness	2	2	2	2	microns	
Copper Stabilizer Thickness	0.04	0.04	n/a	n/a	mm	surround stabilized with rounded corners
Substrate Thickness	0.05	0.05	0.05	0.1	mm	Hastelloy®
Critical Tensile Stress	> 550				MPa	at room temperature
Yield Strength	1200	1200	1200	650	MPa	at 76 K
Critical Bend Diameter in Tension	11			25	mm	at room temperature
Critical Bend Diameter in Compression	11			11	mm	at room temperature
Critical Axial Tensile Strain	0.45%			0.40%		at 76 K
Substrate Resistance	125	125	125	125	micro-ohm cm	higher resistance leads to lower eddy current ac loss
Substrate Magnetic Properties	non-magnetic	non-magnetic	non-magnetic	non-magnetic		non-magnetic substrate leads to lower ferromagnetic ac loss
Joint Resistivity	40-50				$n\Omega cm^2$	
Bend Diameter of Joint	25				mm	
Spiral Winding Pitch	10				cm	around 16 mm dia. core
Overcurrent Capability	22-28				W/cm^2	continuous dc current for 0.04 mm copper stabilizer
AC Losses in a Cable	0.4				W/kA-m	entire cable structure
Hermeticity	24 hrs, 10 atm, LN2					no change in Ic & thickness
SFCL Test Parameters				See front		details on front

* Uniformity in long lengths of SuperPower 2G HTS Wire is better than 5%
* Piece lengths of up to 600 meters are available
* Ic values range from 80 – 110 Amps at 77 K in 4 mm width
* Engineering Current Density (Je) = 21 – 29 kA/cm^2
** *Other custom configurations are also available.* **

Additional product details available on our website: www.superpower-inc.com

We are ready TODAY to discuss your 2G HTS wire needs for a variety of applications.

Please contact us at: info@superpower-inc.com with your specifications, including:

Wire length, width and thickness requirements
Performance characteristics (critical current, stress, etc.)
Silver and/or copper overlayer preference
Other physical or performance characteristics
Delivery timeframe - Application and ultimate end user

Fig. 2.9. Specification card of 2G HTS wire produced by SuperPower Inc. [121]

The specification of 2G high temperature superconducting wire has a number of important mechanical, thermal and electrical parameters such as: mechanical

stress resistance, bend diameter, critical temperature, critical current, join resistivity or AC losses. These parameters are usually offered by manufacturer as the specification card of the wire (Fig. 2.9). In the several recent years, second generation coated superconductors have become commercially available from manufacturers from the USA, Europe and Asia (Table 2.8). Performance of the manufactured 2G wire often meets the application requirements, but there are some industrial applications, where the performance is not sufficient.

Table 2.8 Chosen 2G wire manufacturers and main type production features

Company	Process	HTS deposition technique	Maximum piece length (km)	Production capability (km/year)
American Superconductor Corporation	RABiTS	MOD	0.5	>300
SuperPower Inc.	IBAD	MOCVD	1.4	
Sumitomo Electric Industry	RABiTS	PLD		>1000
Fujikura Electric Industry	IBAD	PLD	1	
SuNAM	RABiTS	RCE	0.1	
Bruker	IBAD	PLD	0.1	

Table 2.9 Industry wire performance requirements for various utility device applications [105]

Application	J_c	B	T	I_c	Bending radius	Cost
	(A/cm^2)	(T)	(K)	(A)	(m)	(USD/kA·m)
Synchronous condenser	10^5	2-3	30-77	100-500	0.1	30-70
Fault current limiter	10^4-10^5	0.1-3	70-77	300	0.1	30-70
Transmission power cable	10^5	0.15	67-77	200	2 (cable)	10-50
Industrial motor	10^5	4-5	30-77	100-500	0.1	10-25
Transformer	over 10^6	0.15	70-77	100 at 0.15 T	0.05	10-25
Generator	over 10^4	2-3	50-65	125 at, 3 T	0.1	5-10

Table 2.9 presents a summary of the industry consensus for chosen applications in the energy sector. Critical current densities and mechanical properties of commercially produced HTS 2G wires closely resemble those required by industrial applications [105].

Critical current densities and mechanical properties of commercially available wires generally meet the industrial application requirements. However, the ratio cost per performance is still high. Today's available tape piece length is 200-300 m and the highest price amounts to about 500 $ per kAm. This presents an opportunity for further development.

Hysteresis losses are an important aspect of HTS coated conductors in AC superconducting devices. These losses are mainly generated in metallic substrate layers of HTS tapes. The value of the losses depends on the substrate type (NiFe, NiCrW), frequency and magnetic flux density value [94, 123].

The first solenoid magnet built of second generation superconducting wire was tested in 2007. The operating temperature of the solenoid is 4.2 K and its magnetic flux density is 26.8 T. Due to improvements in the wire performance, the National High Magnetic Field Laboratory demonstrated operation of the magnet at the temperature of 35.5 T [56].

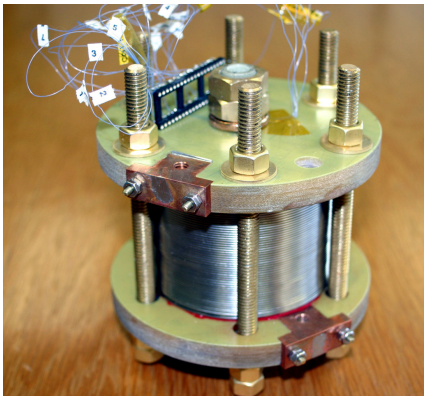

Fig. 2.10. High field magnet built of 2G wire in National High Magnetic Field Laboratory in the USA [56]

Current leads are another device in which superconducting tapes have been used. Within the European Fusion Technology Programme, the Karlsruhe Institute of Technology produced in 2003 the 70 kA HTS current lead for ITER magnets [58]. The constructed current lead has an overall length of 2 m; BSCCO superconductor tapes with an AgAu matrix, produced by AMSC, have been used for its fabrication.

The current lead shown in Fig. 2.11 consists of a high temperature superconductor part (temperatures between 4.5 K and 65 K) and a conventional

heat exchanger (temperatures between 4.5 K and room temperature). The HTS part of the lead is cooled by heat conduction from the 4.5 K end. The middle heat exchanger is cooled with 50 K He. The HTS material is embedded in a stainless steel structure which provides mechanical stability as well as thermal stabilization in case of a failure of the cooling system. The HTS part of current lead consists of sintered AgAu/BSCCO stacks (13 tapes 4.1 mm^2 × 0.2 mm^2 per stack) and 12 panels (7 stacks soldered into stainless steel carriers) [58].

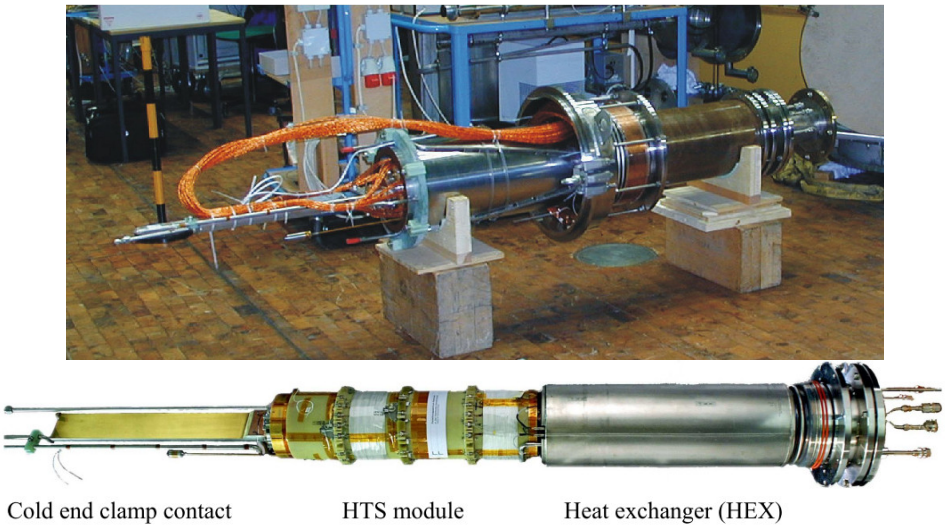

Fig. 2.11. 70 kA HTS current lead for ITER magnets [6]

High temperature superconductors are also used in superconducting power cables. Superconducting power cable systems are installed in electric power grids for transfer of energy, wherever the efficiency of conventional solutions is too small. Albany HTS Cable Project is an example of the superconducting cable application; this project establishes feasibility of operating a 350 m long HTS cable system between two substations of the National Grid Power Company, connecting parts of their real commercial grid [162].

Cable connecting two substations is shown in Fig. 2.12 a) and has the capacity of 800 A at 34.5 kV. Blue line is a 350 m long 1G HTS cable and yellow line is a 30 m long 2G HTS YBCO cable. The YBCO cable was manufactured and shipped to Albany on May 2007. The structure of the 2G HTS cable is shown in Fig. 2.12 b). The three-phase cores are placed in a cable cryostat. This structure has more compact size and lower heat invasion when compared to three single core superconducting cables. Additionally, the three cores are stranded freely to minimize the stress from longitudinal thermal contraction at the initial cooling [162].

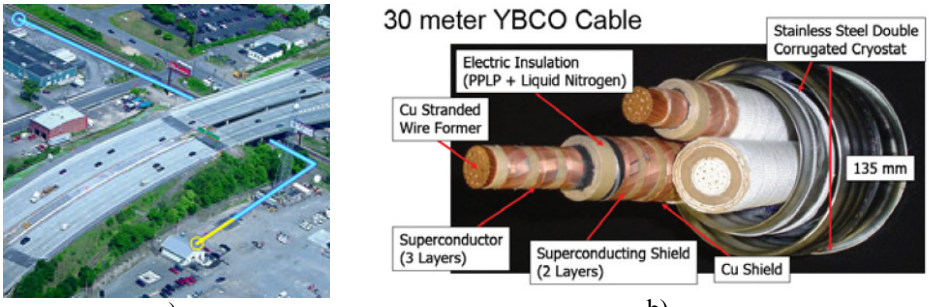

Fig. 2.12. 2G HTS transmission cable in Albany:
a) on site location, b) 2G cable configuration [55]

Race-track coils are also an application of HTS wires. Race-track coils can be used in wind turbine generators. HTS generators for offshore wind turbines are expected to have more than 10 megawatts of electrical power. Abrahamsen *et al*. present the concept of superconducting wind turbine generator with HTS race-track coils (Fig. 2.13) [1].

The stator back iron is holding the three phase stator Cu winding. Superconducting racetrack coils are mounted on the rotor support structure which is holding an inner steel tube to detain the magnetic flux between the rotor and the stator.

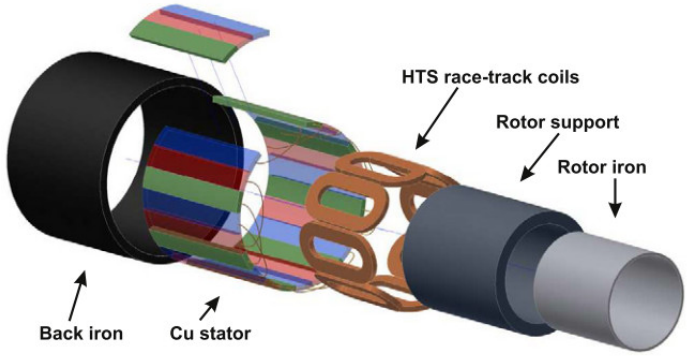

Fig. 2.13. HTS generator layout for multi-mega Watts wind turbines [1]

Coils using HTS wire can change electrical motors and generators to work at much higher power densities; using such technology can help achieve significant reduction in size, when compared to an electrical machine with equivalent output power primarily based on copper wire.

The world's most powerful motor was developed with American Superconductor's first generation HTS wire. AMSC has demonstrated a 5000 horse power (about 3.677 MW), 1800-RPM synchronous motor in 2000. This SuperMotor is shown in Fig. 2.14 and it built with superconducting rotor and conventional stator. The rotor assembly includes the first generation HTS field winding operating at temperature of about 35 K, its support structure, cooling loop, cryostat and electromagnetic (EM) shield. The stator assembly includes AC stator winding, back iron, stator winding support structure, bearing and housing [68].

Fig. 2.14. The AMSC 5000 horse power superconducting motor under tests [68]

The other field where high temperature superconductors can be used are power transformers. Transformers of this type can be used in the civil engineering, energy transfer, railways and other industries. Serious progress in the construction of superconducting transformers dates back to 1960. The initial solutions were based on low-temperature superconductors NbTi and Nb_3Sn. Since 1980, the development of superconducting transformer was driven mainly by ABB and GEC Alsthom in Europe-as well as by various companies and universities in Japan. Advances in the production of high temperature superconducting wires led to a reduction of AC losses. Weight reduction and greater efficiency have been demonstrated on smaller superconducting transformers (power below 100 kVA): 80 kVA single-phase transformer (Alsthom), 30 kVA (Toshiba) and three-phase 40 kVA (Osaka University). Larger superconducting transformers have also been built and successfully tested. Single-phase transformer with a capacity of 330 kVA built by ABB had a security system to protect against quench [15, 22, 42, 82, 84, 85, 161, 164].

In 1996, Kazuo Funaki of Kyushu University presented details of a 500 kVA HTS transformer program that was supported by the collaborative efforts of Fuji

Electric and Sumitomo Electric Corporation. At the CEC/ICMC meeting it was assumed that Sumitomo was responsible for supplying the HTS tapes and Fuji Electric and Kyushu University were responsible for transformer design and construction. The characteristics of HTS strands and winding sequence are shown in Table 2.10.

Table 2.10 HTS strands and winding sequence parameters of Fuji/SEC/Kyushu University HTS Transformer [83]

Strand without insulation	
Superconductor	Bi-2223
Matrix	pure silver
Cross-section	0.22 mm x 3.5 mm
Number of filaments	61
Silver ratio	2.5
Twist pitch	infinite
Critical current	35 A at a self-field, criterion 10^{-13} Ωm
Primary winding	
Type	three parallel
Number of layers	2
Number of turns	50 per layer
Number of transpositions	5 per layer
Secondary winding	
Type	six parallel
Number of layers	2
Number of turns	50 per layer
Number of transpositions	5 per layer

Fig. 2.15. BSCCO HTS transformer unit [83]

Transformer (Fig. 2.15) was cooled with continuous flow of supercooled nitrogen using a refrigerator. In that way, the current-carrying capacity of the winding and dielectric breakdown strength was improved. The parameters of the designed and constructed HTS transformer are shown in Table 2.11. The two values for the winding's primary and secondary diameters refer to sandwiched layers that are constructed so as to reduce the effective self-field [83].

Table 2.11 Transformer design parameters [83]

Parameter	Value
Capacity	500 kVA
Frequency	60 Hz
Voltage (primary/secondary)	6600 V/3300 V
Current (primary/secondary)	76 V/152 A
Core	silicon steel plate
height/width	1580 mm/1110 mm
cross-section	986 cm^2
magnetic field density	1.7 T
Cryostat height/diameter	1210 mm/785 mm
Winding diameter primary/secondary	465.553 mm/509.597 mm
Winding height	748 mm
Secondary load	500 kVA inductive coil

In 2007, also in Japan, a 2 MVA HTS transformer was constructed and tested. The transformer was a single phase unit designed at 66 kV/6.9 kV [15]. Designing and manufacturing the 2 MVA HTS transformer allows for elaboration of essential technology of 10 MVA (66 kV/6.9 kV) class HTS power transformers commonly used in Japan.

Fig. 2.16. The 2 MVA HTS transformer before (left) and after (right) the assembly [15]

The completed 2 MVA HTS transformer is shown in Fig. 2.16. The main parameters of the transformer are shown in Table 2.12.

Table 2.12 Main parameters of 2 MVA HTS transformer [22]

Parameter	Value
Phase	1
Power	2 MVA
Voltage primary/secondary	66 kV/6.9 kV
Current primary/secondary	30.3 A/290 A
Cooling method	Sub-cooled liquid nitrogen 66 K
Wire	BSCCO
Winding	Layer

The tests of the transformer were performed according to the JEC-2200 standard (Japanese Electrotechnical Committee JEC standard). All tests were completed and their results indicate that technologies essential for the development of a 10 MVA class HTS power transformer were established.

The subsequent research on HTS transformers focuses on the design of high power transformers. In Korea in 2004, 60 MVA (154 kV/23 kV) HTS transformer using YBCO coated conductors was designed [84]. The primary winding of the transformer is of the double pancake type and the secondary winding is solenoid type. In 2006 Lee at al. [85] describe the possibility of the design of the 33 MVA transformer (154 kV/22.9 kV) with an on load tap changer (OLTC).

The idea of building superconducting current limiter was established around 1980, but the conditions for its implementation arose around 2000, when high temperature superconducting wires were commercially available, this has also resulted in an expansion of contact cooling systems.

The concept of fault current limiter with a superconducting element is based on the nonlinear characteristics of superconductors, consisting of rapid, automatic transition of the superconducting element, which is in the superconducting state, to the resistive state when the critical current is exceeded.

Components of superconducting fault current limiters can be constructed in the form of:

- stacks of superconducting plates connected in series or in parallel in order to obtain the corresponding value of the limiter current,
- YBCO superconducting thin film,
- massive superconductors BSCCO and YBCO,
- spiral superconducting tapes of BSCCO.

Modular design of superconducting fault current limiters can be used for different levels of voltage and current. SFCL limiters can be adapted to the

specific limiting characteristics in case of occurrence of short circuits. Devices controlling high short circuit currents contribute to significant improvements in system security and more cost-effective design elements of power grids.

Superconducting faults current limiters can be divided into resistive, inductive and diode bridge types due to their activation method [65]. The main parameters of chosen HTS fault current limiters constructed worldwide are presented in Table 2.13.

Table 2.13 Parameters of chosen superconducting fault current limiters built of wired HTS [2, 23, 51, 74, 78, 102, 106, 110]

Constructor	Country / Year	Characteristic	Superconductor	SFCL type
General Atomics	USA / 2002	7.2 kV/1.2 kA	Bi-2212 tape	diode bridge
Yonsei University	Korea / 2002	3.8 kV/200 A	Bi-2212 tape	diode bridge
CAS	China / 2005	6 kV / 1.5 kA	Bi-2212 tape	diode bridge
Innopower	China / 2007	20 kV/1.6 kA	Bi-2212 tape	inductive
KEPRI	Korea / 2004	3.8 kV/200 A	YBCO thin film	resistive
CRIEPI	Japan / 2004	1 kV/40 A	YBCO thin film	resistive
Mitsubishi	Japan / 2004	200 V/1 kA	YBCO thin film	resistive
Alcatel	France / 2001	100 V/1.4 kA	YBCO coated conductor	resistive
IGC Superpower	USA / 2009	80 kV/1.8 kA	YBCO coated conductor	resistive
IEL	Poland / 2010	6 kV/0.6 kA	YBCO coated conductor	inductive
Rolls Royce	UK / 2009	6.6 kV/400 A	MgB_2	resistive

The first superconducting fault current limiter manufactured by Nexans, primarily based on solid superconducting materials, was put in at Boxberg power plant in 2009. Following the successful completion of this project, Nexans has come back to the plant for live testing of anew SFCL device which includes superconducting tapes. These tapes cut back the already low losses within the conductor material by around ninety percent. The thin film HTS tapes additionally offer faster response to short circuit currents than the 1G materials. The new SFCL is designed for a nominal current of 560 A at 12 kV. It is possible to briefly pass current of maximum value up to 2.7 kA without triggering the SFCL. This is a crucial pre-requisite for operation, because of the fact that the coal mills are carrying high current on start-up. The new SFCL is made of YBCO coated conductor tapes [106].

The active part of SFCL consists of 48 superconducting elements per phase, connected in series and placed in a cryostat with liquid nitrogen. Their windings are led outside the cryogenic system through high voltage cryogenic current leads After the occurrence of the short circuit, the current limiter requires a temporary shutdown and cool-down to be able to recover the superconducting properties. Depending on the SFCL type, the period after which the device can return to work in power grid and then respond to the next fault ranges from several seconds to several minutes. The superconducting fault current limiter completed and mounted in Boxberg power plant is shown in Fig. 2.17.

Fig. 2.17. Nexans HTS SFCL mounted in Boxberg power plant [11]

3. Modelling of devices with HTS in transient states

Modern superconducting devices have many parts built of high temperature superconductors. Understanding of electromagnetic and thermal processes occurring during transient states in the devices with high temperature superconductors is the first step in designing and manufacturing efficient superconducting devices. Modelling of the devices built of superconductors is very important for development of new applications [2, 73, 79, 87,114, 117, 118].

A study of transient voltage responses in HTS materials has been performed in the past twenty years; transitions of thin YBCO films from superconducting to resistive state and back induced by a current pulse have been observed in this study [10, 57, 70, 89].

The transient response of BSCCO 2212 tube was investigated by Cha *et al*. [20] by using a pulsed current supply. Analysis of the steady and transient state of the binary current leads for Tevatron accelerator in Fermilab [29] was another attempt. This analysis has emphasised the copper part of the current lead.

The transient stability of BSCCO Ag superconducting multifilamentary tapes calculated with finite element method (FEM) was discussed by Kim and Ishiyama [71]. They have also proposed the most suitable analytical model for analysing behaviours of high temperature superconductors at superconducting transition.

Transient behaviour of a resistive type HTS fault current limiter based on Bi-2212 tubes connected in series has been modelled in [118]. The lumped network model of the limiter has been developed and implemented in PSpice [118] to investigate the transient behaviour of the SFCL.

Simulation of a magnetic shield type high superconducting FCL was carried out by Zhang using Simulink, the parameters were based on the equivalent circuit of a power transformer. Transient response calculation, especially pertaining to the primary short circuit current was presented in [166].

The transient over-current behaviour of the BSCCO silver stabilized HTS tape was examined by Hemmi *et al*. [59]. In this paper, an experiment and a numerical study on transient of the voltage and thermal behaviour of HTS tape have been carried out. In the numerical simulation, the nonlinear dependence of *E-J* characteristic of the tape was assumed [59].

The results of convergence studies of transient thermal and electromagnetic quench analysis of five Super High Momentum Spectrometer (SHMS) superconducting magnets using Vector Fields Quench analysis codes were presented in [142].

Krosny *et al*. [79] described measurements and modelling of transient state phenomena of composite superconducting conductors during pulse excitation of

magnetic flux and current. The NbTi wire (Luvata OK3900 and IMI A60/25) and MgB_2 tape (Columbus Superconductors) were under investigation.

Transient analysis of a 150 kV fault current limiting high temperature superconducting cable working in the power grid was done by Mehairjan *et al*. [97]. The HTS cable was modelled as a part of the infinite powerful grid to which a 23 kV generator is connected through a step-up transformer. The nonlinear resistance of the HTS cable was assumed in that study. Resistance was modelled with analytical equations with dependency on momentary and critical current [97].

Interaction between the SMES and the power system based on the dynamic characteristic of SMES was analysed by Shi *et al*. in [130]. In this study, the energy function method is adopted to analyze the interactions between the SMES and the simple power system. The model was implemented in MATLAB environment [130].

The numerical analysis versus measurements of quenches in the coated conductors was analysed in [125]. The influence of phenomenological formulas on the outputs of a developed finite element model was analysed. The results were compared against experimental voltage curves. The measurements were carried out for pulsed transport currents between 80 A and 160 A and external magnetic fluxes of 0 to 350 mT. The authors conclude that the solution may still be inaccurate at low field values and high current amplitudes, where the curvature of the simulated *E-J* curves is more pronounced [125].

In the above works the nonlinear *E-J* characteristic model or critical state model were often used for calculations. The critical state model is a well-known, macroscopic model that describes partial flux penetration in high temperature superconductor. Furthermore, the flux tubes can start to flow due to the Lorentz-force when a large transport current flows in the superconductor. This produces additional resistive losses which finally increase the temperature.

In this work the real (measured) dependency of the critical parameters and high temperature superconductor properties, as also as nonlinear *E-J* characteristic are taken into consideration in proposed hybrid models. The analysis and measurements were performed for low field magnetic values (self field) and high current amplitudes.

3.1. Hybrid model of coupled problems

Modelling of coupled magneto-dynamic, electrical circuit current flow and heat flow problems in superconducting devices is a complicated issue due to the fact that the properties of superconductors and the critical parameters depend nonlinearly on the temperature; there is also no software on the commercial market which can directly couple these three fields.

Additionally, linkage of the circuit current flow problem and heat flow problem is difficult for devices with HTS superconductors because of significant differences in resistivity of HTS superconductor in the superconducting state ($\rho_s=10^{-24}$ Ωm) and the resistive state ($\rho_r=10^{-5}$ Ωm) [32].

In modelling thin layer 2G high temperature superconducting tapes, disproportion of the HTS layer to width of the tape, still presents a difficulty that needs to be overcome. This often leads to lack of convergence of solutions and the need to rebuild the entire model. The hybrid model of coupled problems has been proposed to tackle the problem of current flow and heat flow fields for different types of superconducting device cooling. Algorithms have been developed for cooling with the cryocooler, where the device is in a vacuum cryostat and in a bath of liquid nitrogen.

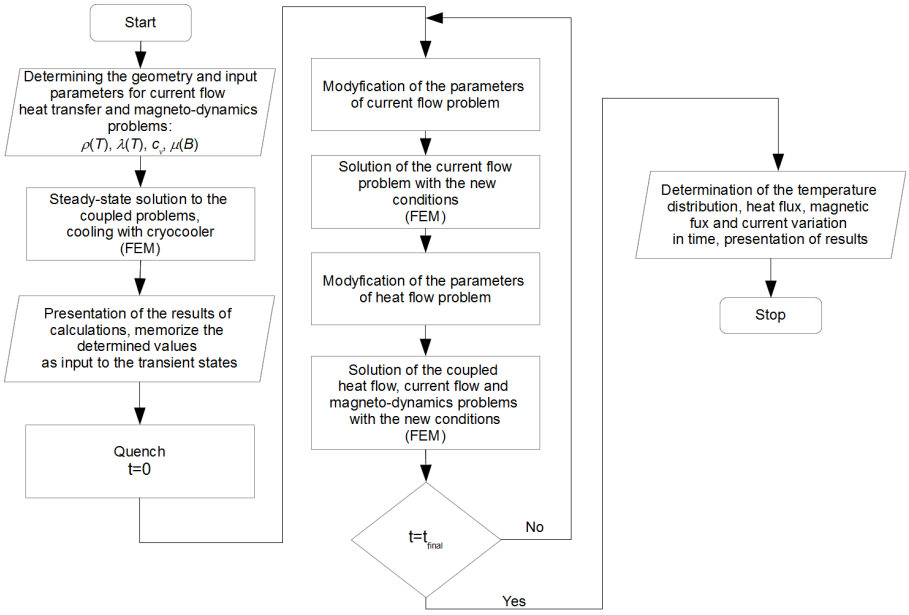

Fig. 3.1. The hybrid model algorithm for contact cooling with cryocooler

The hybrid model consists of: developed models of heat flow (HF), current flow (CF) and magneto-dynamics (MD), which are solved using FEM software and software developed especially for the needs of this study which adds the coupling between the developed models (Fig. 3.1). The steady state is considered as the first step of the algorithm. Elaborated numerical model takes into account nonlinear properties of the materials. In devices built of HTS superconductors these properties mostly depend on temperature, flux density and current intensity. This dependency is usually nonlinear in the temperature range

4 K – 200 K. The response of the high temperature superconductor on the AC magnetic field is achieved according to model elaborated by the author and described in earlier works [33-39].

Steady state solution is taken as the first step of the transient state. The model assumes that the cause of the transient state is quench which occurs in t=0. The input data is stored and then transferred to HF, CF and MD problems, which are solved using FEM method, using FEMM software. Volumetric power from current flow and magneto-dynamic problems are stored in the memory and transferred as input for the heat flow problem. The temperature distribution in the model is calculated in the heat flow problem. New values of temperature dependent properties are also determined and passed to the next step of the solution as input. Magnetic flux density distribution in the model is considered at the same time and the relevant parameters are changed in next step of calculations on the basis of the flux density values. Calculations are stopped after the final run of the programme and the results are stored in data files.

Vacuum of the order of 10^{-2} – 10^{-4} Pa is created in the cryocooler cooled cryostats. The vacuum thermally insulates the device in cryostat; however, there are solutions where additional insulation in form of an inner shell of liquid nitrogen or liquid helium can be met. Cryocooler has two degrees of cooling. The first stage is usually temperature of 40 K, 50 K or 80 K, while the second stage temperature reaches 4.2 K. Cryocooler heads operate in a closed cycle, and thus require only a power supply and water or air to cool the helium compressor and vacuum pumps. Most coolers used in cryogenics are contact cryocoolers working according to the Gifford-McMachon cycle. These cryocoolers are characterized by a relatively large thermal power, wide operating temperature range and low power consumption. In the case of contact cooling with cryocooler, the heat transfer in device built of HTS superconductor is assumed as conduction and radiation.

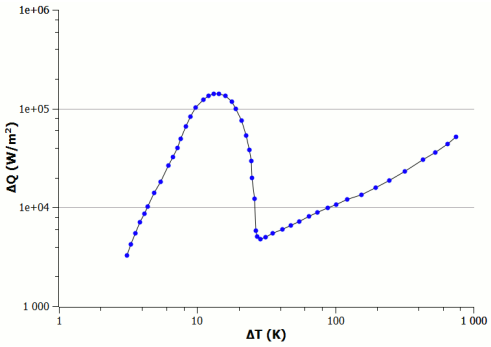

Fig. 3.2. Heat flux ΔQ flowing between the surface and liquid nitrogen (LN_2) as a function of temperature difference ΔT between the surface and the LN_2, technique for cooling in a bath of liquid nitrogen [13, 73, 134]

Completely different cooling conditions are in a liquid nitrogen (LN) bath. All surfaces of the HTS device which are in contact with the LN, are cooled by heat dissipation. The value of this heat dissipation depends on the temperature difference between liquid nitrogen and the cooled surface. This dependency is strongly nonlinear and is shown in Fig. 3.2.

In the temperature difference range of 10 – 50 K an unstable boiling film can be observed on the cooled surface. To take into account the heterogeneous conditions of cooling in a bath of liquid nitrogen, the hybrid model was developed. The algorithm of hybrid model in liquid nitrogen bath cooling is shown in Fig. 3.3.

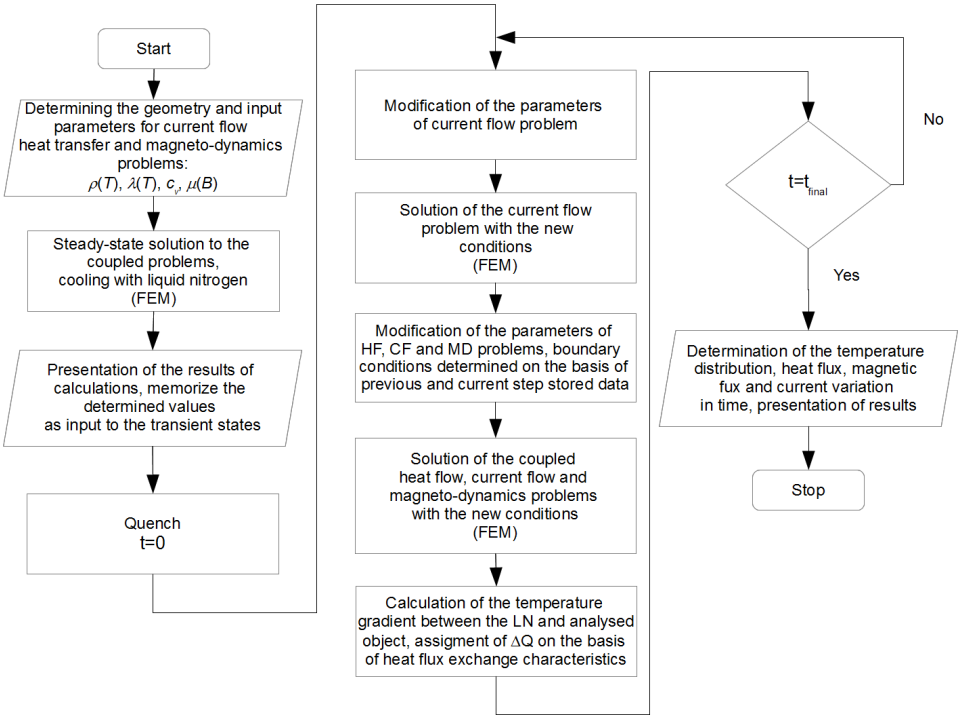

Fig. 3.3. Hybrid model algorithm for cooling with liquid nitrogen bath

Steady state solution is obtained under the assumption that the cooling was performed using the liquid nitrogen bath. In steady state, the temperature at the surfaces of the superconducting device is set to T=77 K. The model assumes that the cause of the transient state is quench which occurs in t=0. The input data is stored and then transferred to HF, CF and MD problems, which are solved using the FEM method. After obtaining the first solution in transient state, the boundary conditions, materials, as well as heat source properties are changed in

all models (i.e. magneto-dynamic, heat transfer and current flow – middle part of algorithm at Fig. 3.3). In the heat flow problem, the temperature difference between the device built of high temperature superconductor and liquid nitrogen is determined. On the basis of this value, the heat flux is assigned from the curve shown in Fig. 3.2. The boundary condition is changed from constant temperature to a heat flux which dependent on temperature difference.

Analogously, the parameters in other models shall be amended accordingly; the whole solution is calculated in the next step. The iteration process stops when it reaches the final time. At each step, the results are stored in the software memory; new values of temperature dependent properties are also determined and passed to the next step of the solution as input.

3.2. Modelling of thermal and magneto-dynamics problems in SFCL

Numerical modelling of the magneto-dynamic and thermal phenomena in AC supplied applications of HTS superconductors will be discussed on the example of inductive type superconducting current limiter (SFCL). The main parameters of the SFCL are shown in Table 3.1.

Table 3.1 Main parameters of superconducting fault current limiter with CST-60/50.2 tube [76]

Primary winding made of Copper	
Wire diameter	0.85 mm
Number of turns	236
Winding height	49 mm
Winding inner diameter	73 mm
Limiting current	2.65
HTS cylinder CST 60/50.2 (BSCCO 2223)	
Critical temperature	108 K
Inner diameter	59 mm
Height	50 mm
Wall thickness	2.5 mm
Critical current at 77 K	625 A
Ferromagnetic core (low carbon steel)	
Core cross section	400 mm^2 (2 cm x 2 cm)
Column height	103 mm
Core window width	36 mm

The measure of the effectiveness of inductive type superconducting current limiters with copper primary winding and HTS secondary winding is the increase of the primary winding impedance caused by the loss of

superconductivity in the secondary winding. In the superconducting state, the secondary winding made of HTS is shielding the ferromagnetic core. Magnetic flux is not allowed to penetrate the inner column of the core. In that case, the influence of the core on the impedance of the limiter in superconducting state can be neglected.

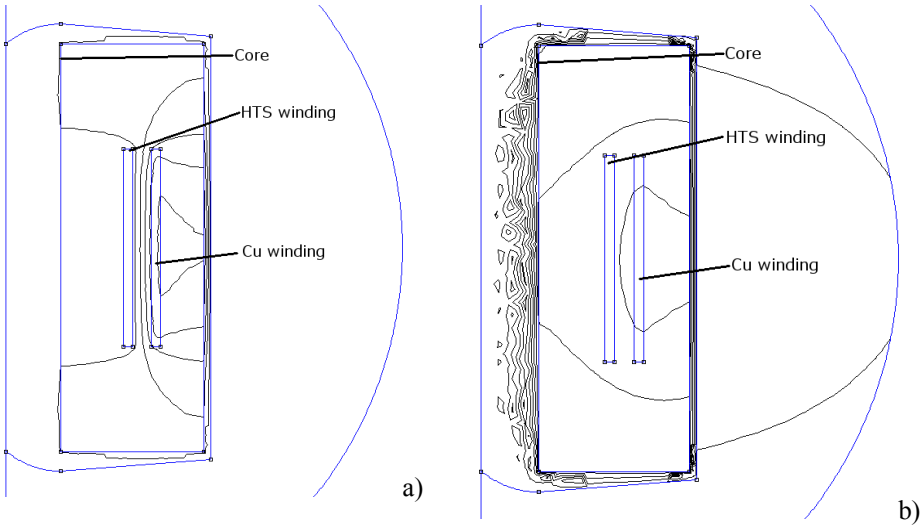

Fig. 3.4. Flux lines in the inductive type of SFCL in: a) superconductive state, b) resistive sate

The results of SFCL modelling and shielding effect are depicted in Fig. 3.4. After limiter went to resistive state, there is no shielding effect caused be secondary HTS winding. It is assumed that the comparison of the limiter impedance without core and with core can be used to assess the degree of current limiting. As the voltage is proportional to the impedance here, the degree of current limiting can be determined by comparing the voltage limiter with a core and without a core.

Modelling of coupled transient magnetics, circuit and thermal problems can be done by using the written software, which can couple these three problems. Most of commercial and freeware software, i.e. FLUX2D, ANSYS, OPERA, FEMM can couple two problems. This limitation can be overcome by writing one's own software, which can control, link and exchange data between the magnetics, circuit finite element analysis application, and thermal problem. Numerical model of inductive type superconducting current limiter with HTS cylinder and closed magnetic core was developed in transient magnetic module coupled to an external circuit in the FEMM application. The basic variable is present in the transient magnetics module, and the vector potential equation is solved [95]:

(3-1) $$\nabla \times \left(\frac{1}{\mu} \nabla \times \boldsymbol{A} \right) = -\sigma \frac{dA}{dt} + J_{src} - \sigma \nabla V$$

where:

A – magnetic vector potential, J − current density , ω − angular frequency , σ − electrical conductivity, μ − magnetic permeablility.

The heat flow problems in FEMM are represented by temperature gradient and heat flux density. The heat flux density must obey the Gauss' law.

(3-2) $$\nabla \cdot F = q$$

where:

F – heat flux density, q – volume heat generation.

Thermal conductivity is often a weak function of temperature. FEMM allows for the variation of conductivity as an arbitrary function of temperature.

FEMM solves the partial differential equation:

(3-3) $$-\nabla \cdot (\lambda \nabla T) = q$$

where:

λ – thermal conductivity, ∇T – temperature gradient.

The geometry of the model consists of HTS and copper windings, ferromagnetic core, and outer area with periodic boundary condition which represent the infinity (Fig. 3.5.).

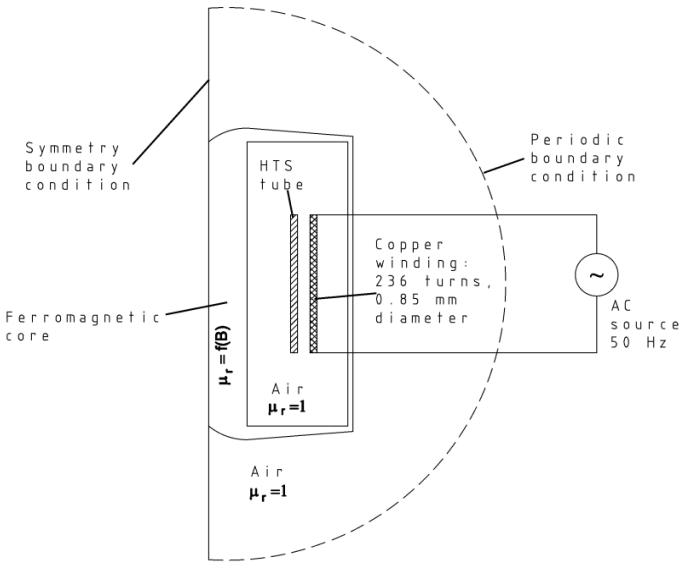

Fig. 3.5. Geometry of the SFCL magnetis model implemented in FEMM

Cooling of HTS winding in liquid nitrogen was assumed in the model. The core of superconducting inductive current limiter has no rotational symmetry. One of the main computational problems when creating a numerical model of the limiter was replacing the three-dimensional geometry of the core with an equivalent axisymmetrical model, allowing the use of the FEMM program.This was achieved by changing the outer diameter and height of the core to keep the constant cross-section (Fig. 3.5).

The copper winding was coupled with electrical circuit, which consists of 236 turns of the wire. The diameter of the wire in the model was equal 0.85 mm.

Work of superconducting inductive current limiter can be seen in two independent states: superconducting and resistive. However, transient analysis was also performed.

The results of calculations of the magnetic flux distribution along the horizontal line of symmetry are presented in Fig. 3.6.

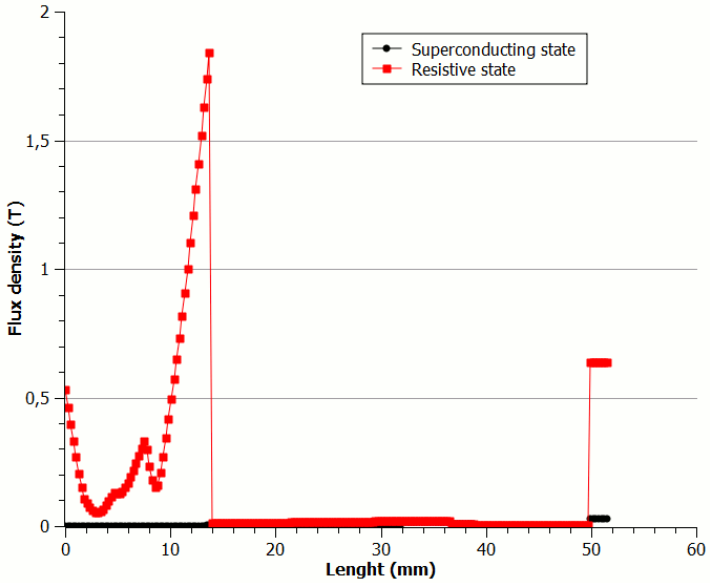

Fig. 3.6. Comparison of the flux density in SFCL model during at the surface of HTS core in superconducting state and resistive state

The shielding effect can be observed in superconducting state, where the value of flux in the inner part of core is almost 0 (analysis line length from 0 to 14 mm). In resistive state of SFCL, flux goes through the inner part of the core and its highest value is about 1.9 T.

Developed coupled magnetics, circuit and thermal model allowed for transient analysis between the superconducting and resistive states.

Fig. 3.7 presents the results of measurements of voltage of the limiter as a function of current at temperature 77 K and the results of calculations using a numerical coupled transient model.

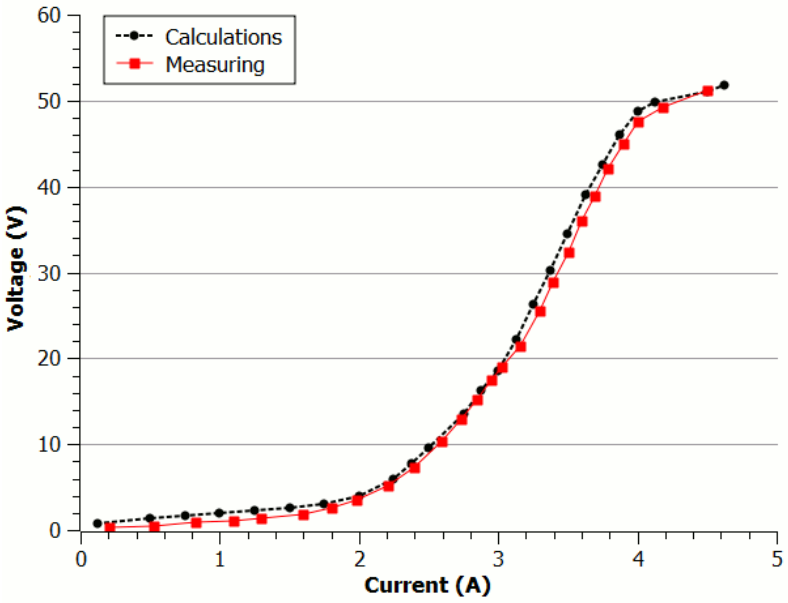

Fig. 3.7. Comparison of the results of measuring and the calculations

The dotted line shows the calculation results which can be compared with measuring (continuous line with square marks). Good agreement of calculation results with measurements can be observed. Similarity of the measured and calculated results can be estimated by calculating the correlation between them.

One of the most important measures used in the correlation analysis is the Pearson correlation coefficient. This coefficient determines the extent to which the variables are interdependent, or otherwise, determines the level of linear dependence between random variables. This coefficient is defined as:

$$r = \frac{\sum(a-\bar{a})(b-\bar{b})}{\sqrt{\sum(a-\bar{a})^2 \sum(b-\bar{b})^2}}$$

where: a and b are random variables.

The sign of the Pearson correlation coefficient can be positive or negative. A positive sign means that as the value of first variable increases, the value of the second variable also increases and as one decreases the other decreases.

Negative sign of the coefficient indicates that as one variable increases, the other decreases, and vice-versa. Assumed on the basis of the result and the sign, the strength and direction of the correlation can be defined as ranges presented in Table 3.2.

Table 3.2 The correlation strength [8, 44]

Range of values	Description
[0.0 – |±0.2|]	very weak correlation
(|±0.2| – |±0.4|]	weak correlation
(|±0.4| – |±0.6|]	moderate correlation
(|±0.6| – |±0.8|]	strong correlation
(|±0.8| – |±1.0|]	very strong correlation

The voltage-current characteristic obtained from the result calculation was compared with the measured result, and Pearson correlation coefficient was calculated. Relative error and absolute error were also determined. The results are presented in Table 3.3.

Table 3.3 Hybrid model versus measurement result comparison

Description	Value
Pearson correlation coefficient	0.9993
Average absolute error	0.9762
Average relative error	10.17%

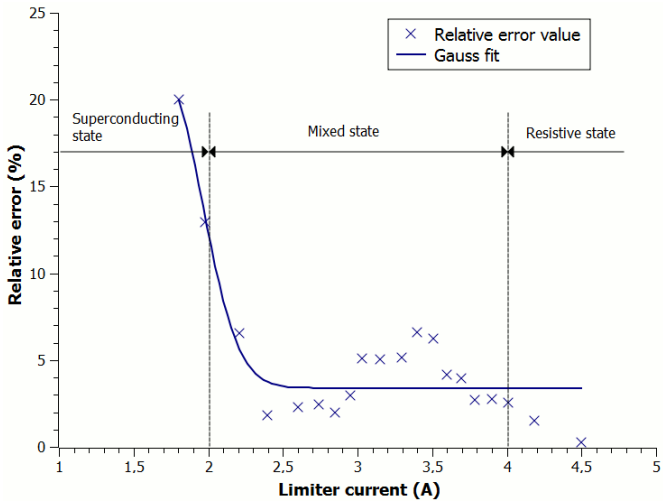

Fig. 3.8. Relative error change versus limiter current

For measured and calculated *V-I* curves shown in Fig. 3.7 the Pearson correlation coefficient is very high (almost 1) and thus it can be concluded that there is a very strong correlation between the proposed hybrid limiter model results and measurements. Calculated average relative error is about 10%, which is not high comparing to finite element analysis method error. In transient state, when the superconductor leaves the superconducting state and goes to the state of resistivity, the value of relative error drops below 10% (Fig. 3.8). It can be observed that in the range of the supplying current from 2 A to 4 A relative error value is mostly below 6% and when limiter is in resistive state the error value descends below 1%. This shows very good agreement of the results obtained from proposed hybrid model of limiter and the results obtained from measurements.

Coupled heat transfer model was also implemented in FEMM software and additionally consists of liquid nitrogen tank. The geometry of the model is shown in Fig. 3.9.

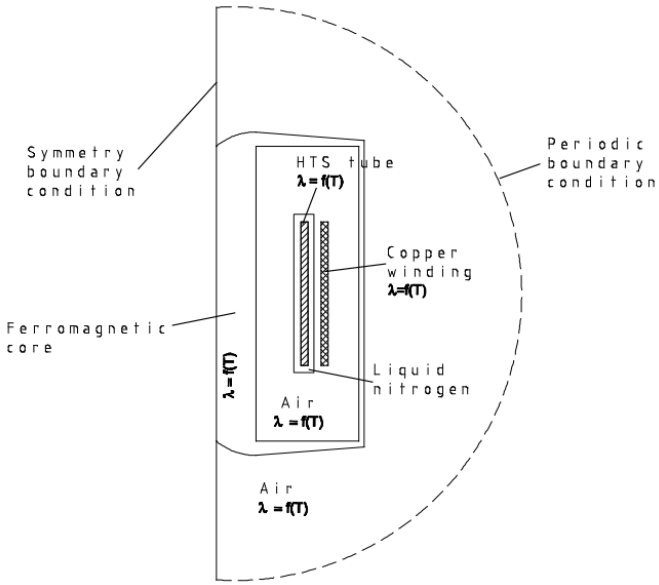

Fig. 3.9. Geometry of the SFCL heat transfer model implemented in FEMM

The HTS tube of current limiter is in the liquid nitrogen bath. On the contact surface of the liquid nitrogen-HTS tube the exchange heat flux boundary condition is used. The nonlinear dependence of the heat flux on the temperature difference is *assumed* (Fig. 3.2). The nonlinear dependence of the thermal conductivity on the temperature for all materials was assumed. Additional heat sources are generated during quench, when the high temperature superconductor

goes to resistive state. These sources have been taken into account in the form of volumetric heat generated in HTS tube. Hybrid model of the superconducting fault current limiter allowed on calculation the temperature distribution in the model (Fig. 3.10) and changes in temperature distribution during transient states (Fig. 3.11).

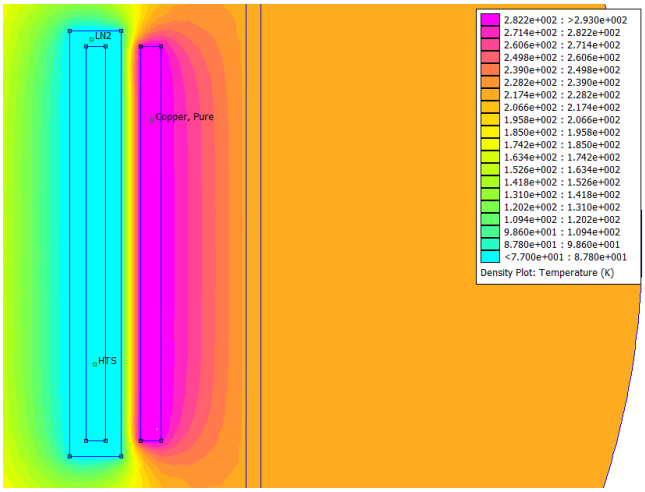

Fig. 3.10. Temperature distribution in the magnified SFC windings

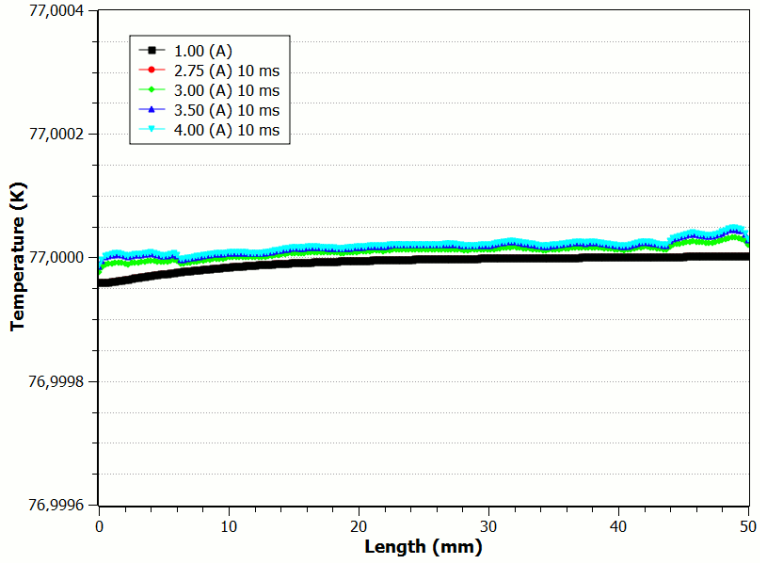

Fig. 3.11. Temperature distribution along the HTS tube height for chosen SFCL currents after 10 ms from quench appearing (black line for current equal 1 A added as reference)

After the quench the temperature in the HTS tube of SFCL does not change significantly. Cooling in liquid nitrogen bath is efficient enough to overcome the additional heat sources. In the Fig. 3.11 the temperature distribution along the HTS tube height for limiter current equal 1 A is marked black (covered with the red one). In the case of current equal 2.75 A after the 10 ms from quench appearing, the temperature distribution is the same as before.

For higher currents a very small change may be noticed, however this change does not overcome the calualtion error margin and it can be assumed that the temperature is still equal 77 K.

3.3. Modelling of the current lead built of 2G HTS thin layer tape

Development of HTS tape manufacturing technologies leads to evolution of many superconducting devices. It is possible to build the current lead based on high temperature superconducting tapes (Fig. 3.12). For this kind of current leads it is very important to keep heat sources and AC losses on the very low level (even 1 Joule) [21, 54, 127, 158].

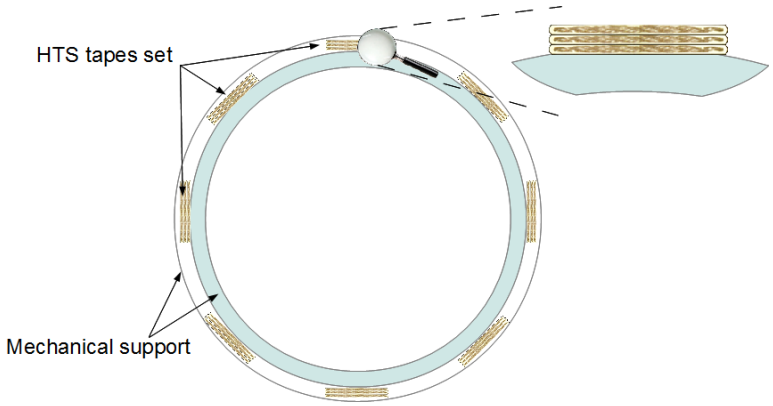

Fig. 3.12. Idea of current lead built of HTS tapes

Suitable analysis of HTS 2G YBCO tape is the first step in the process of constructing the current lead model. To complete this task an appropriate FEM model of HTS 2G tape should be built. Modelling of the second generation HTS wire is a difficult task because of the large disparity of thickness to width of the tape [49, 93, 125]. The width of the tape is at least 30 times bigger then its thickness and the ratio of thickness of superconducting layer to overall width of tape can be as high as 1:10000. Construction of the 2G HTS tape FEM model (Fig. 3.13) was the first step of the simulation.

The model used is based on the SCS3050 tape produced by the SuperPower Company. The model consists of: thin layer of (RE)BCO superconductor (thickness 1 μm), substrate made of hastelloy (50 μm), silver overlayer (2 μm) and copper stabilizers (20 μm each). Width of the tape is 3 mm.

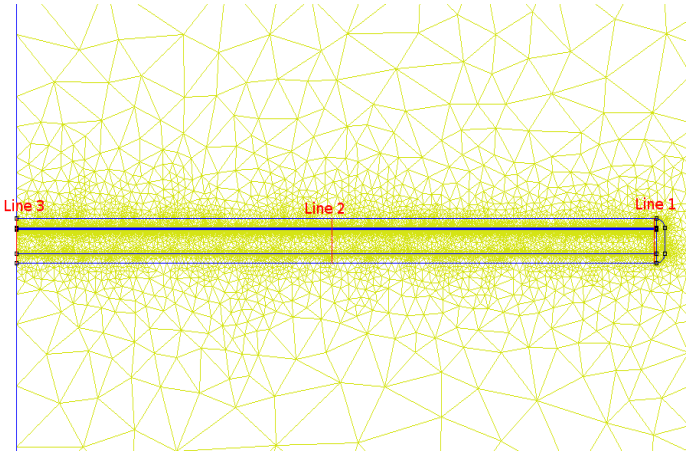

Fig. 3.13. FEM model of the second generation HTS tape

When building the mesh, it is very important to obtain good quality elements in the HTS layer, this will ensure the correct results. The value of the current is 50 A and it is lower than the critical current for this type of tape, which equals I_c=60 A.

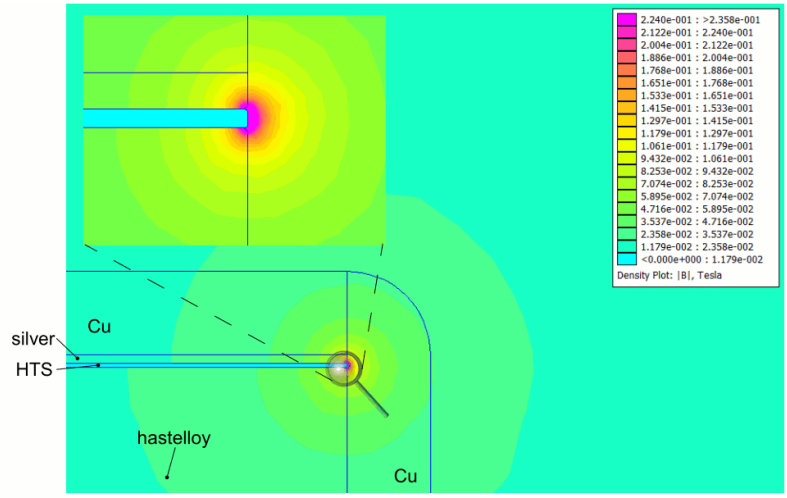

Fig. 3.14. Distribution of the flux density in the model (self field)

The tape was modelled in superconducting state. After solution the flux distribution was obtained (Fig. 3.14).

The inhomogeneities in the distribution of magnetic flux at the end of the wire can be noticed. This leads to an increase of AC losses in the tape.

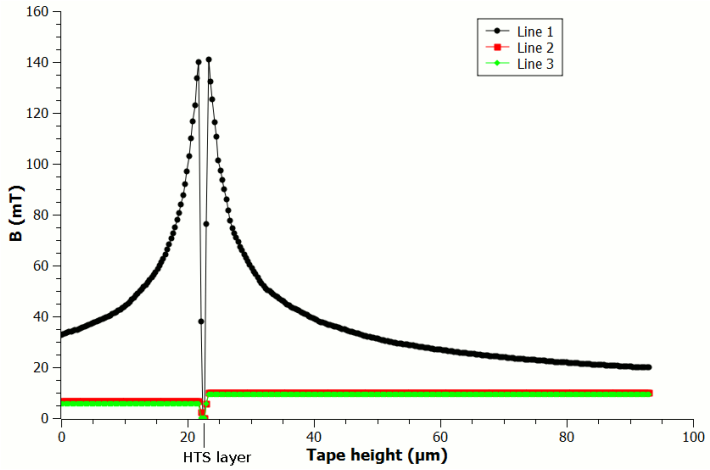

Fig. 3.15. Flux density versus height of tape

Highest values of flux were obtained in hastelloy substrate, silver overlayer and copper stabilizers near the end of the HTS layer (Fig. 3.15). Transport current flows mostly in the HTS superconductor layer as shown in Fig. 3.16.

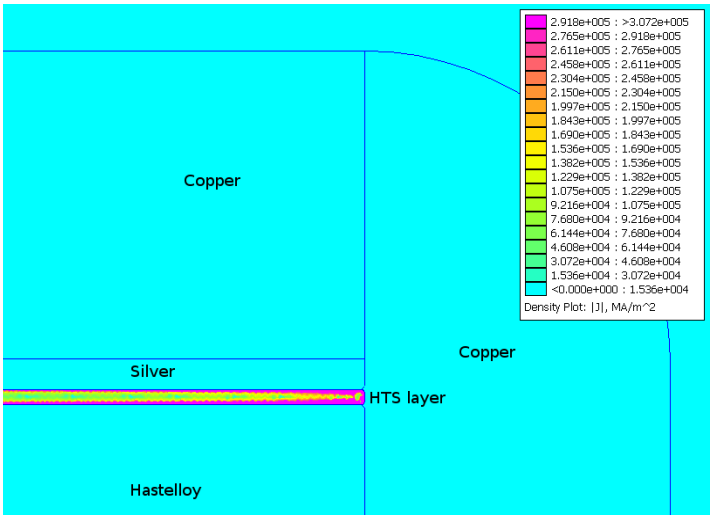

Fig. 3.16. Distribution of the current density in HTS SCS3050 tape model

In the model total power losses were calculated. The highest values were obtained in the copper laminations as shown in Fig. 3.17.

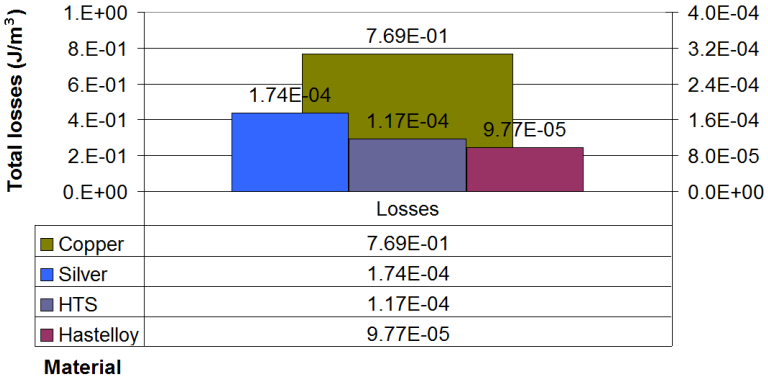

Fig. 3.17. Total power losses per cycle in SCS3050 tape model

For hybrid model verification the numerical model based on existing HTS design was build.

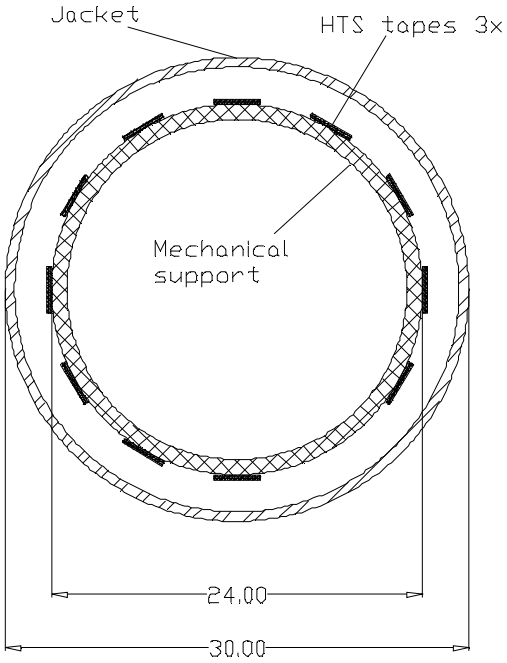

Fig. 3.18. Current lead supplying the LHC superconducting magnets [14]

Current lead is made of HTS tapes connected together as shown in Fig. 3.18. HTS tape pieces are placed on tube support made of copper or stainless steel. The outer jacket performs the function of electrical insulation and mechanical protection. Mechanical support is usually made of stainless steel or other nonferromagnetic material [14].

The current lead consists of HTS tapes placed by a few at a time on facets of a polyhedral stainless steel tube of length 350 mm (Fig. 3.18).

The symmetry of the geometry was assumed and quarter of the lead was considered for modelling of the current lead. Because of a large disproportion of the HTS superconducting layer to other dimensions of the current lead (thickness of HTS layer is 1 μm and inner diameter of the lead is 24000 μm), magnification of the model part was shown in Fig. 3.19.

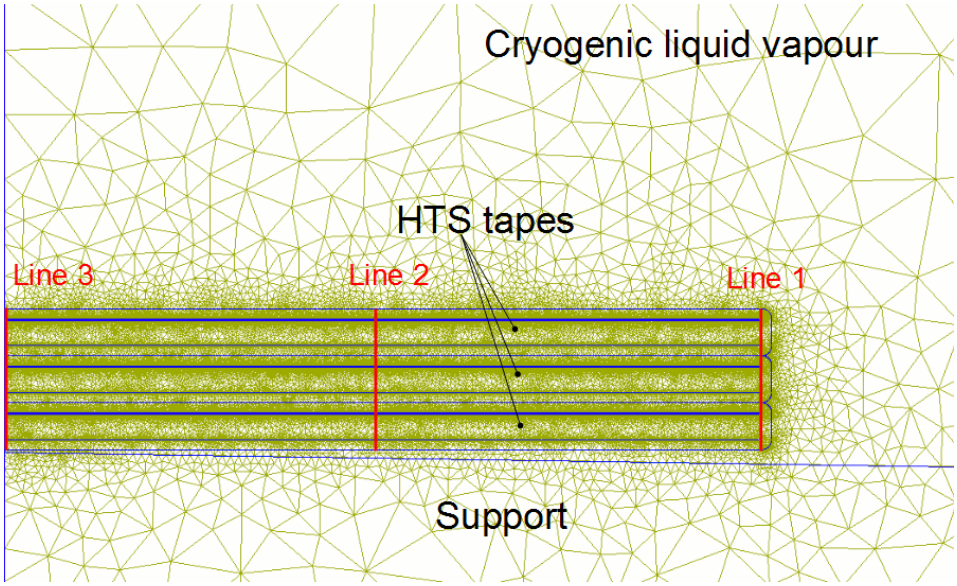

Fig. 3.19. Magnification of the HTS current lead model tapes placed on the mechanical support

The highest values of flux (similarly to the HTS tape model) were obtained in hastelloy substrate, silver overlayer and copper stabilizers near the end of HTS layer (Fig. 3.20).

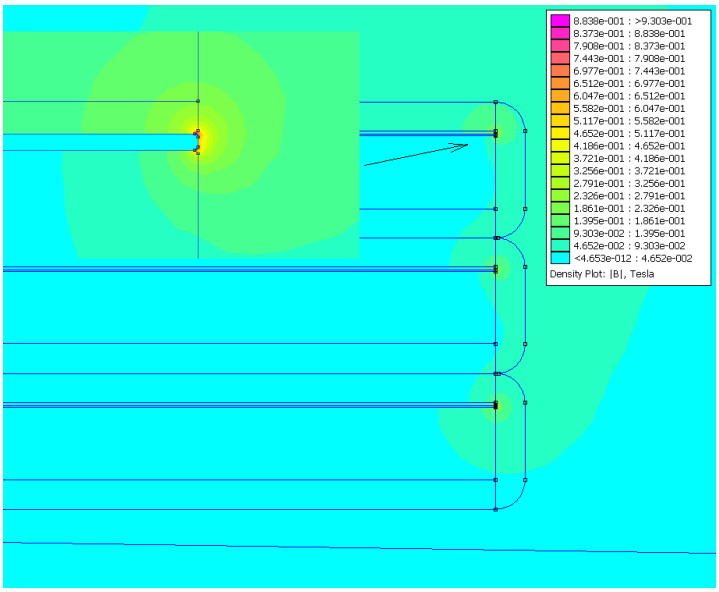

Fig. 3.20. Distribution of the flux density in the current lead model (self field)

Investigating the flux density distribution along the analysis lines, it can be noticed that the most significant inhomogeneities are present at the ends of the HTS layer (Fig. 3.21).

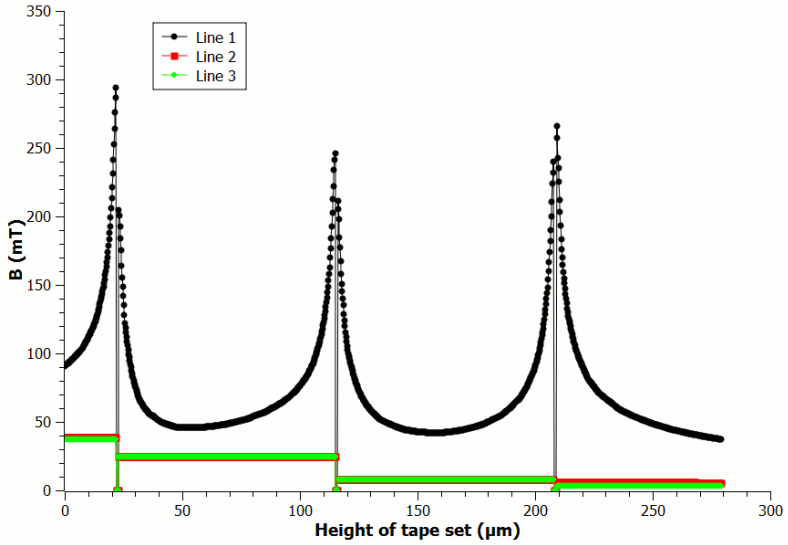

Fig. 3.21. Flux density versus height of tapes set along the analysis lines

Comparing the values of magnetic flux density obtained in current lead model to a single tape model, it can be noticed that the maximum value is at least twice higher in the current lead (Fig. 3.15 and Fig. 3.21).

Total losses (AC and resistive) in the current lead were calculated. The highest value of power losses was obtained in the copper stabilizer and is equal to about 1.7 J/m^3 per cycle (Fig. 3.22).

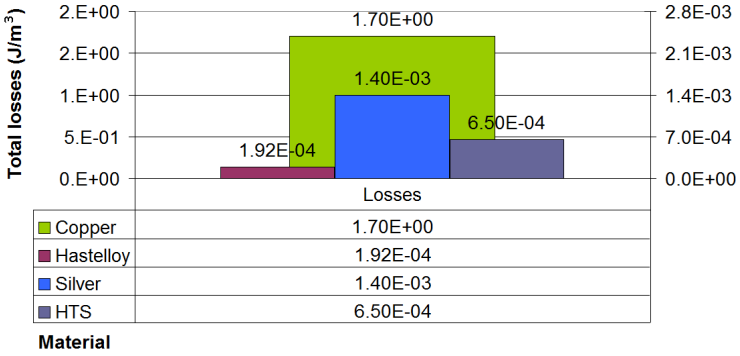

Fig. 3.22. Total power losses per cycle in HTS current lead model

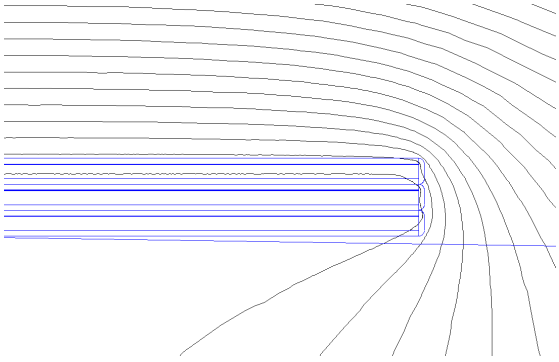

Fig. 3.23. Magnification of the magnetic field lines surrounding the HTS tapes of current lead

It seems that this value should not be too much of a problem for the cooling system, in the case of liquid nitrogen or liquid helium cooling, this value is negligible, but in the case of contact cooling, where cryocoolers are used, this value may be about 0.1% of the power capacity of the second stage of cryocooler. When designing the current leads for contact cooling, it is very important to minimize additionally generated power losses and heat sources and keep them even at the level of 20 mJ per cycle. The value obtained places at a similar level as values given by calculations made by Nguyen *et al.* in [109] and Kajikawa *et al.* in [67].

Distribution of the magnetic field lines in and around the HTS tape set was obtained (Fig. 3.23). Higher density of the magnetic field lines at the ends of the HTS tapes can be noticed.

Physical properties of HTS superconductors vary widely and their relation to the temperature, current and magnetic field is very difficult for implementation in electromagnetic model representation. Another difficult task during modelling is the large disproportion of the superconducting layer thickness to overall dimensions of the current lead model.

The highest values of flux density and AC losses were obtained in the copper stabilizer of the HTS tape. Too large values of magnetic flux and current density at the ends of the tape can cause resistive zones. Resistive zone appearance may cause unstable operation of current leads built of HTS tapes.

3.4. Modelling of the second generation HTS wire in transient states

The modelled wire was a second generation tape produced by SuperPower. The wire type is SF12050 utilizing the 50 µm thickness of highly resistive substrate. The width of wire is 12 mm and its thickness is 55 µm. Using a FEM simulation, which is considered to be optimal if the finite elements of the mesh are regular, allows for transient analysis. The geometric aspect ratio of this wire is 3272 (180 mm length versus 55 µm total thickness) and requires a very fine mesh with a huge number of elements, over $3 \cdot 10^6$ in case of coarse mesh and over $6 \cdot 10^6$ in case of fine mesh.

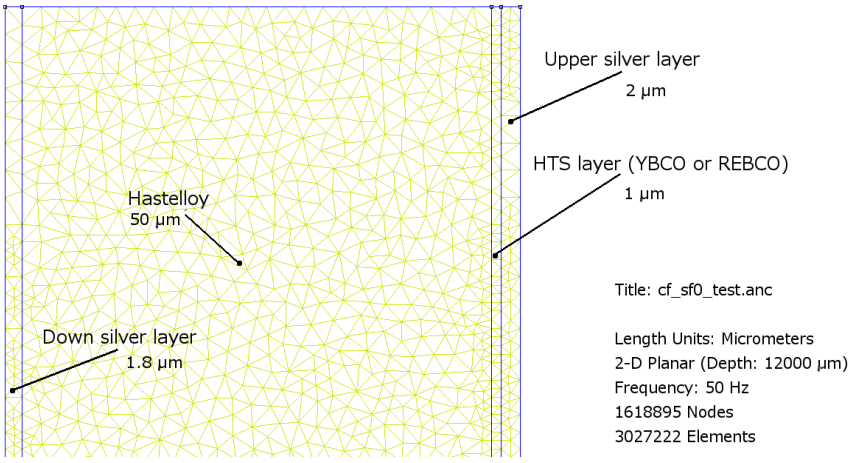

Fig. 3.24. Magnification of the part of SF12050 HTS wire, model with real dimensions (buffer stack neglected)

Such geometry results in an enormous consumption of CPU calculation time and memory usage. Decreasing the finesse of the mesh results in significantly extended elements along the length of the HTS tape. It leads to problems with the convergence of the algorithm and, in consequence, to erroneous results.

To avoid the geometry scale problem in transient current flow model, the thickness of the layers in model was multiplied by a factor, which is equal to 1000 for the simulations of SF12050 2G HTS wire. Using a lower factor, which is closer to reality, requires significantly more computational resources.

The 2G HTS wire model consists of four layers: two silver layers named upper and down, hastelloy and HTS layer (Fig. 3.24).

In order to verify the correctness of the model parameter modified by the specific factor, a comparison with the real scale model was made. The critical current I_c of the HTS layer and the resistances of the silver and hastelloy layers depend on the cross section, therefore they also depend on the thickness. Thus, the following electric parameters of the current flow model have been modified as:

(3-4) $$\rho_{\mathrm{Ag}} = \rho^{\bullet}_{\mathrm{Ag}} \times factor$$

(3-5) $$\rho_{\mathrm{Hastelloy}} = \rho^{\bullet}_{\mathrm{Hastelloy}} \times factor$$

(3-6) $$\rho_{\mathrm{YBCO}} = \rho^{\bullet}_{\mathrm{YBCO}} \times factor$$

(3-7) $$J_{\mathrm{c}} = J^{\bullet}_{\mathrm{c}} / factor$$

where $J^{\bullet}_{\mathrm{c}}$ is the value of the critical current density of the high temperature superconducting material and $\rho^{\bullet}$ is the electrical resistivity of the silver, YBCO superconductor and hastelloy used in the simulations in real scale model.

These parameters were respectively equal to: $\rho^{\bullet}_{Ag} = 0.285 \cdot 10^{-8}$ Ωm in 77 K, $\rho^{\bullet}_{Hastelloy} = 12.35 \cdot 10^{-8}$ Ωm in 77 K and $J^{\bullet}_{c} = 2.7 \cdot 10^{4}$ A/mm^2 and are the real resistivity of the silver layer and hastelloy layer and real critical current density defined with the standard 1 μV/cm electric field criterion. In this way, the HTS critical current I_c and the resistance of the silver and hastelloy layers do not change. Thus, the critical current I_c of the simulated tape is equal to 270 A, just like in the reality.

To verify the above assumptions, two models of the HTS wire current flow were compared, one in real scale and the second one, with its width multiplied by factor (Fig. 3.25).

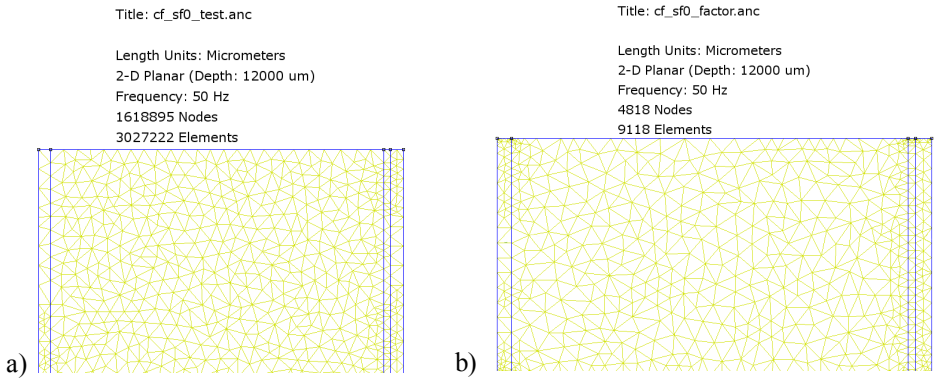

Fig. 3.25. Comparison of the geometry and meshes in the
a) real scale model and b) scale factor model

Real scale model consists of over 1.6 million nodes and 3 million elements and scale factor model consist of about 4.8 thousand nodes and 9 thousand elements. Computational time on the same machine (HP ProLiant ML110 G6 Intel Xeon X3430 Quad Core 2.40 GHz), was about 86 hours for the real model and about 5 minutes for the scale factor model.

A current of 10 A flows through the tape. For both models, selected results were compared, i.e. distribution of the current density in the wire and real power generated in each layer.

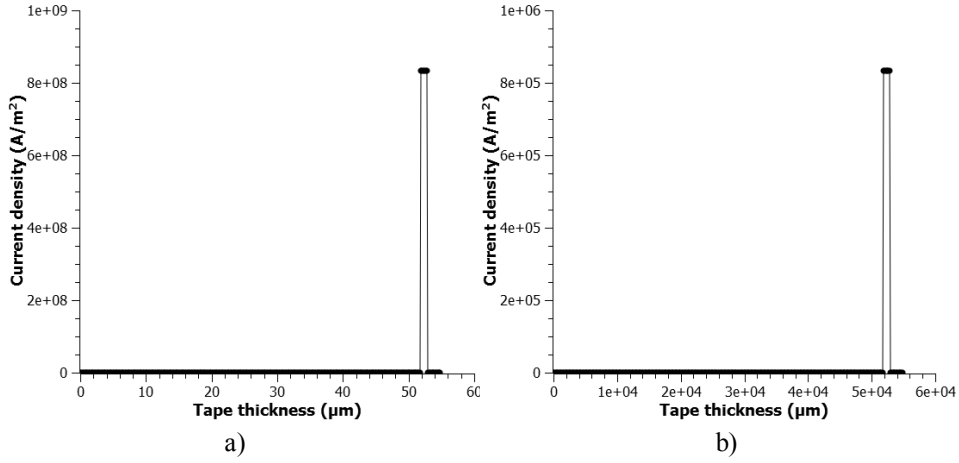

Fig. 3.26. Comparison of the current density along tape thickness in the
a) real scale model and b) scale factor model

The distribution of the current density along the tape thickness is shown in Fig. 3.26. It can be noticed that almost the whole current is flowing through the HTS layer and the values of the current density are 1000 times smaller in the case of scale factor model.

Table 3.4 Real power generated in layers of the models

Layer name	Real power (W)	
	real scale model	scale factor model
Down silver	$2.24811 \cdot 10^{-9}$	$2.24811 \cdot 10^{-9}$
Hastelloy	$5.05643 \cdot 10^{-10}$	$5.05643 \cdot 10^{-10}$
YBCO superconductor	$1.24895 \cdot 10^{-5}$	$1.24895 \cdot 10^{-5}$
Top silver	$2.4979 \cdot 10^{-9}$	$2.4979 \cdot 10^{-9}$

The same values of power generated in each layer of both models confirm the correctness of the scale factor model. Next, the data from current flow model is transferred to heat flow model. Heat flow model assumes that each volume can be heated with external sources with parameter called volume heat generation, as well as through heat conduction and radiation. From the current flow model, the volume heat generation is transferred to the heat flow problem by using software written in LUA programming language.

Because values of volume heat generation depend on the geometry, the correct values are obtained after taking into account the scale factor.

In case of heat transfer modelling, the real scale model has the same number of mesh elements as current flow. It is computationally expensive. Taking it into consideration, the scaling law was applied to the heat transfer model.

It can be assumed that the geometry of the thin layer HTS wire (like SF12050) is similar to the assembly of the flat plates. The whole model has steady fixed temperature. In the time t=0, the temperature on both outer surfaces rises to the desired value. At the same time, internal heat sources start to operate. Assuming that the thermal material parameters are constant, conductivity equation can be written as (3-8) [139]:

$$div\left(-\lambda grad T\right)+\rho \cdot c_p \cdot \frac{\partial T}{\partial t} = q_{\mathrm{v}} \tag{3-8}$$

In the two dimensional problem in XY plane and for the model with no scale (index 1) this equation can be written as:

$$-\lambda_{1x} \frac{d^2 T_1}{dx_1^{\,2}} - \lambda_{1y} \frac{d^2 T_1}{dy_1^{\,2}} + \rho_1 \cdot c_{p1} \cdot \frac{\partial T_1}{\partial t_1} = q_{\mathrm{v}1} \tag{3-9}$$

For the scale model (index 2), in which the all parameters change, it can be written as:

(3-10) $$-\lambda_{2x}\frac{d^2T_2}{dx_2^{\,2}}-\lambda_{2y}\frac{d^2T_2}{dy_2^{\,2}}+\rho_2\cdot c_{p2}\cdot\frac{\partial T_2}{\partial t_2}=q_{v2}$$

The scale factors have been defined as follows

(3-11) temperature factor – $$\frac{T_2}{T_1}=m_T$$

(3-12) X dimension factor – $$\frac{x_2}{x_1}=m_x$$

(3-13) Y dimension factor – $$\frac{y_2}{y_1}=m_y$$

(3-14) thermal conductivity factor in X direction– $$\frac{\lambda_{2x}}{\lambda_{1x}}=m_{\lambda x}$$

(3-15) thermal conductivity factor in Y direction – $$\frac{\lambda_{2y}}{\lambda_{1y}}=m_{\lambda y}$$

(3-16) specific heat capacity factor – $$\frac{\rho_2\cdot c_{p2}}{\rho_1\cdot c_{p1}}=m_{cp}$$

(3-17) time factor – $$\frac{t_2}{t_1}=m_t$$

(3-18) volume heat source factor – $$\frac{q_{v2}}{q_{v1}}=m_{qv}$$

Substituting all defined factors into equation (3-10) it can be written as:

(3-19) $$-(\lambda_{1x}\cdot m_{\lambda x})\frac{d^2(m_T\cdot T_1)}{m_x^{\,2}dx_1^{\,2}}-(\lambda_{1y}\cdot m_{\lambda y})\frac{d^2(m_T\cdot T_1)}{m_y^{\,2}dy_1^{\,2}}+m_{cp}\cdot\rho_1\cdot c_{p1}\cdot\frac{\partial(m_T\cdot T_1)}{m_t\cdot\partial t_1}=m_{qv}\cdot q_{v1}$$

By introducing constant values before differentials, it can be written as:

(3-20) $$-(\frac{m_T\cdot m_{\lambda x}}{m_x^{\,2}})\cdot\lambda_{1x}\cdot\frac{d^2T_1}{dx_1^{\,2}}-(\frac{m_T\cdot m_{\lambda y}}{m_y^{\,2}})\cdot\lambda_{1y}\cdot\frac{d^2T_1}{dy_1^{\,2}}+\frac{m_{cp}\cdot m_T}{m_t}\cdot\rho_1\cdot c_{p1}\cdot\frac{\partial T_1}{\partial t_1}=m_{qv}\cdot q_{v1}$$

Equations (3-9) and (3-20) should be equivalent, therefore it can be stated:

(3-21) $$\frac{m_T \cdot m_{\lambda x}}{m_x^{\,2}} = 1$$

(3-22) $$\frac{m_T \cdot m_{\lambda y}}{m_y^{\,2}} = 1$$

(3-23) $$\frac{m_{cp} \cdot m_T}{m_t} = 1$$

(3-24) $$m_{qv} = 1$$

Substituting (3-22) into (3-21) it can be obtained:

(3-25) $$\frac{m_T \cdot m_{\lambda x}}{m_x^{\,2}} = \frac{m_T \cdot m_{\lambda y}}{m_y^{\,2}}$$

And in the next step:

(3-26) $$\frac{m_{\lambda x}}{m_x^{\,2}} = \frac{m_{\lambda y}}{m_y^{\,2}}$$

Because the X dimension should be rescaled in the model, the Y dimension factor is equal to 1 (equation (3-27)).

(3-27) $$m_y = 1$$

Temperature distribution in the scale factor model should be the same as in the original geometry model, therefore it can be assumed that:

(3-28) $$m_T = 1$$

Substituting (3-27) and (3-28) into (3-22) it can be written that:

(3-29) $$m_{\lambda y} = 1$$

Substituting (3-27) and (3-29) into (3-25) it can be assumed that:

(3-30) $$m_{\lambda x} = m_x^{\,2}$$

Substituting (3-30) into (3-14) it can be written that:

(3-31) $$\lambda_{2x} = m_x^{\,2} \cdot \lambda_{1x}$$

Conducting from the above relationships and assuming that temperature field should be the same in both models during transients, it can be derived that time factor and specific heat capacity factor should be equal to 1.

Finally, the equation (3-10) can be written as:

(3-32) $$-m_x^{\,2} \cdot \lambda_{1x} \frac{d^2 T_2}{dx_2^{\,2}} - \lambda_{1y} \frac{d^2 T_2}{dy_2^{\,2}} + \rho_1 \cdot c_{p1} \cdot \frac{\partial T_1}{\partial t_1} = q_{v1}$$

The exchange of the additional heat sources generated during current flow can be done by volume heat generation part (q_v).

The equation (3-8) can be rewritten as:

(3-33) $$\rho \cdot c_p \cdot \frac{\partial T}{\partial t} = q_v + div(\lambda gradT)$$

For quasi static electric field it can be written:

(3-34) $$div(gradV / \rho(T)) = 0$$

Heat source term can be defined as:

(3-35) $$q_v = \frac{1}{\rho(T)}(-gradV)^2$$

Resistivity $\rho(T)$ of the hight temperature superconductor can be implemented using empirical laws

(3-36) $$\rho(T) = \frac{E(J_c, T)}{J}$$

or measured characteristic (see chapter 4.2).

The equation (3-32) can be implemented in the hybrid model. The implementation of anisotropy of thermal conductivity was implemented in external program written in LUA language (see Appendix A). Geometry and FEM solution were implemented in FEMM software (Fig. 3.27).

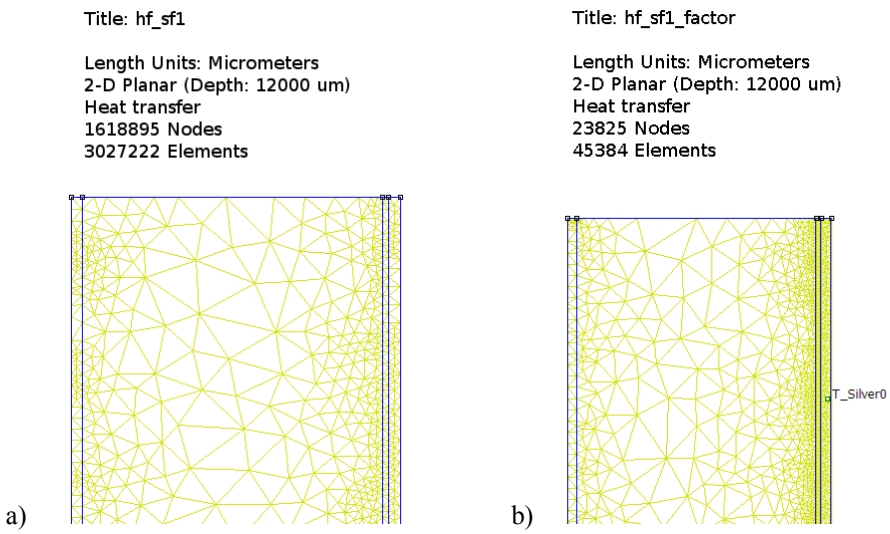

Fig. 3.27. Comparison of the geometry and meshes in the a) real scale model and b) scale factor model of the heat transfer

Because the nonlinear thermal conductivity in the case of scale factor model reveals anisotropy, all heat transfer material property changes were implemented in the external LUA program.

The SF12050 wire scale factor heat transfer model consists of four layers and eight segments. The layers in each segment are named after materials i.e.: T_Silver0 (top silver layer in segment 0), ReHTS0 (REBCO/YBCO high temperature superconductor in segment 0), Hastelloy0 (hastelloy layer in segment 0) and D_Silver0 (down silver layer in segment 0) shown in Fig. 3.28 a).

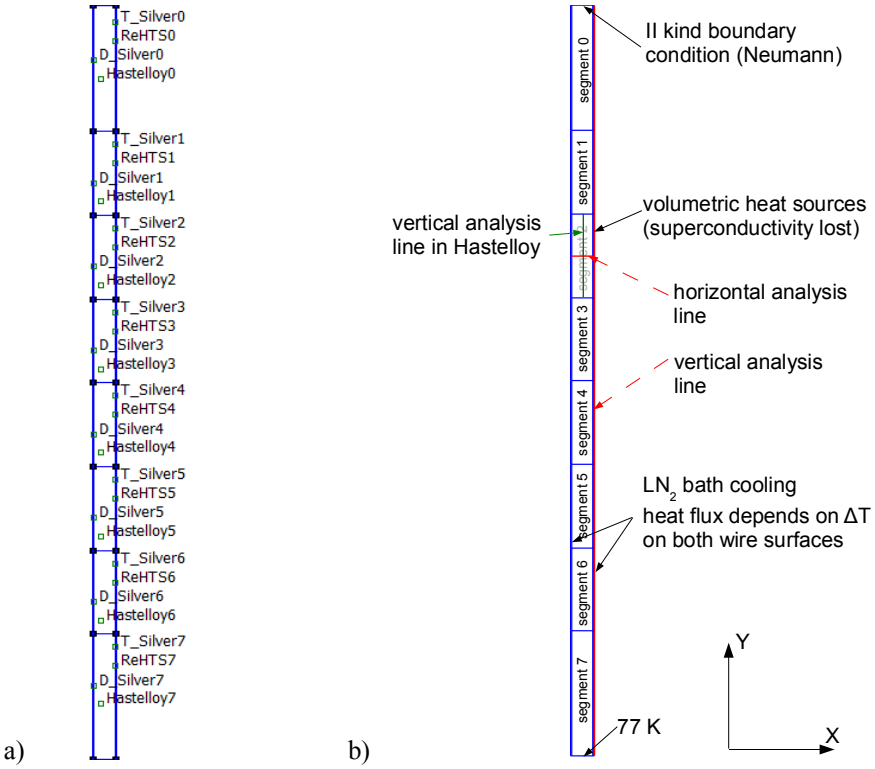

Fig. 3.28. Heat transfer scale factor model
a) materials and layers b) boundary conditions and analysis lines

In the steady state, the whole wire is placed in liquid nitrogen bath and the temperature is uniform across the whole model. In transients, segment 2 losses its superconductivity and additional volumetric heat sources are generated.

The heat sources are calculated in current flow model and transferred to heat flow scale factor model. Each segment of the model has its own boundary conditions; each material in the segment also has assigned volumetric heat sources. Transient state models, in which nonlinear temperature dependence and anisotropy were taken into consideration, were built and solved. Results obtained in the two models were compared along the horizontal and vertical analysis lines shown in Fig. 3.28 b) after two seconds of transient state.

Temperature distribution along the vertical analysis line is shown in Fig. 3.29. There is a very good correlation between the scale factor model results and real scale model results.

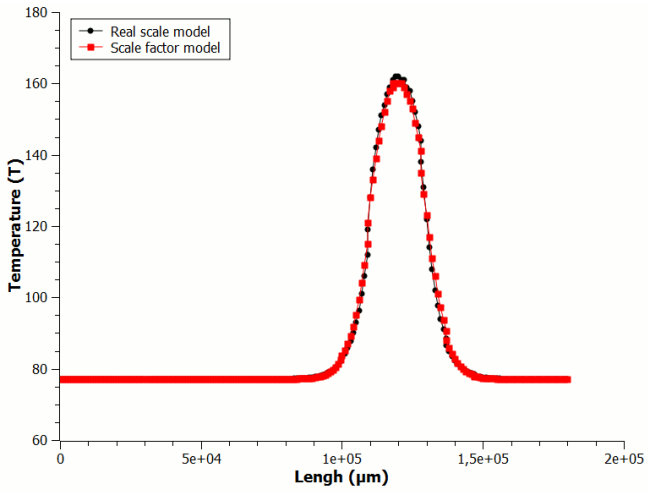

Fig. 3.29. Temperature distribution along the vertical analysis line in real scale and scale factor models

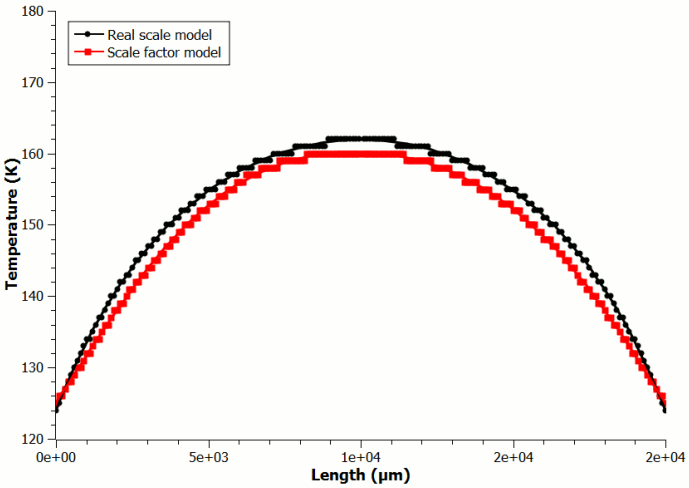

Fig. 3.30. Temperature distribution along the vertical analysis line in "Hastelloy2" layer in real scale and scale factor models

The difference in maximum values of calculated temperatures is equal to about 1.6 K, which is a 0.988 % of the real scale model value. The distribution

of the temperature, where it reaches maximum values, along the vertical analysis line in hastelloy and horizontal analysis line is shown in Fig. 3.30 and Fig. 3.31 respectively.

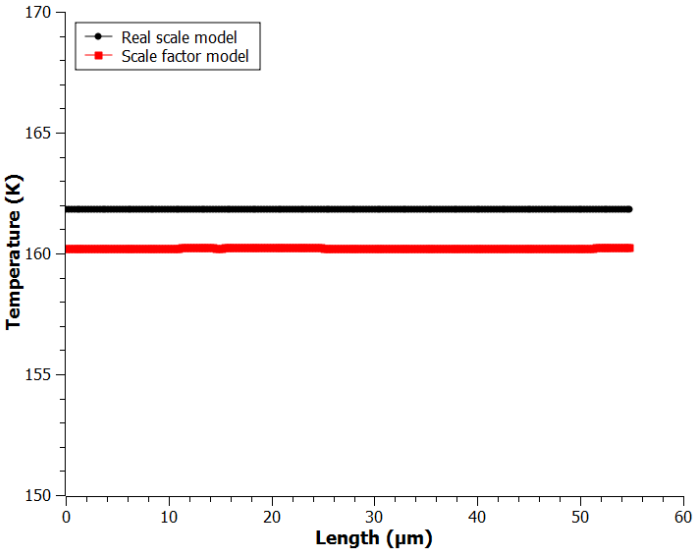

Fig. 3.31. Temperature distribution along horizontal analysis line in real scale and scale factor models

To assess the accuracy of the results of the scale factor model comparing with the real scale one, Pearson correlation coefficient and relative error has been calculated (Table 3.5).

Table 3.5 Real scale and scale factor model result comparison

Description	Value
Vertical analysis line	
Pearson correlation coefficient	0.9991
Minimum relative error	0 %
Maximum relative error	3.92 %
Average relative error	0.44 %
Horizontal analysis line	
Pearson correlation coefficient	0.8603
Minimum relative error	0.97 %
Maximum relative error	1 %
Average relative error	0.99 %

The real scale model results were taken as the reference values. The Pearson correlation coefficient value, in both cases i.e. the vertical and horizontal analysis lines, is high and so it can be concluded that there is a very strong correlation between the real scale and scale factor models. The average relative error value is very small, below 1 %, so it can be assumed that the scale factor model gives very good results, with 99 % accuracy comparing to real scale model. The scale factor was implemented in the hybrid model of SF12050 wire, in the current flow and heat transfer problems. The geometry of SF12050 wire was modelled according to the manufacturer specifications. The Super Power Company provides information on structure of SF12050 wire (Fig. 4.1). Hybrid model FEM geometries rely on physical structure of the wire (Fig. 3.32). In case of current flow geometry, the dimensions on the abscissa were scaled by the factor m_c=1000.

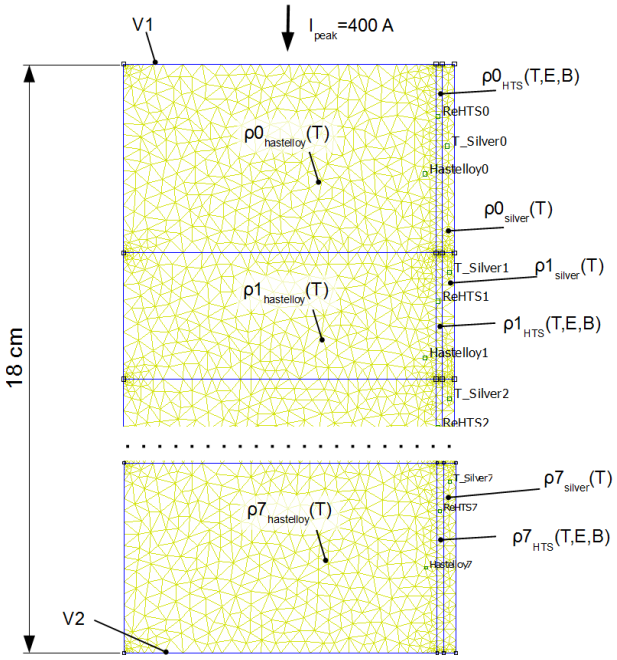

Fig. 3.32. Current flow model geometry and parameters, abscissa dimensions multiplied by factor m_c

The model consists of an 18 cm long part of the SF12050 wire, as it is presented in measurements described in section 4 of this monograph. Modelled case corresponded to measurements carried out where the current peak value was equal to 400 A. The model was divided into eight parts, so that they correspond to the measured sections of wire (see Fig. 3.32 and Fig. 4.5). Tape

thickness in the CF model is equal to 53μm×m_c. Each section of the modelled wire has appriopriate material properties, which in the case of silver and hastelloy basically depend on the temperature ($\rho_{hastelloy}(T)$, $\rho_{silver}(T)$) and in the case of high temperature superconductor depends on temperature, magnetic flux density and electric field intensity ($\rho(T,E,B)$). Electrical parameters were modified due to the scaling law as described in equations (3-4) to (3-7). The boundary conditions in the model were set to potential difference (V1 and V2 in Fig. 3.32) to reach the peak value of current equal to 400 A at the beginning of quench, when the wire was in superconducting state. This approach allowed the modelling of change in current amplitude at the transition from superconducting state to resistive state of the HTS wire. The results of current flow modelling were transferred to the heat flow and magnetics problems according to the hybrid model algorithm with liquid nitrogen bath.

Second constructed geometry contains the transient magnetics model of the SF12050 wire. Due to the 2D modelling limitations, the geometry contains the cross-section of the wire with current flowing perpendicularly to the XY plane (Fig. 3.33).

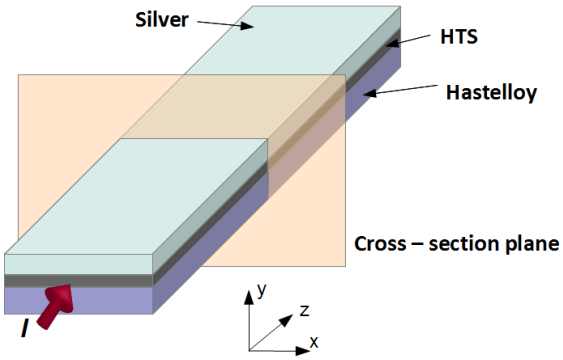

Fig. 3.33. Idea of magnetics model of SF12050 wire (not in scale)

Similarly like in previous cases the scale factor model for magnetics 2D problem has been developed. It was assumed that in XY plane only the dimensions in Y axis will be scaled by factor m_y. The partial differential equation for time-varying magnetic problems can be written as [95]:

$$\nabla \times \left(\frac{1}{\mu} \nabla \times \boldsymbol{A} \right) = -\sigma \frac{d\boldsymbol{A}}{dt} + J_{src} - \sigma \nabla V \tag{3-37}$$

This equation is solved in FEMM magnetics problem. Assuming the two dimensional problem on the XY plane, current flowing in Z direction, anisotropy of magnetic permeability and the model with no scale (index 1) this equation can be written as:

(3-38) $$-\frac{1}{\mu_{1x}}\cdot\frac{d^2A_{1z}}{dx_1^{\,2}}-\frac{1}{\mu_{1y}}\cdot\frac{d^2A_{1z}}{dy_1^{\,2}}=-\sigma_1\frac{dA_{1z}}{dt_1}+J_{1src}-\sigma_1\frac{dV_1}{dz_1}$$

For the scale model (index 2), in which the all parameters change, it can be written:

(3-39) $$-\frac{1}{\mu_{2x}}\cdot\frac{d^2A_{2z}}{dx_2^{\,2}}-\frac{1}{\mu_{2y}}\cdot\frac{d^2A_{2z}}{dy_2^{\,2}}=-\sigma_2\frac{dA_{2z}}{dt_2}+J_{2src}-\sigma_2\frac{dV_2}{dz_2}$$

The scale factors have been defined as follows

(3-40) magnetic permeability factor in X dimension – $\dfrac{\mu_{2x}}{\mu_{1x}}=m_{\mu x}$

(3-41) magnetic permeability factor in Y dimension – $\dfrac{\mu_{2y}}{\mu_{1y}}=m_{\mu y}$

(3-42) X dimension factor – $\dfrac{x_2}{x_1}=m_x$

(3-43) Y dimension factor – $\dfrac{y_2}{y_1}=m_y$

(3-44) Z dimension factor – $\dfrac{z_2}{z_1}=m_z$

(3-45) magnetic vector potential factor– $\dfrac{A_{2z}}{A_{1z}}=m_A$

(3-46) current density factor – $\dfrac{J_{2src}}{J_{1src}}=m_J$

(3-47) electrical conductivity factor – $\dfrac{\sigma_2}{\sigma_1}=m_\sigma$

(3-48) electric potential factor – $V_2/V_1=m_V$

(3-49) time factor – $t_2/t_1=m_t$

Substituting all defined factors into equation (3-39) it can be written as:

(3-50) $$-\frac{1}{m_{\mu x}\mu_{1x}}\cdot\frac{d^2(m_AA_{1z})}{d(m_xx_1)^2}-\frac{1}{m_{\mu y}\mu_{1y}}\cdot\frac{d^2(m_AA_{1z})}{d(m_yy_1)^2}=$$
$$-m_\sigma\sigma_1\frac{d(m_AA_{1z})}{d(m_tt_1)}+m_JJ_{1src}-m_\sigma\sigma_1\frac{d(m_VV_1)}{d(m_zz_1)}$$

By introducing the constant values before differentials it can be written as:

$$-\frac{1}{m_{\mu x}\mu_{1x}}\cdot\frac{m_A}{m_x^2}\cdot\frac{d^2A_{1z}}{dx_1^{\ 2}}-\frac{1}{m_{\mu y}\mu_{1y}}\cdot\frac{m_A}{m_y^2}\cdot\frac{d^2A_{1z}}{dy_1^{\ 2}}= \tag{3-51}$$
$$-\frac{m_\sigma m_A}{m_t}\sigma_1\frac{dA_{1z}}{dt_1}+m_J J_{1src}-\frac{m_\sigma m_V}{m_z}\sigma_1\frac{dV_1}{dz_1}$$

If the distribution of magnetic vector potential should be the same in both models, the equations (3-38) and (3-51) should be equivalent. Thus, it can be written:

$$\frac{1}{m_{\mu x}}\cdot\frac{m_A}{m_x^2}=1 \tag{3-52}$$

$$\frac{1}{m_{\mu y}}\cdot\frac{m_A}{m_y^2}=1 \tag{3-53}$$

$$m_\sigma m_A=1 \tag{3-54}$$

$$m_J=1 \tag{3-55}$$

$$\frac{m_\sigma m_V}{m_z}=1 \tag{3-56}$$

Substituting (3-52) into (3-53) it can be obtained that:

$$\frac{m_{\mu x}}{m_{\mu y}}=\frac{m_y^2}{m_x^2} \tag{3-57}$$

Because the scale factor will be implemented only in the Y direction, it can be assumed that $m_x=1$ and $m_{\mu x}=1$. From (3-56) it can be obtained that:

$$\frac{1}{m_{\mu y}}=\frac{m_y^2}{1} \tag{3-58}$$

Scale factor for magnetic permeability in Y direction can be obtained from that and wriiten as:

$$m_{\mu y}=\frac{1}{m_y^2} \tag{3-59}$$

Magnetic vector potential distribution in the scale factor model should be the same as in original geometry model, therefore it can be assumed that:

$$m_A=1 \tag{3-60}$$

Thus from (3-54) it can be obtained that:

$$m_\sigma=1 \tag{3-61}$$

Substituting (3-61) into (3-56) it can be assumed that:

$$m_V/m_z=1 \tag{3-62}$$

and

(3-63) $$m_V = m_z$$

The time domain shoud be the same as original thus it can be assumed:

(3-64) $$m_t = 1$$

Because there is no change of geometry in the Z direction, the Z direction factor is equal to 1 and it can be derived that electrical voltage factor should also be equal to 1.

Finally, the equation (3-39) can be written as:

(3-65) $$-\frac{1}{\mu_{1x}} \cdot \frac{d^2 A_{1z}}{dx_1^{\,2}} - \frac{m_y^2}{\mu_{1y}} \cdot \frac{d^2 A_{1z}}{dy_1^{\,2}} = -\sigma_1 \frac{dA_{1z}}{dt} + J_{1src} - \sigma_1 \frac{dV_1}{dz_1}$$

The equation (3-65) can be implemented in the hybrid model. It can be done by introducing the anisotropy of magnetic permeability of the material and divide the Y-value of magnetic permeability by square of scale factor value.

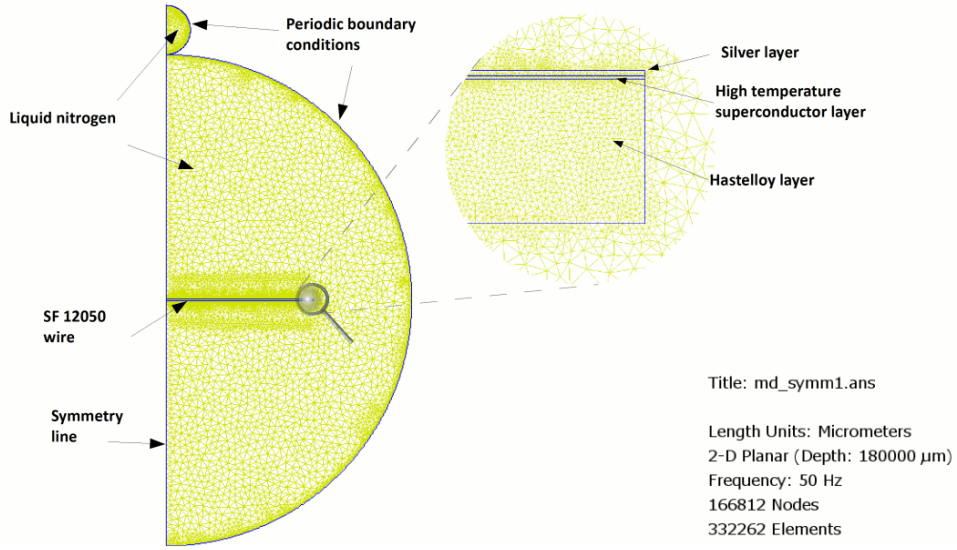

Fig. 3.34. Geometry and boundary conditions of magnetics model of SF12050 wire (in scale)

Constructed transient magnetics model of SF12050 wire contains superconducting wire and liquid nitrogen region. Because of symmetry of the model along 0Y line, only the half of the wire was modelled. The wire was cooled with liquid nitrogen bath and the infinity region was applied (Fig. 3.34).

Modelling of infinity region is done by adding the area outside the main geometry with imposed periodic boundary condition type (additional semicircle

above main geometry in Fig. 3.34). This type of boundary condition must also be imposed on the edge of the main area of modelling. The geometry of the SF12050 wire is set according to the manufacturer specification and the scale of the wire has been preserved [144].

The SF12050 wire consists of three layers of materials: hastelloy, high temperature superconductor and silver shown in magnification in Fig. 3.34.

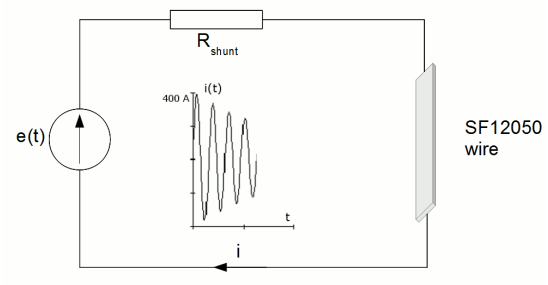

Fig. 3.35. Circuit connected with the magnetic model

Transient magnetic model is coupled with circuit one, as shown in Fig. 3.35. The current in the circuit is set to sinusoidal one, with amplitude decreasing exponentially from 400 A to 200 A.

The change in current amplitude was simulated (taking into account changes in resitance of SF12050 wire) to reflect the curve of the current recorded during the measurement experiment described in section 4.2.

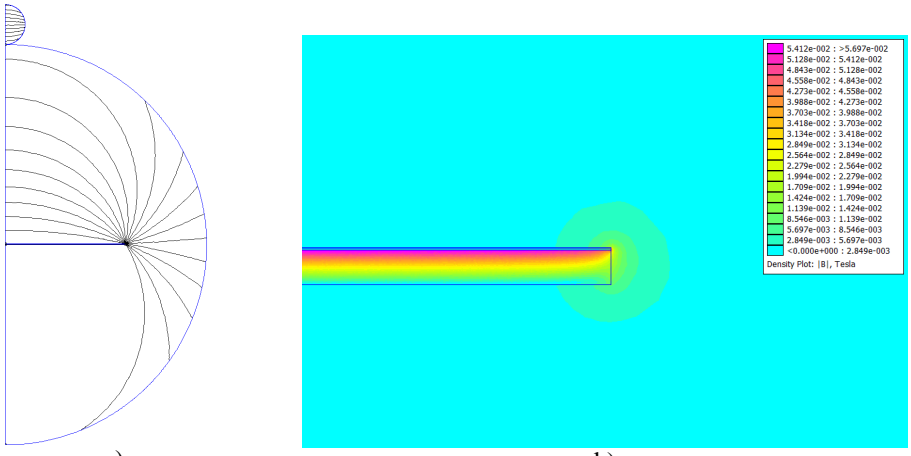

a) b)

Fig. 3.36. Magnetic field distribution before the quench in the HTS wire model:
a) field lines b) flux density at the edge of the wire

Additional AC losses generated in segments of wire, according to the hybrid model algorithm, were saved and implemented as heat sources in the heat transfer problem. Calculation results of hybrid model allow for determination of values, which are in fact non-measurable or difficult to measure (i.e. flux density distribution, current density distribution). The magnetic field distribution in the SF12050 wire model in the moment before the quench is shown in Fig. 3.36.

During normal work of the tape (i.e. superconducting state) the magnetic shielding effect can be observed and the magnetic field penetrates the areas around the superconducting layer.

After the quench, when parts of the superconductor layer go into the resistive state, the magnetic field starts to partially penetrate the HTS wire. The magnitude of the magnetic field density decreases due the decreasing magnitude of transport current. Distribution of the magnetic field in the moment after the quench is shown in Fig. 3.37.

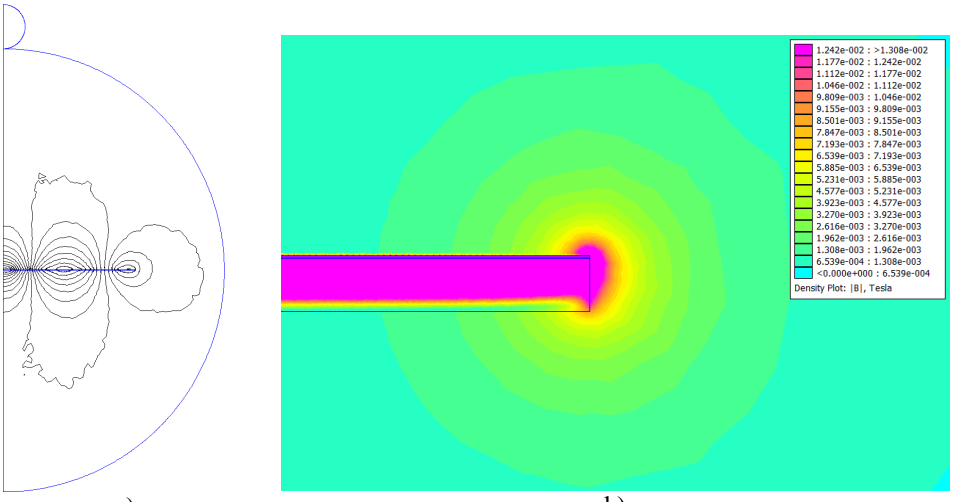

a) b)

Fig. 3.37. Magnetic field distribution after the quench in the HTS wire model: a) field lines b) flux density at the edge of the wire

Almost all current flows through the superconducting layer in the superconducting state (Fig. 3.38 a). After the quench, in the areas where the superconductor loses its superconductivity, the current starts to flow through the silver layer (Fig. 3.38 b).

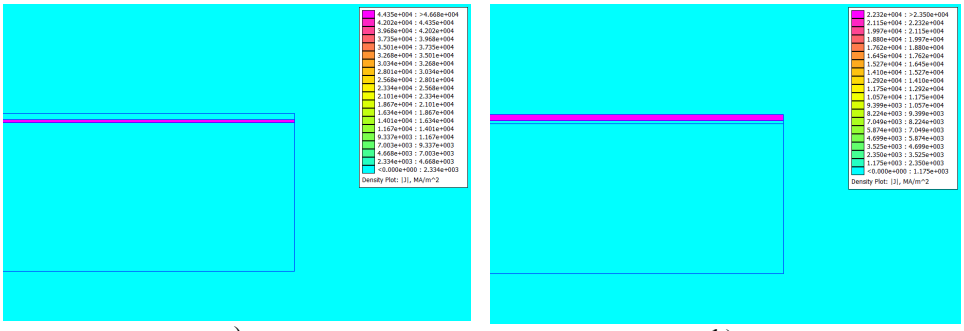

a) b)

Fig. 3.38. Current density distribution: a) before the quench b) after the quench

Calculation results of magnetic part of hybrid model allow for determination of the changes of flux density in time. The analysis point was located at the end of the wire, near the YBCO layer, where the magnetic flux density reaches the highest values (Fig. 3.39).

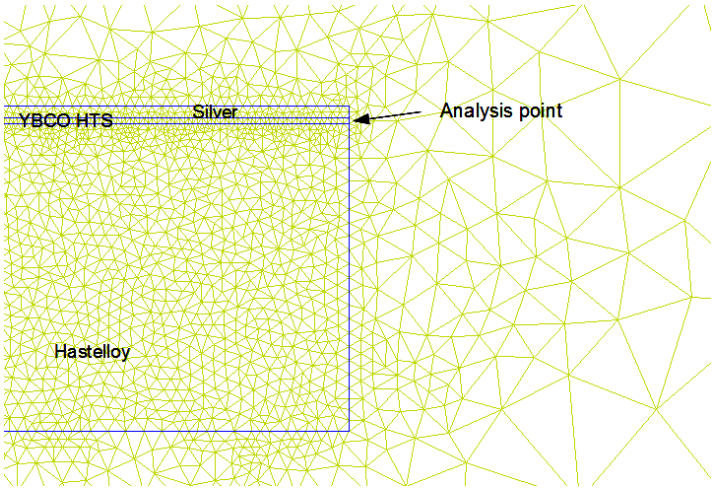

Fig. 3.39. Analysis point located at the right end of the wire

Flux density during quench decreases exponentially (Fig. 3.40). The maximum value of flux density drops in the first period (20 ms) almost twice. However, the maximum reach value (about 48 mT) is too low to significantly decrease the critical current. In the case of YBCO high temperature coated superconductors, such a small flux density value almost does not alter the critical temperature value and critical current value [90, 145, 154, 163].

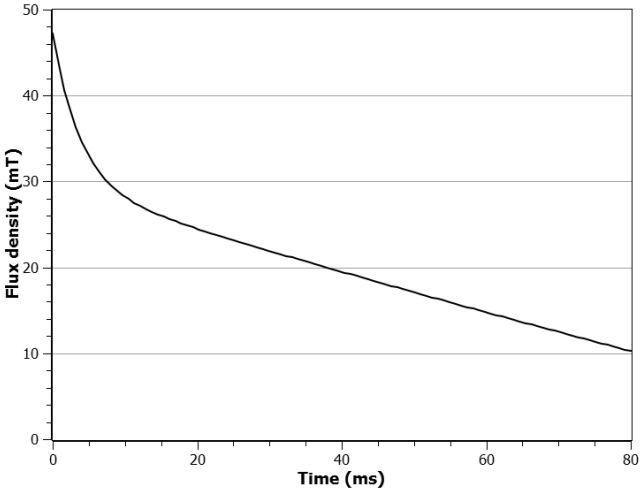

Fig. 3.40. Peak value of magnetic flux density versus time in the analysis point

The heat transfer problem is solved as the last one in one calculation loop of the hybrid model of SF12050 wire. The geometry, material properties and boundary conditions of the heat transfer model are shown in Fig. 3.41. The geometry is analogous to the current flow problem, but the abscissa dimensions are multiplied by the scale factor m_h=100. Because of applied scaling law, as described above in equations (3-8) to (3-32), the anisotropy of the heat conductivity of each layer of the modelled SF12050 wire was implemented in external software SF1250ANISOTROPY.LUA (Appendix A page 156). At every step of the simulation, properties of the materials change due to the change of temperature and are set in the model.

In the areas, where the wire is fitted with the copper connectors, the boundary conditions are set to constant temperature of 77 K (upper and lower lines of the model in Fig. 3.41). At the surfaces where the HTS wire is cooled with liquid nitrogen, the nonlinear change of heat flux is assumed (boundary conditions $\boldsymbol{q}_D$ and $\boldsymbol{q}_T$) according to dependence shown in Fig. 3.2. Change of boundary conditions due to the temperature change and different cooling conditions was implemented in written software LN2cooling.LUA (Appendix A page 159).

During the quench caused by current exceeding the critical value, when some segments of the wire go from the superconducting state to the resistivity state, additional power losses are generated in those segments. These losses are then transformed into Joule heat. It can be assumed that in each segment and layer of the HTS wire model, Joule heat is represented by volumetric heat sources. These volumetric heat sources are the excitations in the thermal part of SF12050 wire hybrid model.

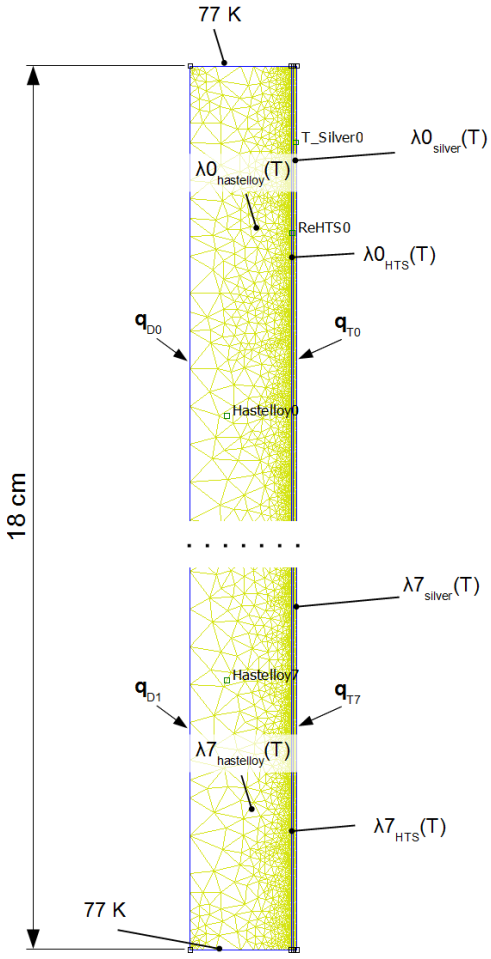

Fig. 3.41. Heat flow model geometry and parameters, abscissa dimensions multiplied by factor m_h

Solution of the hybrid model in transients gives the information on the parameters which are very difficult to measure or are not measurable at all.

Temperature is one of such parameters. In transient states, it can be measured indirectly, which was described in detail in section 4. Determination of the temperature distribution in the wire cannot, however, be made directly due to small thickness of wire (about 53 μm) and its cooling in liquid nitrogen bath.

In that case, FEM modelling is very useful for determining the temperature distribution. Proposed hybrid model of thin layer high temperature superconducting wire allows for calculation of temperature distribution in transients. Changes of temperature in the segment which loses its superconductivity are shown in Fig. 3.42.

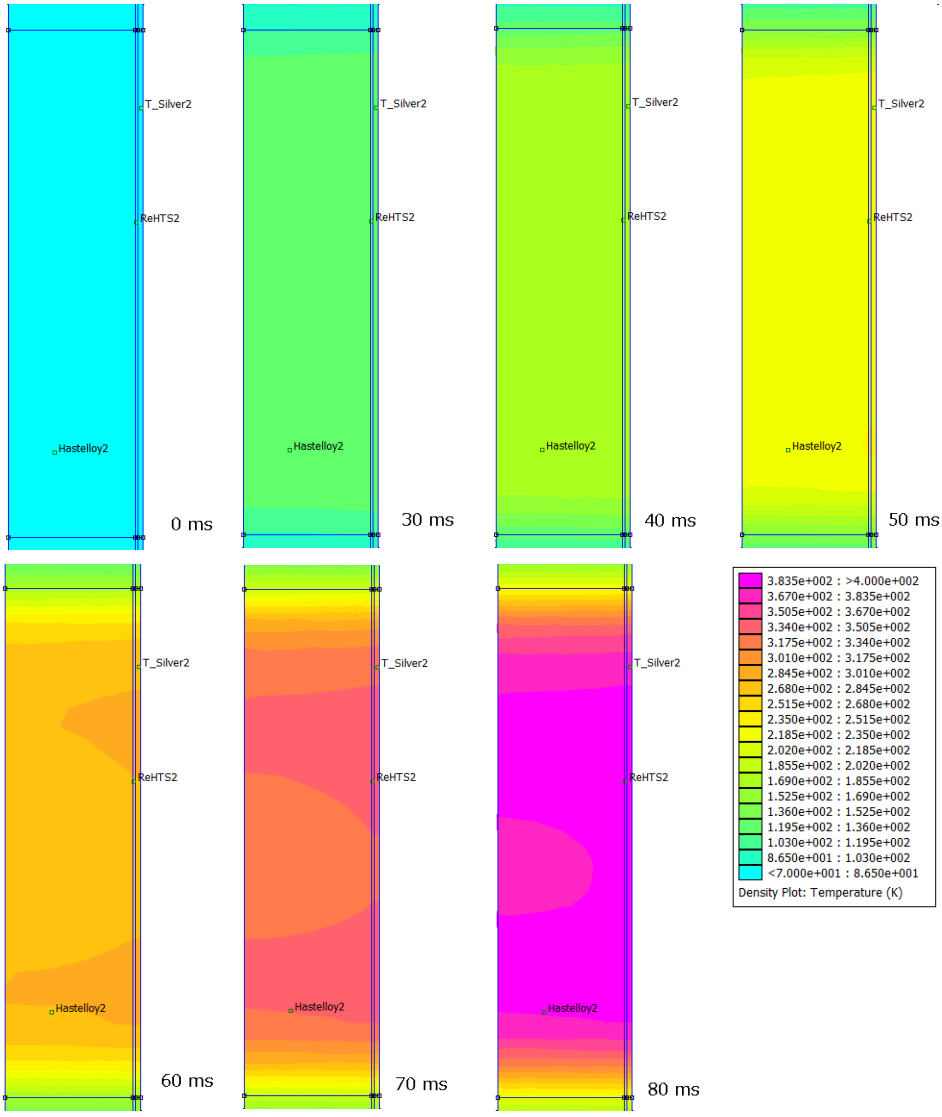

Fig. 3.42. Changes of temperature distribution in segment of SF12050 wire model in subsequent time steps

It can be observed that the higher temperature zone is rapidly expanding from the HTS layer to the silver layer and a little bit slower to the hastelloy layer. After 80 ms from the quench, the temperature rises to about 370 K. Obtained hybrid model results allow for determination of the temperature rise in time, in the segment 2 of the wire. The temperature change of segment 2 of the SF12050

wire was measured as described in section 1 of this work The measured and approximated curves for the quench caused by current with peak value equal to 400 A are shown in Fig. 3.43.

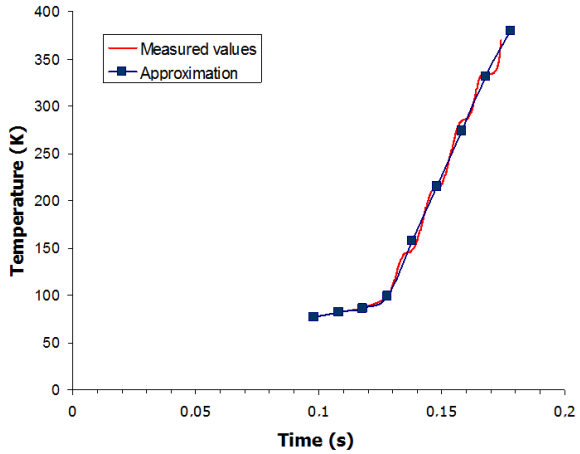

Fig. 3.43. Measured and approximated values of temperature in segment 2 of the SF12050 wire

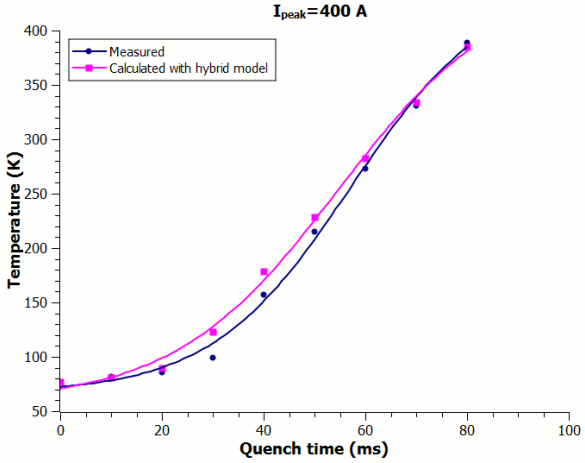

Fig. 3.44. Comparison of temperature changes in segment 2 of SF12050 wire

The results measured during quench were compared with calculated ones and the results are shown in Fig. 3.44. The accuracy of the results of the scale factor model comparing with actual measurements was assessed with the Pearson correlation coefficient and relative error – both presented in Table 3.6.

Table 3.6 Measurement and hybrid model result comparison

Description	Value
Pearson correlation coefficient	0.9966
Minimum relative error	0 %
Maximum relative error	23.5 %
Average relative error	6.05 %

Correlation coefficient value is close to 1, therefore very strong correlation between compared curves can be assumed. Maximum relative error between measured and calculated values occurred after 30 ms from quench beginning, and is equal to about 23 %. Average relative error is not high and equal to about 6 %, therefore very good agreement between hybrid model results and measurement results can be assumed.

The hybrid model of the SF12050 tape additionally was compared with the 2D tape model built in COMSOL environment.

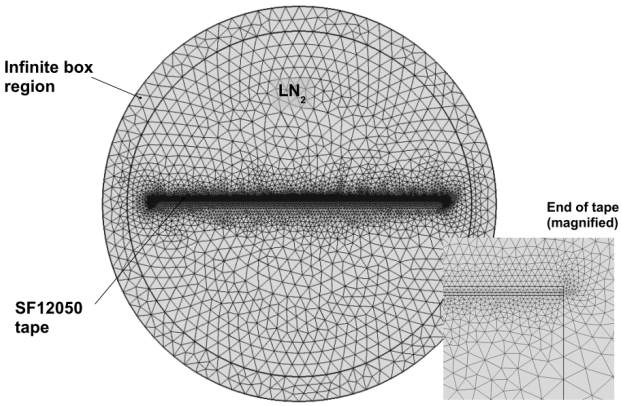

Fig. 3.45. Model of SF12050 tape elaborated in COMSOL environment

Model built in COMSOL environment consists of: infinite box region (which properly reflects the infinite area), liguid nitrogen area (LN_2), and SF12050 tape (structure analogous like in hybrid model) Fig. 3.45.

In the model the coupling of three problems i.e. magnetic field (mf), heat transfer (ht) and elactrical circuit (cir) were implemented. Such complex calculation task required the efficient computing platform. The platform was built basing on the grid computing architecture. The structure and the performance of the computing cluster built by the author was described in [40] and together with coauthors in [41].

For COMSOL environment the Linux cluster was set up according the specification of the COMSOL manufacturer [30]. In hybrid model and

COMSOL model the SF12050 tape was supplied with AC current with beginning amplitude equal to 380 A (same as in measurements). After the quench, when the superconducting tape goes to the resisitivity state, the magnetic field starts to penetrate the tape interior. The results of the flux density distribution in both models are shown in Fig. 3.46.

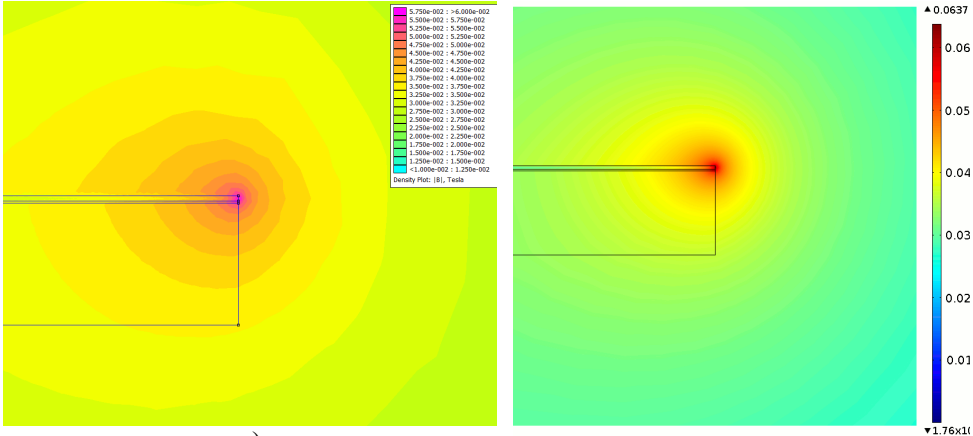

Fig. 3.46. Comparison of flux density distribution of SF12050 tape model: a) hybrid, b) COMSOL (values given in Teslas, defined the same range values)

The distribution in both models is the same however the maximum value of the flux density is slightly different. Thus the estimation of the discretisation error has been done. Using Richardson extrapolation method the more exact solution is defined as k_{ex} and two solutions with different discretisations (k_o, k_p) of the same problem are known [9, 43, 62, 63]. Both solutions only differ in their meshe's triangle step size. The second solution uses the mesh where the elements are linearly twice time less than first one. The exact solution value can be written as:

$$k_{ex} = k_p - \frac{k_o - k_p}{1 - \left(\frac{p}{o}\right)^r} \tag{3-66}$$

where: k_{ex} – exact solution, k_o – solution with initial mesh step size, k_p – solution with higher order mesh step size, o – initial mesh step size, p – higher order mesh step size, r – order of error which depends on convergence.

Assuming pessimistically $r = 1$, the error is overestimated, but this assumption gives the safe top estimation. The relationship of o and p dimensions are equal to 2 and the nominative case is simply becoming equal to one.

Therefore it can be written:

(3-67) $$k_{ex} - k_p \le k_p - k_o$$

Knowing the exact solution, it is possible to estimate the discretization error made during the calculations with hybrid model. The exact solution can be obtained analytically, hovewer because of the HTS tape geometry it will be very difficult. Another way is the use the calculation software with much better accuracy. COMSOL is computing environment with such capabilities [16, 61, 63, 151].

Maxium value of the magnetic flux density at the edge of the SF12050 tape calculated in COMSOL was equal to 63.16 mT. Using the hybrid model the values of magnetic flux density were equal respectively: to 57.394 mT – for model with initial mesh step size and to 60.454 mT – for model with the mesh where the elements are linearly twice time less than first one. Thus in can be written:

(3-68) $$k_{ex} = 63.16 \text{ mT};\ k_o = 57.394 \text{ mT};\ k_p = 60.454 \text{ mT}$$

and finally substituting these values to (3-67) for identitiy checking

(3-69) $$2.706 \le 3.06$$

Because the identity is satisfied there is no need to made more dense mesh and the upper estimation of the flux density value can be calculated in (3-70).

(3-70) $$B_{upper} = 60.454 \text{ mT} + 3.06 \text{ mT} = 63.514 \text{ mT}$$

Without nowing the exact solution it can be assumed that the value of flux density is equal to 62 mT ± 2.5%. The error estimation of hybrid model of SF12050 tape of magnetic and other solutions is shown in Table 3.7.

Table 3.7 Estimated discretization error values of hybrid model

Description of problem	Estimated error [%]
Magnetic	2.5
Heat transfer	3
Current flow	1.8

It can be concluded, on the basis of obtained calculation results, that the maxium discretization error of hybrid model is equal to 3 percent.

3.5. Modelling of the current lead built of bulk high temperature superconductor in transient states

The hybrid model contains the aspects of current flow, heat transfer and the effect of magnetic field on current lead work. The modelled current lead is a commercial product available from Can Superconductors and the type of the

lead is CSL-12/120.2. This current lead is built of superconducting tube of BiPbSrCaCuO (Bi-2223 phase) ceramics with silver covered ends of low contact resistance. The HTS tube is fitted in the protective case made from a metal of low thermal conductivity. The case is made of a CuNi tube and the ceramic HTS tube is extended by power leads from a flat braided copper cable [19].

Table 3.8 Parameters of the commercially available CSL current leads [19]

	Dimensions				Critical current (higher than)		Approx. critical current[1] (77 K) at longitudinal[2] magnetic field			Conductive heat leak per pair between temperatures[3]	
Type	Outer dia.	Length	Cross-section area	Silver contact lenght	at 77 K	at 64 K	25 mT	50 mT	100 mT	77 K - 4 K	64 K - 4 K
CSL-5/70.1	5 mm	70 mm	7 mm^2	10 mm	35 A	70 A	12 A	8 A	5 A	0.04 W	0.02 W
CSL-5/70.2	5 mm	70 mm	7 mm^2	10 mm	60 A	120 A	20 A	13 A	8 A	0.04 W	0.02 W
CSL-7/70.1	6.6 mm	70 mm	14 mm^2	10 mm	60 A	120 A	20 A	13 A	8 A	0.08 W	0.05 W
CSL-7/70.2	6.6 mm	70 mm	14 mm^2	10 mm	100 A	200 A	33 A	20 A	13 A	0.08 W	0.05 W
CSL-7/120.1	6.6 mm	120 mm	14 mm^2	10 mm	60 A	120 A	20 A	13 A	8 A	0.04 W	0.02 W
CSL-7/120.2	6.6 mm	120 mm	14 mm^2	10 mm	100 A	200 A	33 A	20 A	13 A	0.04 W	0.02 W
CSL-10/80.1	9.6 mm	80 mm	22 mm^2	10 mm	100 A	200 A	30 A	20 A	0	0.10 W	0.07 W
CSL-10/80.2	9.6 mm	80 mm	22 mm^2	10 mm	170 A	340 A	50 A	30 A	20 A	0.10 W	0.07 W
CSL-12/80.1	12.0 mm	80 mm	34 mm^2	12 mm	150 A	300 A	50 A	33 A	20 A	0.17 W	0.12 W
CSL-12/80.2	12.0 mm	80 mm	34 mm^2	12 mm	250 A	500 A	90 A	50 A	33 A	0.17 W	0.12 W
CSL-12/80.3	12.0 mm	80 mm	34 mm^2	12 mm	370 A	740 A	180 A	110 A	70 A	0.17 W	0.12 W
CSL-12/120.1	12.0 mm	120 mm	34 mm^2	12 mm	150 A	300 A	50 A	33 A	20 A	0.10 W	0.07 W
CSL-12/120.2	12.0 mm	120 mm	34 mm^2	12 mm	250 A	500 A	90 A	50 A	33 A	0.10 W	0.07 W
CSL-12/120.3	12.0 mm	120 mm	34 mm^2	12 mm	370 A	740 A	180 A	110 A	70 A	0.10 W	0.07 W
CSL-12/160.1	12.0 mm	160 mm	34 mm^2	12 mm	150 A	300 A	50 A	33 A	20 A	0.07 W	0.05 W
CSL-12/160.2	12.0 mm	160 mm	34 mm^2	12 mm	250 A	500 A	90 A	50 A	33 A	0.07 W	0.05 W
CSL-12/160.3	12.0 mm	160 mm	34 mm^2	12 mm	370 A	740 A	180 A	110 A	70 A	0.07 W	0.05 W
CSL-18/80.1	18.0 mm	80 mm	78 mm^2	15 mm	300 A	600 A	120 A	80 A	50 A	0.40 W	0.30 W
CSL-18/80.2	18.0 mm	80 mm	78 mm^2	15 mm	450 A	900 A	200 A	120 A	80 A	0.40 W	0.30 W
CSL-18/80.3	18.0 mm	80 mm	78 mm^2	15 mm	750 A	1500 A	430 A	300 A	190 A	0.40 W	0.30 W
CSL-18/120.1	18.0 mm	120 mm	78 mm^2	15 mm	300 A	600 A	120 A	80 A	50 A	0.20 W	0.16 W

[1] Values at 64 K and at double magnetic field are twice higher than the values at 77 K.
[2] Respective values at transversal magnetic field are lower by apporx. 20 %.
[3] Values without vapor cooling; if cooled in vapor the values are substantially lower.

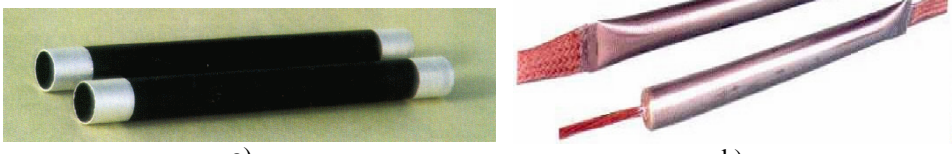

a) b)

Fig. 3.47. High temperature superconducting current leads produced by CAN Superconductors a) Bi 2223 tube b) tube fitted in CuNi case

The geometry of the CSL-12/120.2 current lead model is shown in Fig. 3.48. The model is built in axisymmetrical geometry and the copper braided cables are simplified as tube copper connectors (Fig. 3.48 a).

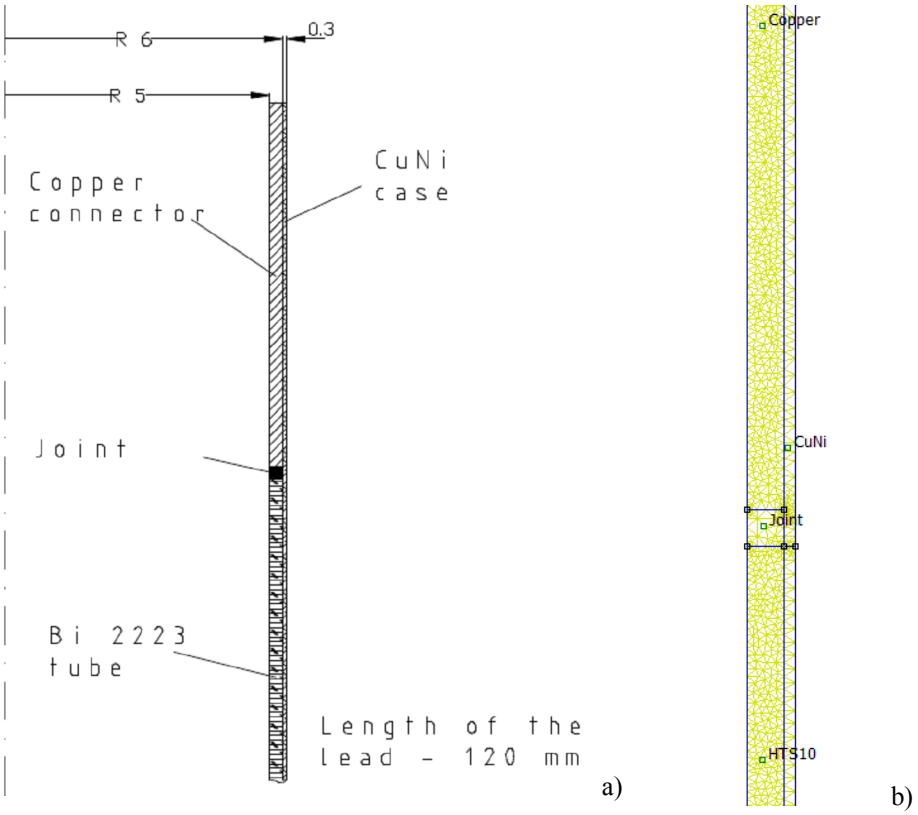

Fig. 3.48. Geometry of the modelled current lead: a) dimensions and materials b) magnification of FEM model with generated mesh in the junction of HTS tube with copper

Joint resistance was simulated as additional material which connects copper in series with high superconducting material. Constructed hybrid model allows for researching of the coupling circuit, as well as thermal and magnetic field problems. Properties of materials used for HTS current lead building depend nonlinearly on the temperature and, in the case of high temperature superconductor, also on the value of the flowing current and magnetic flux density.

Verification of the model was performed by comparing the results obtained in the measurement experiment carried out by Plechacek and Hejtmanek in [119] and the computational experiment results.

In the measurement experiment the HTS current lead fitted in CuNi tube was immersed in liquid nitrogen bath and supplied with current of different values.

The voltage was measured on the whole length of the current lead including ceramic tube and hidden part of the copper cable (approx. 6 cm) and parallel connected CuNi tube. The critical current of value 234 A was determined from

the extrapolated linear part of the *V-I* characteristic under criterion of 100 μV/cm. The voltage versus current characteristic of the encased tube, measured at 77 K, is shown in Fig. 3.49. [119]

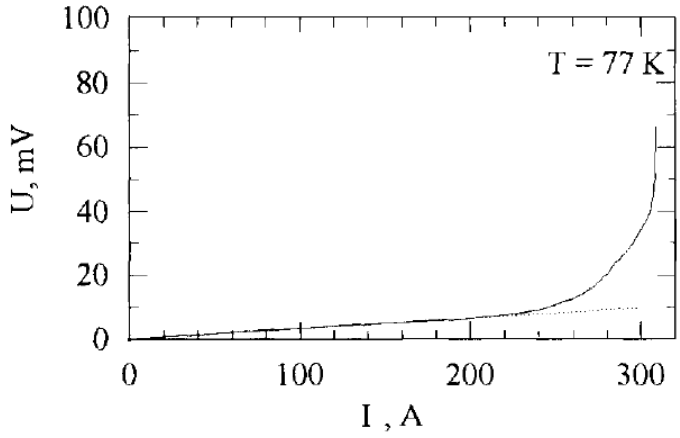

Fig. 3.49. *V-I* characteristic of encased CSL-12/120.2 superconducting lead [119]

Hybrid model of HTS current lead consists of three coupled sub-problems. First one is a heat transfer problem, where the nonlinear changes of thermal conductivity of the materials and inhomogeneous cooling in liquid nitrogen bath were assumed. Second one is a current flow problem, where nonlinear electrical conductivity, which depends on the temperature in the case of copper and CuNi alloy. The electrical conductivity of Bi 2223 was modelled as nonlinear function of the current density and electric field intensity. In the case of high temperature superconductors, current density also depends on magnetic flux density. The electrical conductivity of high temperature superconductor is given by equation:

$$\delta(E,B) = \frac{J_c(B)}{E_c^{\frac{1}{n}}} \cdot |E|^{\left(\frac{1-n}{n}\right)}$$

where:

δ – electrical conductivity,

J_c – value of critical current density,

E_c – value of critical electric field intensity,

n – power factor which depends on the high temperature superconductor material.

Last one is magnetic field problem, where the materials parameters also depend on the temperature, and in the case of high temperature superconductor additionally on flux density and current density.

For verification of the hybrid model, the voltage current characteristic of CSL-12/120.2 lead was calculated and compared with the measured result. Summary of the two characteristics is shown in Fig. 3.50.

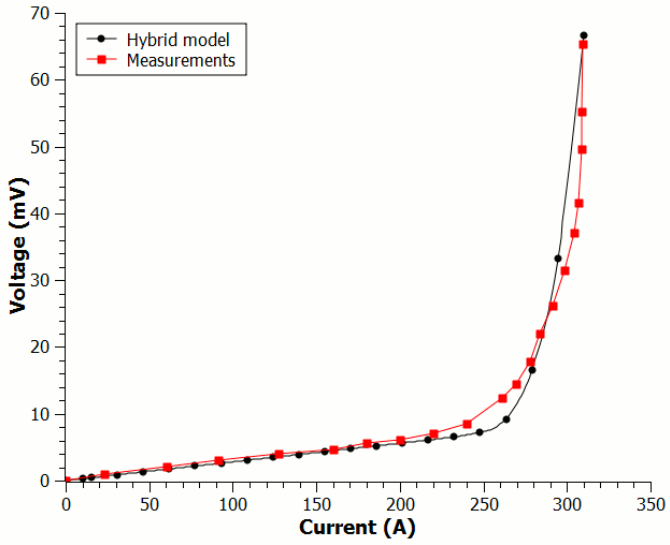

Fig. 3.50. Comparison of measured and calculated *V-I* characteristic of encased CSL-12/120.2 superconducting lead

Comparing the characteristics of both waveforms, it can be concluded that the hybrid model of current lead has a significant level of comparability with the real object.

Table 3.9 Comparison of the measured *V-I* curve with the curve calculated by the hybrid model

Description	Value
Pearson correlation coefficient	0.9957
Minimum relative error	1.11 %
Maximum relative error	28 %
Average relative error	13.1 %

Pearson correlation coefficient and relative error were calculated for both waveforms (Table 3.9). Correlation coefficient value is close to one, thus there is very strong correlation between the actual measurement and hybrid model results. Average relative error is about 13 %. Taking above into consideration it can be concluded that proposed hybrid model of the superconducting lead reflects the phenomena occurring in the real object with high accuracy.

Two cases of current lead cooling, using proposed hybrid model, have been analyzed. First one was contact cooling with cryocooler, with the temperature of the lower stage equal to 4 K and upper stage equal to 77 K, and the second one the cooling in liquid nitrogen bath (boiling point of liquid nitrogen, approximately 77 K). The idea of the model and cooling concepts is shown in Fig. 3.51.

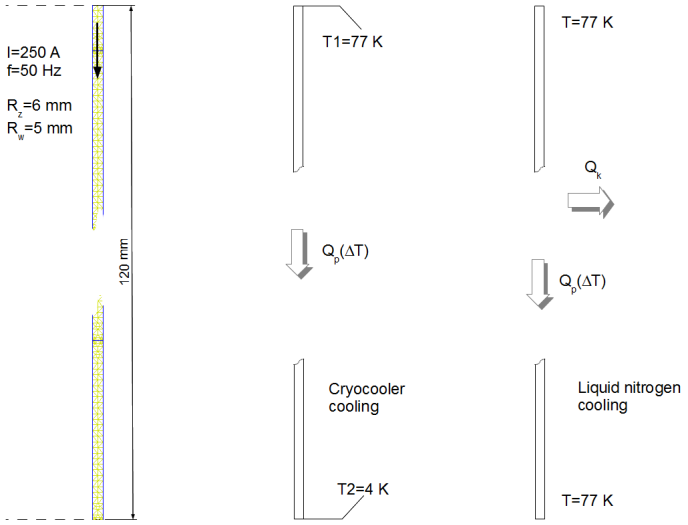

Fig. 3.51. Idea of different type of cooling in hybrid superconducting current lead model

On the contact cooling, where the current lead was cooled with liquid nitrogen, it is assumed that the current lead is in a vacuum cryostat and heat transfer takes place only by conduction.

Non-linear dependence of heat exchange is incorporated at the interface between surface of the liquid nitrogen-current lead according to the temperature difference and the flow of heat by conduction.

Developed computational models made it possible to conduct a series of simulations of the current lead. Velocity of resistive zone spreading for both cooling instances was analyzed. Calculations were carried out on the assumption of a disturbance in the bottom part of the current lead. The time in which the temperature inside the lead exceeds the critical temperature superconductor BSCCO was analyzed. In this case, the value of critical temperature was 107 K.

The temperature changes at the transition of lower part of lead from the superconducting state to resistive state are shown in Fig. 3.52. Superconductor resistivity increases at this point about 10^{20} times and this generates the additional losses which are converted into Joule's heat. This is directly reflected in the local increase of temperature in the current lead.

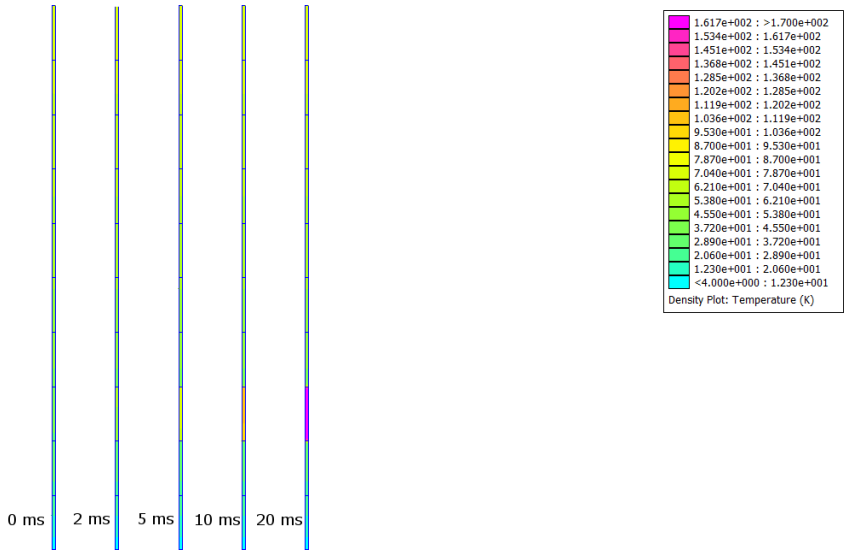

Fig. 3.52. Map of temperature distribution in the current lead model in a state of transition (contact cooling with cryocooler)

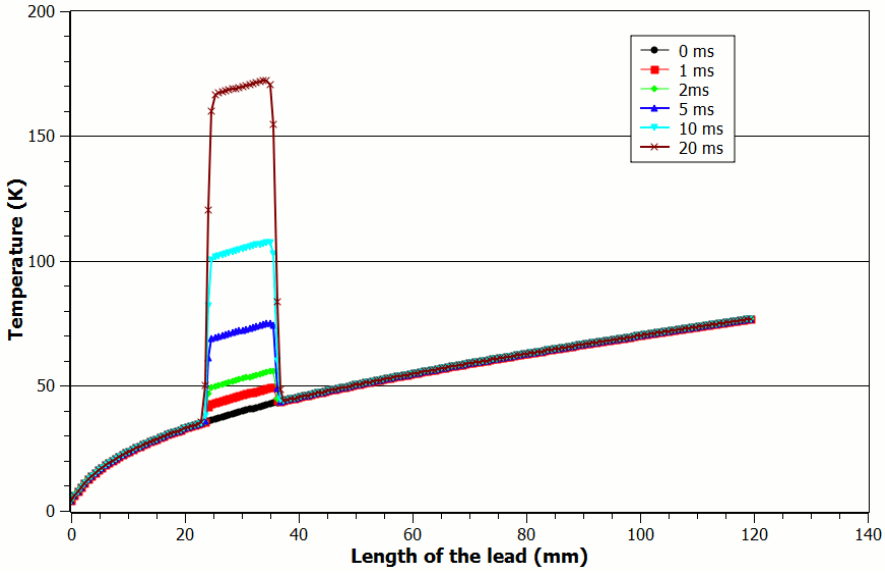

Fig. 3.53. Temperature distribution on the surface of the current lead cooled with cryocoolers; calculations performed at time increments subsequent to quench

Fig. 3.53 shows the temperature distribution on the outer surface of current lead cooled with cryocoolers occurring after the quench. A similar analysis was

carried out for the cooling of the current lead in liquid nitrogen bath and the results are shown in Fig. 3.54. Analyzing the distribution of temperature in successive time steps it can be seen that a local increase in temperature of about 130 K occurs in both cases after 20 ms.

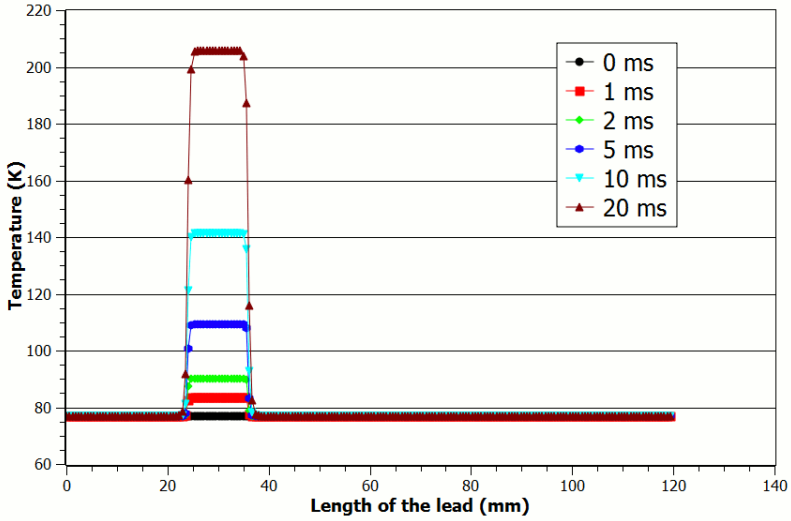

Fig. 3.54. Temperature distribution on the surface of the current lead, cooled in liquid nitrogen bath; calculations performed at time increments subsequent to quench

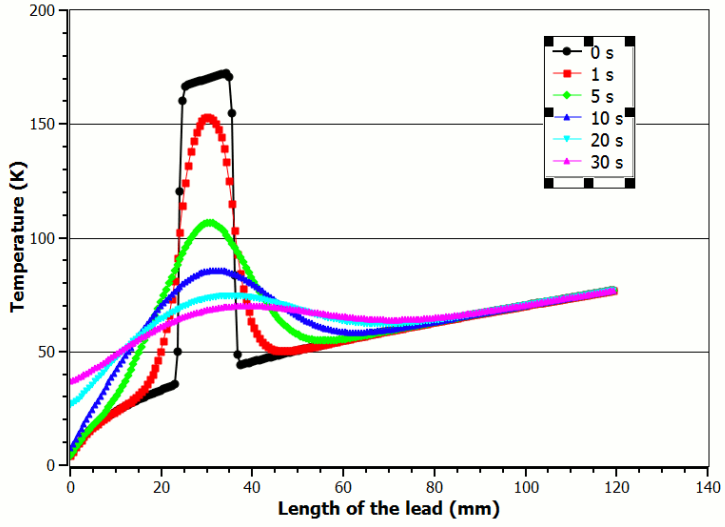

Fig. 3.55. Temperature distribution on the surface of the current lead, cooled with cryocoolers; calculations performed at time increments subsequent to quench cessation

For cooling with cryocooler, the temperature rises above the critical value after the time equal to 10 ms in the area of quench. In case of cooling in liquid nitrogen bath, the temperature rises above the critical value after the time equal to 5 ms on the loss of the superconductivity state in lower part of current lead. This time is shorter due to higher initial temperature of the current lead before the quench.

Another computational experiment was carried out for the current lead returning to a steady state after disturbance cessation. Temperature distribution on the surface of current lead is shown in Fig. 3.55 and Fig. 3.56 for the two types of cooling.

Analyzing temperature distribution subsequent to the quench for the contact cooling, it can be observed that the temperature on the surface of the current lead falls below a critical value after about 6 seconds. This is not a sufficient condition to ensure that the device can be switched on again, especially when taking into account the fact that the temperature of the lower part of the current lead rises much above 4 K (up to about 40 K).

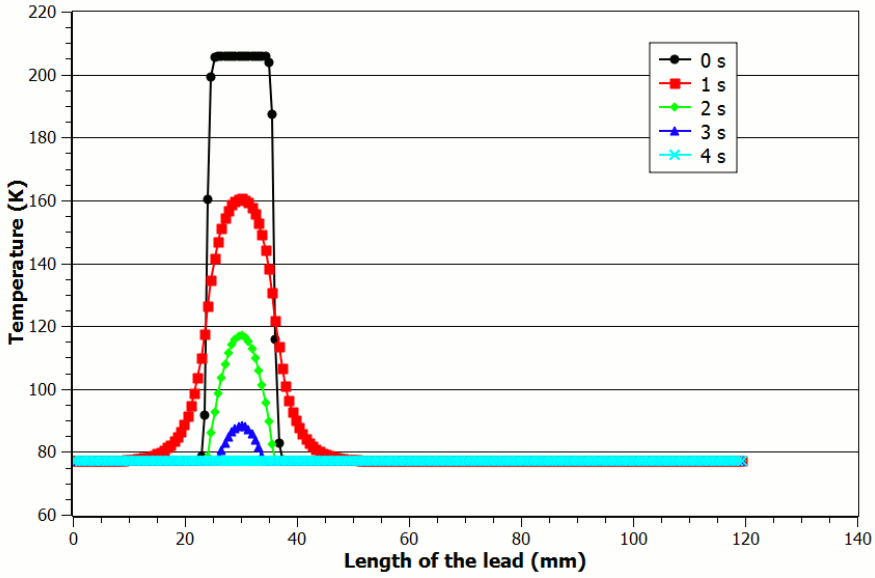

Fig. 3.56. Temperature distribution on the surface of the current lead, cooled in liquid nitrogen; calculations performed at time increments subsequent to quench cessation

The temperature rise of the lower end of the HTS lead results in an increased need for heat removal. The efficiency of the lower stage of cryocooler is very low and amounts to about 1 W. Thus, the temperature of the current lead stabilizes after a longer period of time (over 1 minute).

In the case of cooling in liquid nitrogen bath, temperature distribution in the lead stabilizes much faster due to much better cooling conditions. The temperature is fixed in the whole HTS lead at the value of about 77 K after 4 seconds.

The speed of the resistive zone spreading has a very large impact on the stability of the superconducting devices regardless of the method of cooling. Times where the temperature rises above the critical value for the superconducting device reach several milliseconds. It is very important for stability of superconducting device to limit quench sources as soon as possible.

Second constructed model of CSL 12/120.2 consists of Bi 2223 tube, copper connectors and CuNi tube casing (Fig. 3.48). In this case, the experiment focused on examining the impact of CuNi casing on the stability of working conditions in transient state.

Comparison of the model's geometry of the CLS-12/120.2 current lead with casing and without it is shown in Fig. 3.57.

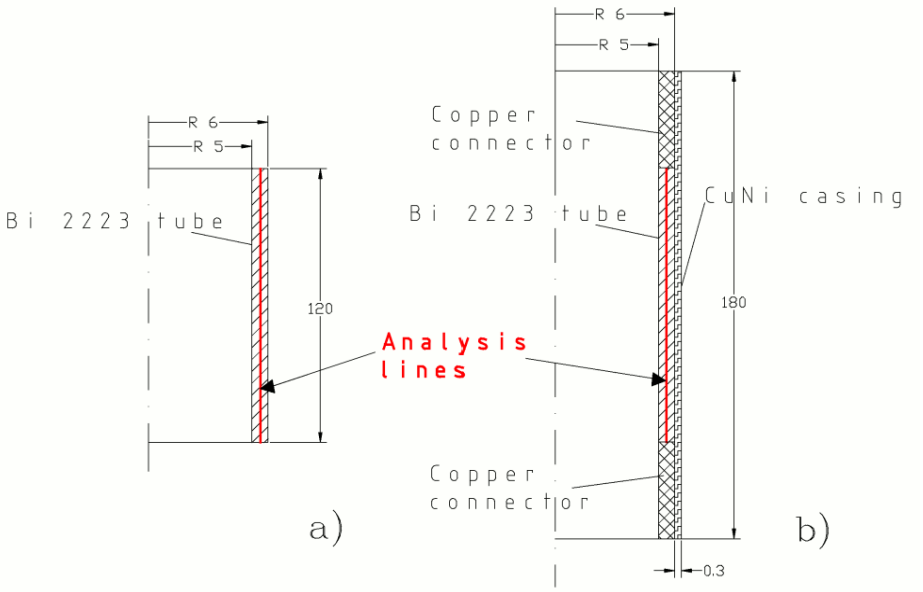

Fig. 3.57. Geometry of the CLS-12/120.2 current lead a) without and b) with CuNi casing

Similarly to the previous calculation experiment the two cases of cooling were considered: cooling with cryocooler and cooling in liquid nitrogen bath.

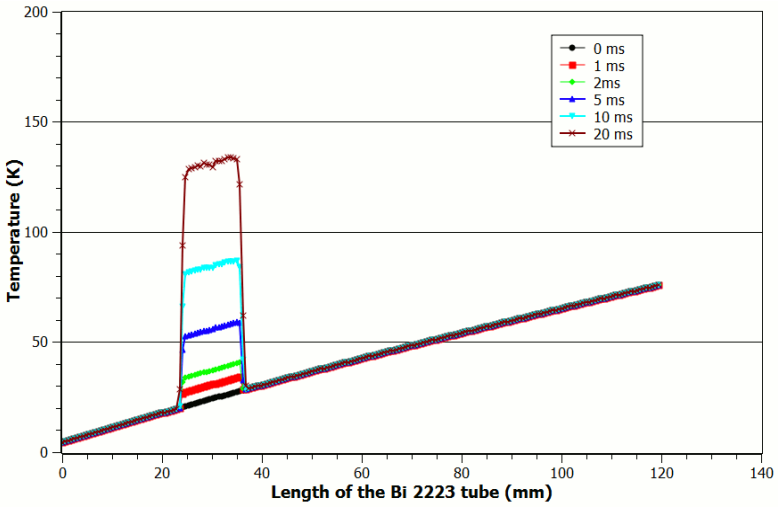

Fig. 3.58. Temperature distribution along analysis line of the current lead in CuNi casing cooled with cryocoolers; calculations performed at time increments subsequent to quench

The temperature distribution along the analysis line shown in Fig. 3.57 has been determined. In the case of contact cooling after the quench occurred, the temperature increased locally in 20 ms to the value of 140 K. The greatest difference between the temperatures established before the quench (about 20 K at 30 mm length) and 20 ms after the quench is 120 K (Fig. 3.58).

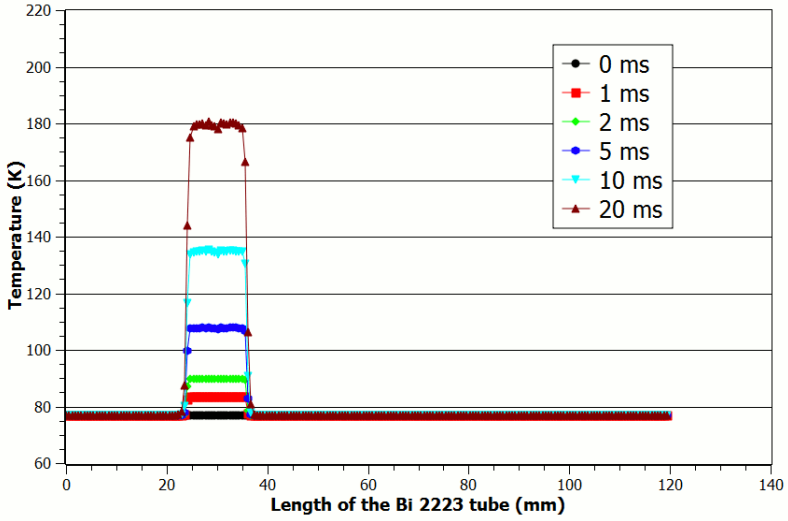

Fig. 3.59. Temperature distribution along analysis line of the current lead in CuNi casing, cooled in liquid nitrogen bath; calculations performed at time increments subsequent to quench

When the current lead is cooled in liquid nitrogen bath, the temperature rises locally to the value of 180 K. The greatest difference between the temperatures established before the quench (about 77 K at 30 mm length) and 20 ms after the quench is 103 K (Fig. 3.59). The increase in temperature value is lower by 14 percent comparing to contact cooling with cryocooler.

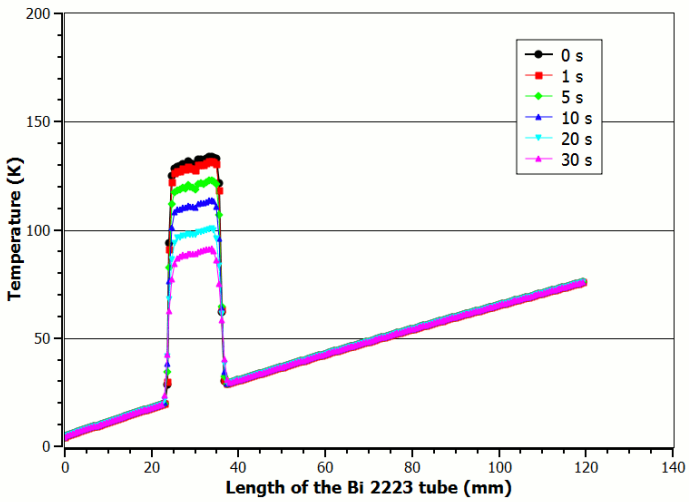

Fig. 3.60. Temperature distribution along analysis line of the current lead in CuNi casing, cooled with cryocoolers; calculations performed at time increments subsequent to quench cessation

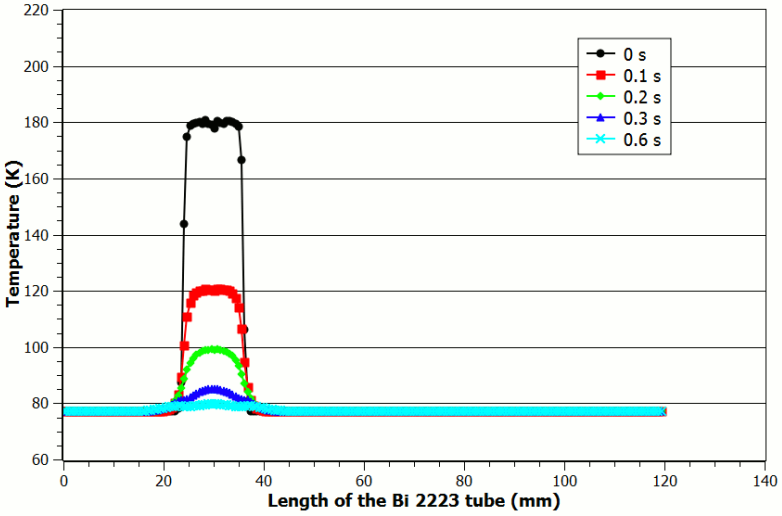

Fig. 3.61. Temperature distribution along analysis line of the current lead in CuNi casing, cooled in liquid nitrogen bath, calculations performed at time increments subsequent to quench cessation

Return to steady state after quench cessation was also considered in both cooling cases. The results of temperature distribution along analysis line are shown in Fig. 3.60 and Fig. 3.61. In the case of contact cooling with cryocooler, current lead with CuNi casing returns to the steady state after long time (about 4 minutes). When the HTS current lead is cooled in liquid nitrogen bath, temperature drops more rapidly, and the steady state is achieved after 0.6 seconds.

Comparison of the CSL-12/120.2 current lead model with and without the CuNi casing has been made. The most interesting element of superconducting devices from the point of view of work stability with increasing temperature is the fact that they have a spot, in which temperature rises more quickly.This "hottest" point is located about 35 mm from the lower part of HTS lead (see Fig. 3.53 and Fig. 3.58). The change of temperature in time was calculated for this point for both types of current leads.

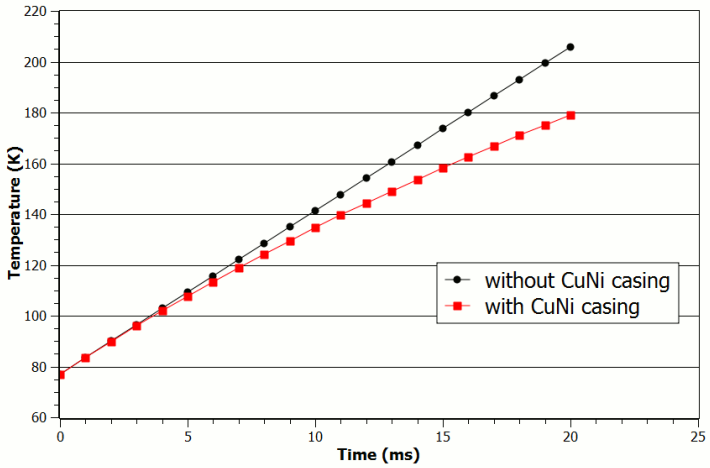

Fig. 3.62. Temperature versus time in the hottest point of CSL-12/120.2 current lead without and with CuNi casing, liquid nitrogen bath cooling (t=0 quench occurred)

When the current lead is cooled in liquid nitrogen bath, the temperature rises quickly after the quench. In the first 5 ms, the temperatures of both types of the HTS current leads are almost the same. After this time, the temperature of the HTS current lead without CuNi casing rises faster then that of the current lead with casing (Fig. 3.62). The temperature of the HTS current lead without CuNi case at the end of quench (t=20 ms) is higher by about 25 K, when compared to the encased current lead. After quench cessation (Fig. 3.63), there are no heat sources and temperature returns to the value of about 77 K. In the case of the HTS current lead with CuNi casing, this time is shorter and equal to 0.6 seconds.

In the current lead without the casing, the temperature returns to the established value after 4 seconds.

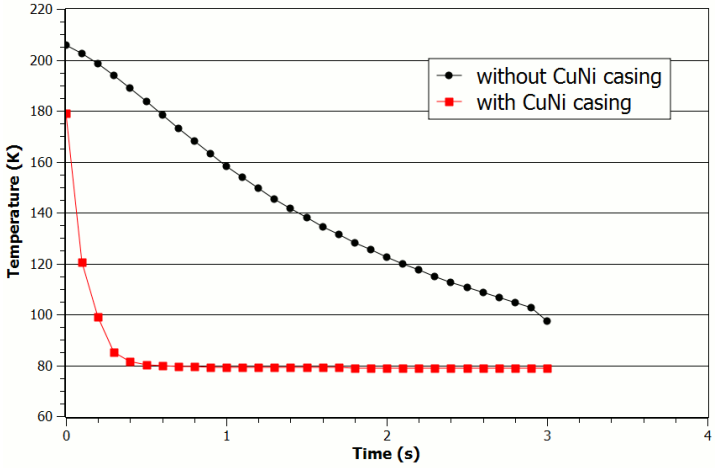

Fig. 3.63. Temperature versus time in the hottest point of CSL-12/120.2 current lead without and with CuNi casing, liquid nitrogen bath cooling (t=0 quench cessation)

It may by noted that the bulk HTS current lead in liquid nitrogen bath behaves quite differently, depending on the technical design. When the lead is in CuNi casing, the rise of temperature is slower and the return to the working temperature is faster (Fig. 3.62 and Fig. 3.63). This kind of solution offers better and more stable operation of HTS current lead.

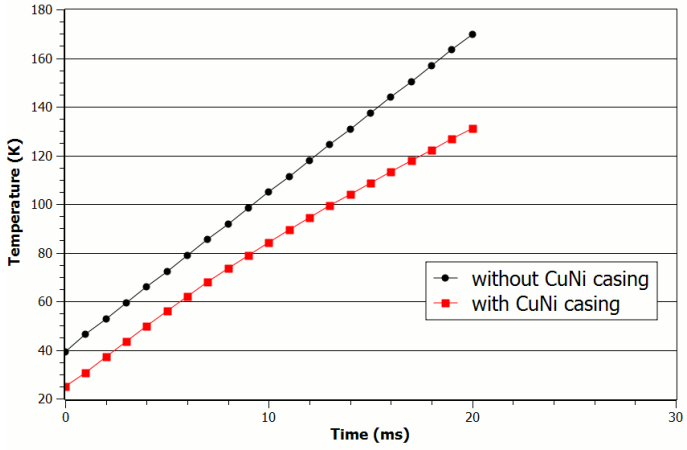

Fig. 3.64. The temperature versus time in the hottest point of CSL-12/120.2 current lead without and with CuNi casing, cryocooler cooling (t=0 quench occurred)

Different behaviours can be observed in contact cooling with cryocooler. The distribution of temperature along the analysis lines is different for both technical solutions (Fig. 3.53 and Fig. 3.58). For HTS lead in CuNi casing the temperature diagram is more linear and the temperatures are lower.

In the case of HTS current lead without the casing, temperature of the analysed point rises a little bit faster and reaches the value of about 170 K (Fig. 3.64). After quench cessation, the temperature drops below the critical value (107 K) quite quickly (about 6 seconds) as shown in Fig. 3.65.

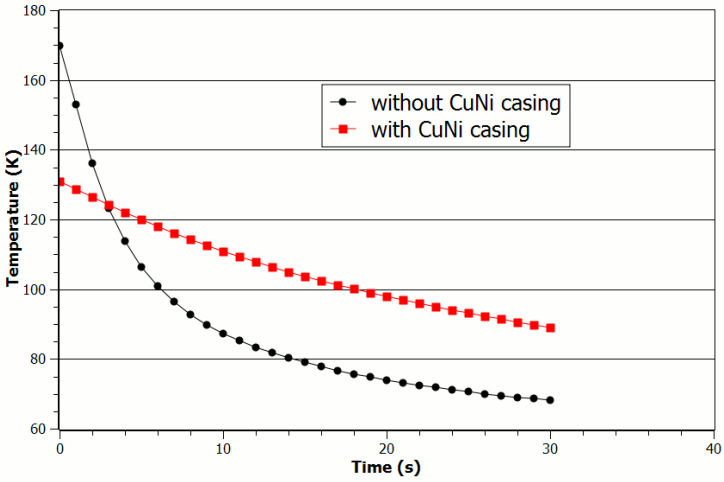

Fig. 3.65. Temperature versus time in the hottest point of CSL-12/120.2 current lead without and with CuNi casing, cryocooler cooling (t=0 quench cessation)

Different behaviour can be observed when current lead with CuNi casing returns to steady state after quench cessation. The time of temperature decrease to below critical value is about 16 seconds. It is almost three times longer than in the case of HTS lead without the CuNi thecasing. It is caused by different technical construction of current lead in the casing. Additional elements such as CuNi casing and copper connectors heat after quench and the total heat capacity of this solution is greater than that of the HTS lead without casing.

4. Measurements

For verification of the developed algorithms and models the measuring verification of the HTS tape was performed. The tape, produced by SuperPower, is the second generation high temperature superconductor thin layer tape. The HTS layer thickness in the SF12050 tape is 1 μm and the tape has high critical current value that ranges form 200 A to 300 A. The SF12050 tape has no copper stabilizers and its structure is shown in Fig. 4.1.

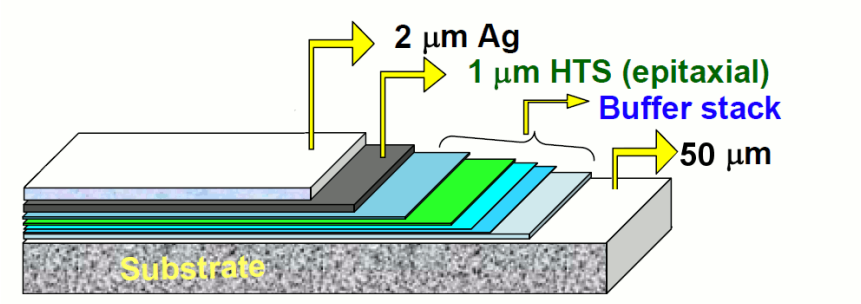

Fig. 4.1. Structure of SF12050 SuperPower 2G HTS tape [144]

Substrate is usually a nonmagnetic stainless steel and in the case of SF12050 it is Hastelloy C276, a substance well described in literature [86, 96, 104]. Tape parameters are shown in Table 4.1.

Table 4.1 Second generation SF12050 HTS tape parameters

Parameter	Value
Producer	Super Power
Tape width	12 mm
Tape thickness	0.055 mm
Critical temperature	93 K
Critical current at 77 K (self field)	200-300 A
Critical flux	Above 5T
Joint/splice resistance	~40 nΩ/cm^2
HTS (Re)BCO thickness in tape	1 μm
Substrate – hastelloy C276 thickness	50 μm
Silver overlayer thickness (upper/lower if exists)	2/1.8 μm
Buffer stack	0.2 μm
Substrate reistivity of 1 cm of tape	125 μΩcm

The idea of the experiment was to measure the changes of voltage and the resistance of the SF12050 tape parts in transient states. Knowing the voltage and current waveforms allows for calculation of temperature in each segment of the tested tape.

Having the instantaneous value of power obtained from current and voltage waveforms, the heat quantity per pulse can be calculated (equation (4-1)).

$$Q = PT = \int_0^{T_s} p(t)dt \tag{4-1}$$

where: Q – generated heat, $p(t)$ – instantaneous power, T_s – time period, P – active power

Assuming adiabatic heating of the tape in cycle of AC current, the temperature in HTS tape can be obtained from equation (4-2) on heat quantity:

$$Q = m \cdot c(T) \cdot \Delta T \tag{4-2}$$

where: $c(T)$ – specific heat capacity (temperature dependent), m – mass of an object, $\Delta T = T_1 - T_0$ – temperature difference

Deriving from (4-2) the temperature of the segment of tape can be obtained:

$$T_1 = \frac{Q}{m \cdot c(T)} + T_0 \tag{4-3}$$

The mass m of the segment can be calculated from:

$$m = \rho \cdot V \tag{4-4}$$

where: ρ – mass density, V – volume of the segment

According to Alferov *et al.* in [2], average mass density and specific heat capacity for the SF12050 tape are equal to, respectively:

$$\rho = 8600 \ \mathrm{kg/m^3} \tag{4-5}$$

$$c(T) = 369.7 + 0.19 \cdot T \ \ \mathrm{J/(kg \cdot K)} \tag{4-6}$$

where: T – temperature given in K.

Another way of determining the temperature is the knowledge of resistance versus temperature curve of SF12050 wire. This can be done by measurements described in section 4.3 of this work. Knowing the instantaneous values of voltage and current, resistance of the HTS wire can be obtained from Ohm law. After this the temperature of the tape can be determined from the $R(T)$ curve.

This method of temperature determination can be used when the increase in temperature above the critical value is the cause for the loss of the superconducting state. In the case when the HTS thin layer tape loses its

superconductivity due to the current greater than critical, equations (4-1) to (4-6) should be used for temperature calculations.

During the first experiment, two transient state situations were observed: one – when tape loses its superconducting state and goes to resistive state, second – when tape returns from resistive state to superconducting state after quench.

Test stand consists of three main elements shown in Fig. 4.2.

Fig. 4.2. The test stand for measuring the parameters of tape in transient states: 1 – computer controlled supplying system, 2 – data acquisition stand, 3 – HTS 2G tape with quench system

Computer controlled supplying system (1) allows for automatic switching on and off of the power supply voltage and for introducing changes in the amplitude by the use of computer software. Data acquisition stand (2) consists of National Instrument DAQ Card, PC computer and software for data acquisition written in LabView environment. The last element is the HTS 2G tape with installed quench generating system and measuring probes.

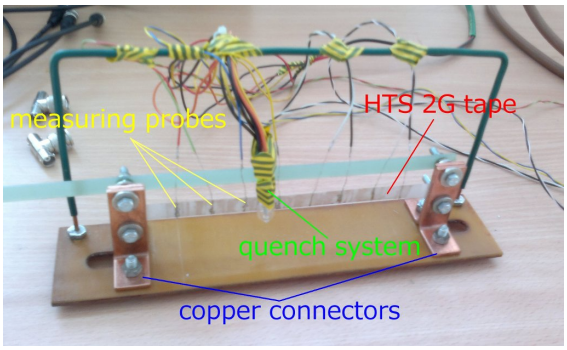

Fig. 4.3. HTS 2G tape set in for measuring

Measuring probes are silver wire soldered with the surfaces of the HTS tape (Fig. 4.3.). Quench generating system is a heater, which can raise the temperature of the tape in liquid nitrogen bath above the critical value 108 K. Tape is connected to the supplying system through copper connectors allowing the flow of current critical value and higher.

The idea of measurement system is shown in Fig. 4.4. The system is using the NI DAQ 6251 PCI card [107] for data acquisition in transient states. The voltages obtained from measuring probes, and from shunt resistor are collected by means of written software in LabView environment [108, 152].

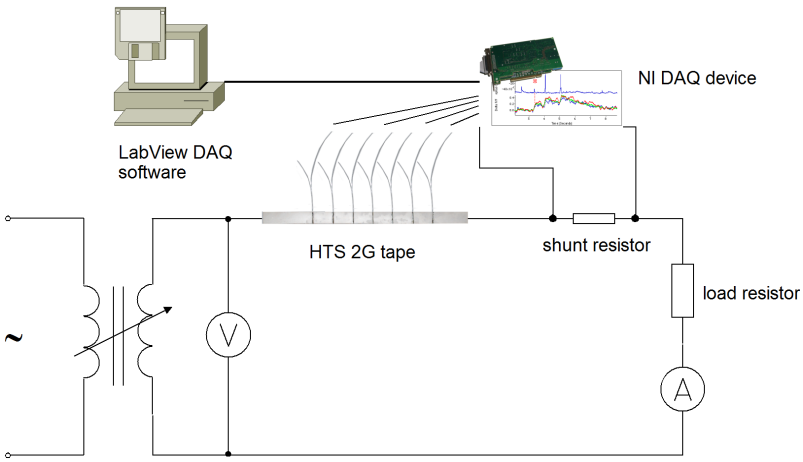

Fig. 4.4. The measurement system to determine the characteristics of the HTS 2G

Computerised data acquisition system can record transient states in HTS tape with sampling rate of 200 per sine interval per channel in the case of quench casused by local temperature rise.

NI DAQ card records data from measuring probes and shunt resistor. Measuring probes were spread at equal distances of 2 cm from each other. Each probe consisted of silver-plated wire and was soldered to the tape (Fig. 4.5).

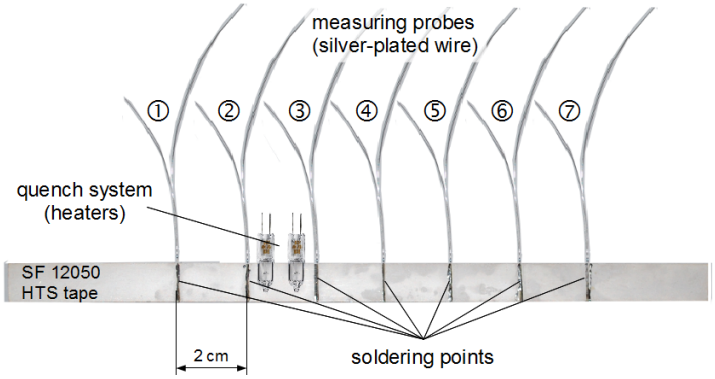

Fig. 4.5. Measurement probes fitted on HTS tape

Quench system consisted of heaters, which were in contact with HTS tape and were placed between second and third measuring probe (Fig. 4.5).

The SF12050 tape was fitted in copper connectors and the measuring probes were soldered to the measuring cables. To remove the influence of residual inductance, the shielded twisted pair measuring cable was used (Fig. 4.6) [153].

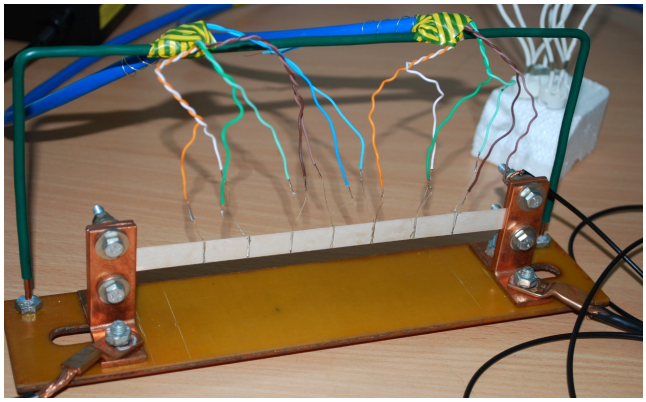

Fig. 4.6. Tape fitted in copper connectors with attached measuring cables

Measurements were performed for a few values of supplying alternating current i.e.: 3 A, 10 A, 20 A and 40 A.

4.1. Measurement results of quench caused by local temperature rise

Voltages, as well as current flowing through the tape were recorded on each measuring probe during the experiment. Constructed measuring system allowed to register the transient states of the voltage and current in each piece of tape (Fig. 4.7).

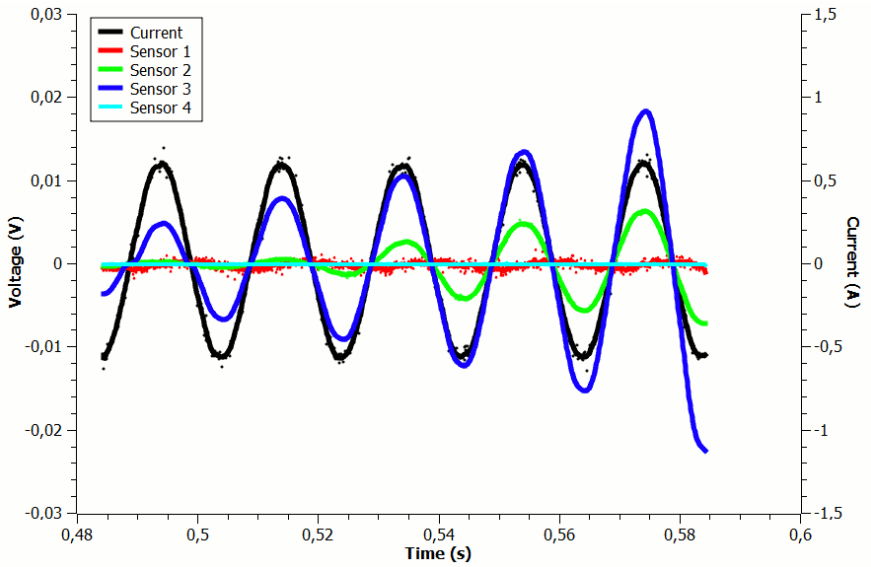

Fig. 4.7. Voltage on sensors No 1, 2, 3, 4 and current in tape versus time

Change of the voltage amplitude during heating of the tape was observed at the first three segments of wire (probes 1-2, 2-3 and 3-4). On the other probes (starting from 4), voltage is equal to 0 during the measurements (Fig. 4.7). Therefore, in further work, the voltage and current changes recorded in the first three probes will be considered.

During each experiment, the quench system heats the tape to reach temperature above the critical value and is turned off after 3 to 4 seconds. The tape returns to the superconducting state after some time, which depends in the experiment on the supplying current. The cooling conditions do not change; the tape remains in liquid nitrogen bath throughout all the measurements.

In the first experiment, the SF12050 wire was supplied with current with RMS value equal to 3A. The changes of the voltage amplitude in time were observed at the first three segments (Fig. 4.8 and Fig. 4.12). At the other segments of the tape, the amplitude of the voltage in time remains at same level, which is close to zero. Voltages described in following figures correspond to

voltages on segments 1, 2 and 3 and are described as Probe 1, Probe 2 and Probe 3.The first two segments lose their superconducting state at the same time (Probe 1 and Probe 2 lines in Fig. 4.8). Third segment loses its superconductivity about 3 seconds later and the recorded voltage had lower amplitude.

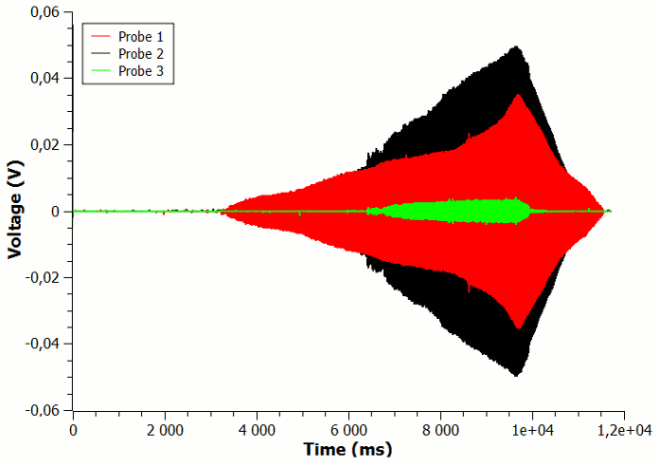

Fig. 4.8. Voltage amplitude on probes No 1, 2, 3 versus time (supplying current $3A_{RMS}$)

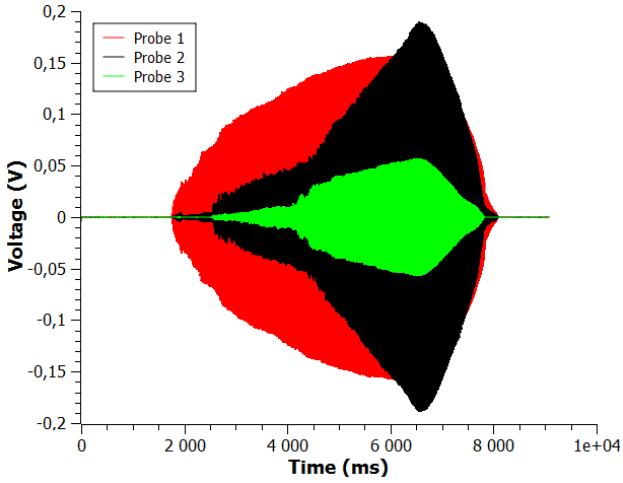

Fig. 4.9. Voltage amplitude on probes No 1, 2, 3 versus time (supplying current $10A_{RMS}$)

In the second experiment, the SF12050 wire was supplied with current of 10 A_{RMS} value. In that case, the first two measurement segments of wire lose superconductivity state almost at the same time, but the voltage on segment

No. 1 grows more rapidly comparing to others (Fig. 4.9). The highest value of voltage is obtained on the segment with installed quench system.

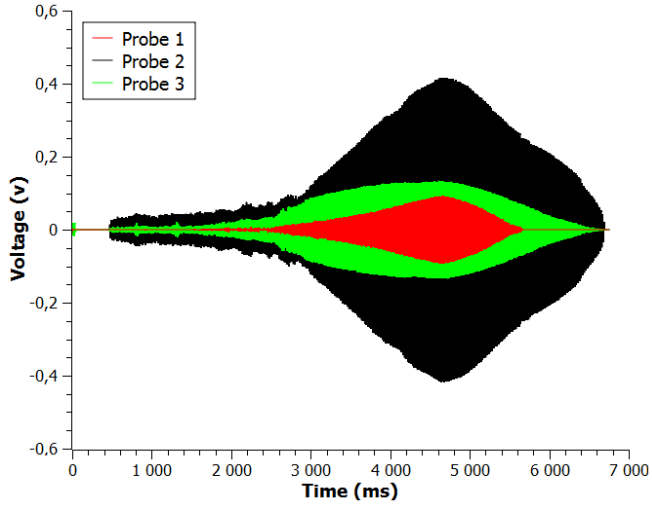

Fig. 4.10. Voltage amplitude on probes No 1, 2, 3 versus time (supplying current 20A_{RMS})

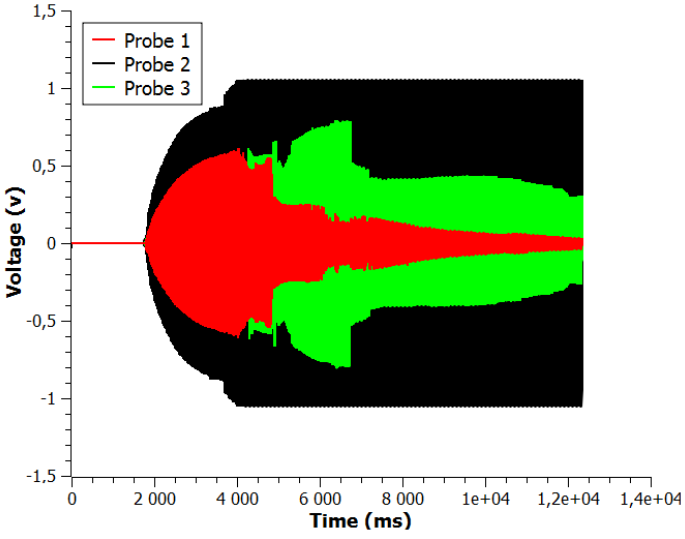

Fig. 4.11. Voltage amplitude on probes No 1, 2, 3 versus time (supplying current 40A_{RMS})

In the last two experiments, the SF12050 wire was supplied with current of 20 A_{RMS} and 40 A_{RMS} value (Fig. 4.10 and Fig. 4.11). Greatest voltage jump can

be observed at the second segment (Probe 2 on Fig. 4.10 and Fig. 4.11). In case of 40 A supplying current, the tape quickly loses superconducting state and gets damaged after about 1.7 seconds due to thermal effects. It can be observed at Fig. 4.11 at the time starting from 4 seconds, where the voltage amplitude exceeded the value of the 1 V set at the DAQ device card.

After turning off the quench system, wire is cooled down and segments which have lost superconductivity return to superconducting state. This time depends on the initial temperature of the wire segments and on the supplying current. In the case of small currents, i.e. 3 and 10 A, this time is similar and is about 1.5 seconds (Fig. 4.8 and Fig. 4.9). Higher supplying current will extend the cooling time to over 2 seconds in the case of 20 A supplying current (Fig. 4.10) and to over 8 seconds in the case of 40 A (Fig. 4.11).

Which part of the wire loses its superconductivity first is also an important aspect. The effect of loss of superconductivity by a part of the wire is the further spread of resistive zone. During measurements, the transient state of wire losing its superconductivity was recorded. In the case of $3A_{RMS}$ supplying current, the first two segments lost superconductivity at the same time (Fig. 4.12).

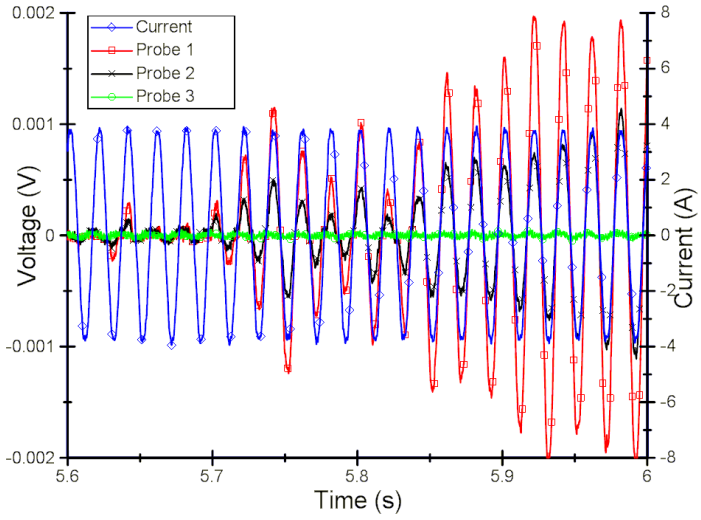

Fig. 4.12. Voltage on probes No 1, 2, 3 and current in wire during superconductivity loss (supplying current $3A_{RMS}$)

When the HTS wire is supplied with $10A_{RMS}$ current, the second segment loses its superconductivity state first of all, next is the third segment and the first segment is the last one to lose its superconductivity state (Fig. 4.13).

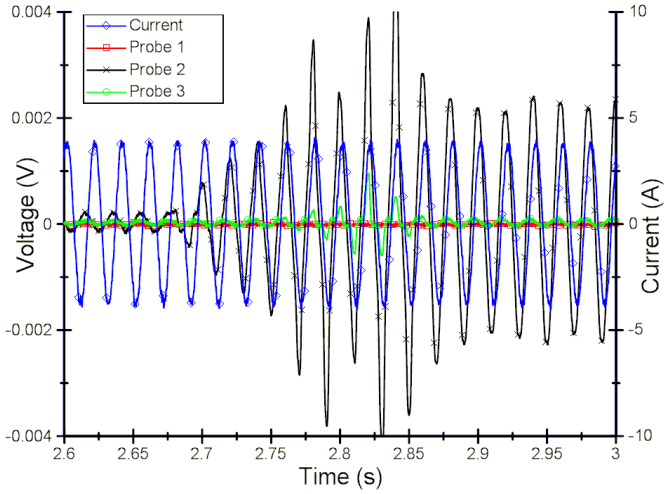

Fig. 4.13. Voltage on probes No 1, 2, 3 and current in wire during superconductivity loss (supplying current 10 A_{RMS})

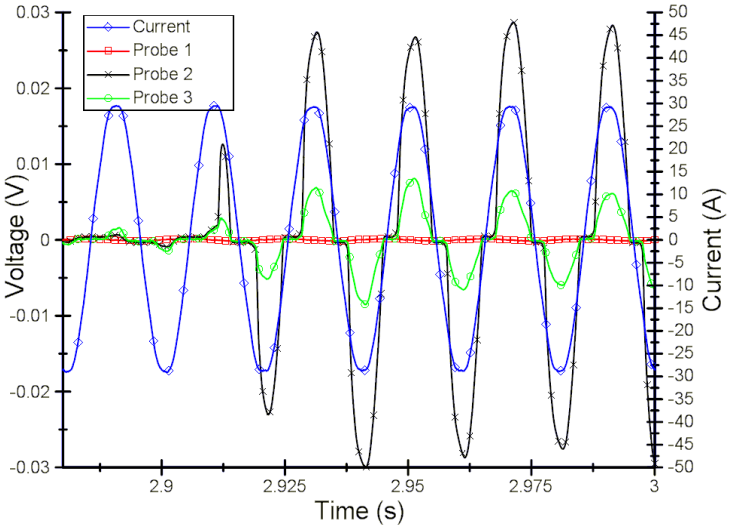

Fig. 4.14. Voltage on probes No 1, 2, 3 and current in wire during superconductivity loss (supplying current 20 A_{RMS})

Supplying the SF12050 wire with higher values of current i.e. 20 A and 40 A results in faster loss of superconductivity. The second and third segment of wire go into the state of resistivity almost at the same time (Probe 2 and Probe 3 lines at Fig. 4.14 and Fig. 4.15)

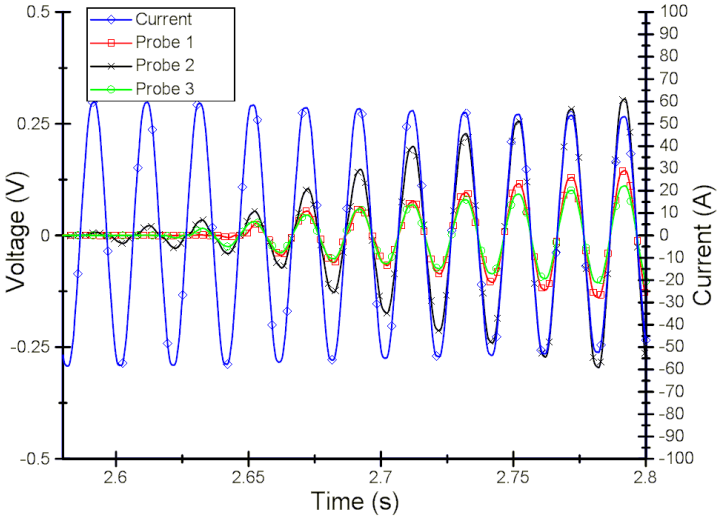

Fig. 4.15. Voltage on probes No 1, 2, 3 and current in wire during superconductivity loss (supplying current 40 A_{RMS})

The resistance of each tape segment was calculated due to the Ohm's law. Only segments which losses their superconductivity state were presented. The changes of resistance in time for different supplying current values are shown in Fig. 4.16 to Fig. 4.19.

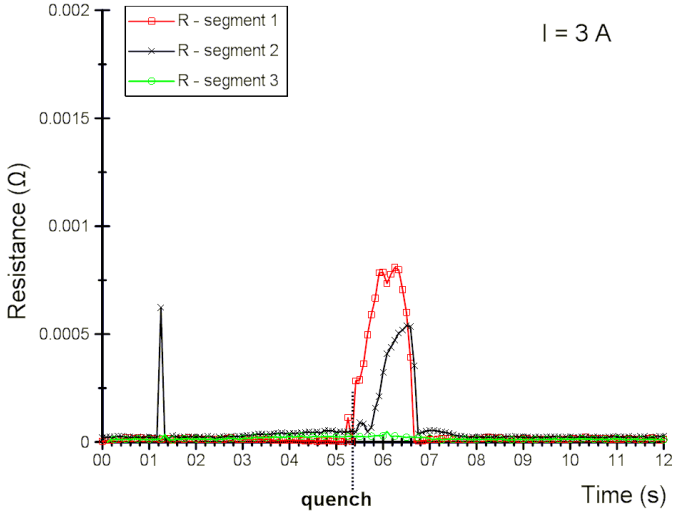

Fig. 4.16. Resistance change of segments No 1, 2, 3 versus time (supplying current 3 A_{RMS})

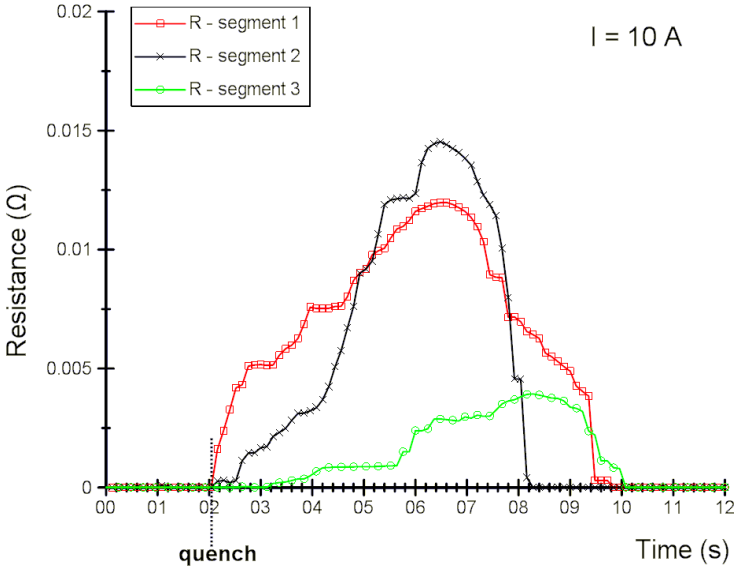

Fig. 4.17. Resistance change of segments No 1, 2, 3 versus time (supplying current 10 A_{RMS})

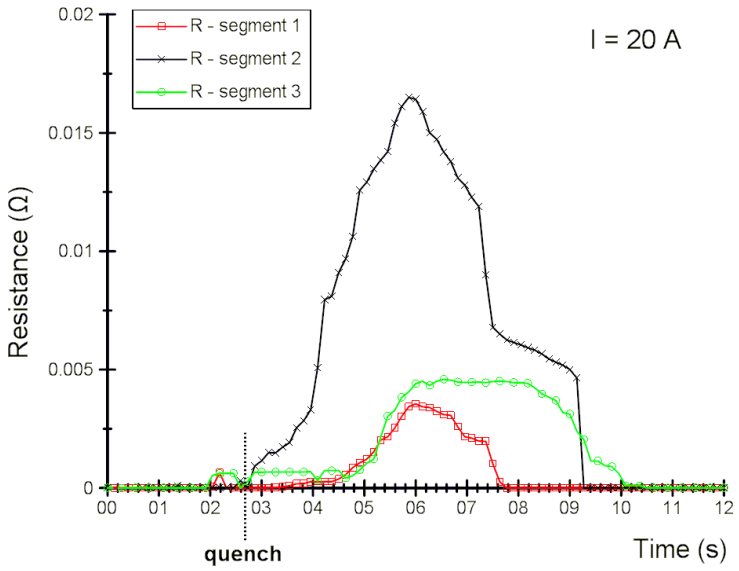

Fig. 4.18. Resistance change of segments No 1, 2, 3 versus time (supplying current 20 A_{RMS})

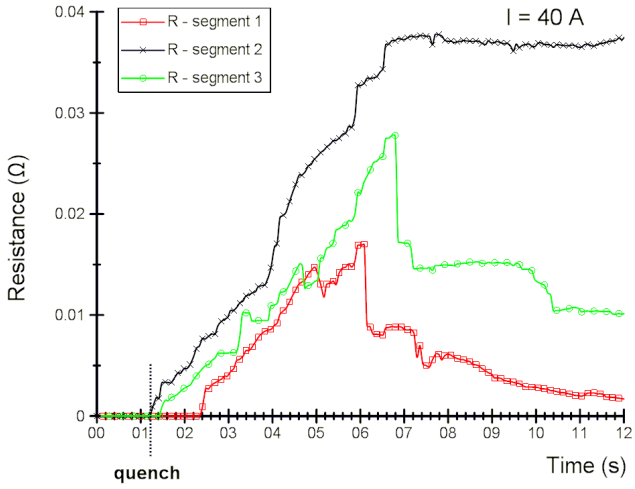

Fig. 4.19. Resistance change of segments No 1, 2, 3 versus time (supplying current 40 A_{RMS})

It can be noticed that for supplying current equal to 40 A the resistance of segment 2 of the tape remained at the value of 0.038 Ohms. It happened due to overheating of the tape segment, and the tape material has been destroyed.

Knowledge of the resistance versus temperature curve of the SF12050 tape obtained in measurements described in section 4.3, allows for the determination of temperature changes in time.

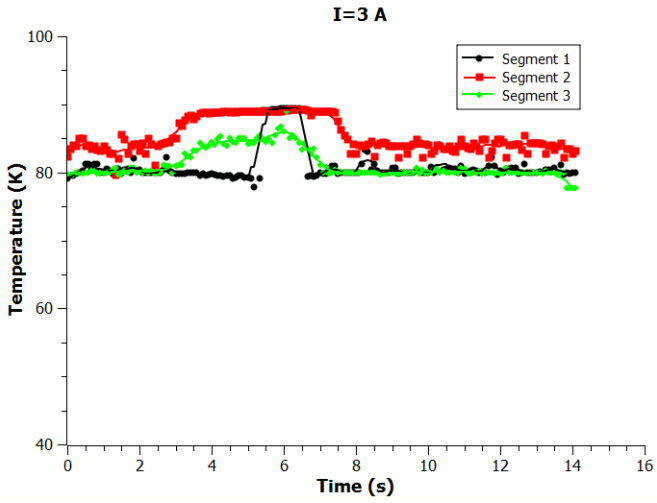

Fig. 4.20. Temperature changes of segments No 1, 2, 3 (supplying current 3 A_{RMS})

The measurement results of temperature changes in transients are presented only for tape which did not overheat Fig. 4.20, Fig. 4.21 and Fig. 4.22.

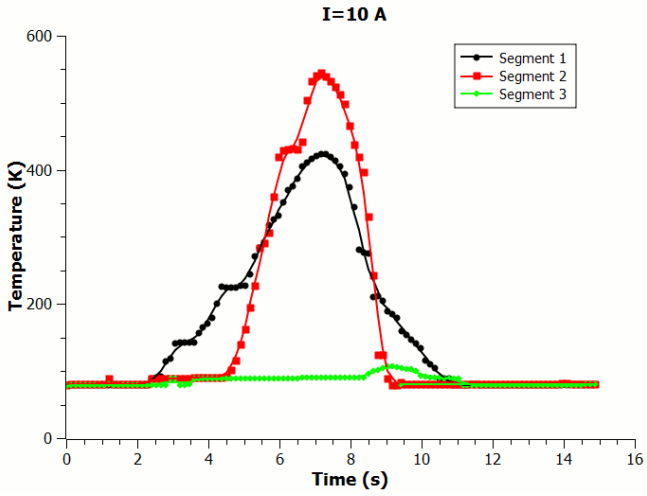

Fig. 4.21. Temperature changes of segments No 1, 2, 3 (supplying current 10 A_{RMS})

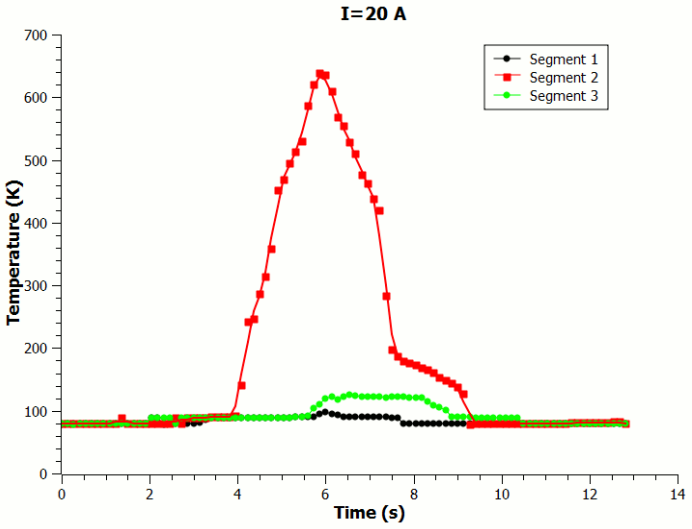

Fig. 4.22. Temperature changes of segments No 1, 2, 3 (supplying current 20 A_{RMS})

For the supplying current equal to 3A, the temperature of the segments slightly exceeds the critical temperature (highest segment temperature equal to 90 K).

For the currents equal to 10 A and 20 A, the temperature rises quickly to the maximum values of about 550 K and 650 K, respectively. In the case of 20 A current supply, it can be noticed that the temperature of adjacent segments 1 and 3 of SF12050 tape did not grow to high values. This is because segment 2 loses its superconducting state much earlier and starts to limit the supplying current.

4.2. Measurement results of quench caused by transport current rise

Another performed experiment was to examine the HTS tape in transient states when the supplying current exceeds the critical value. The experiment was performed in the test stand shown in Fig. 4.2. The second generation SF12050 tape was fitted in copper connectors. Seven measuring probes were soldered on the tape (Fig. 4.23).

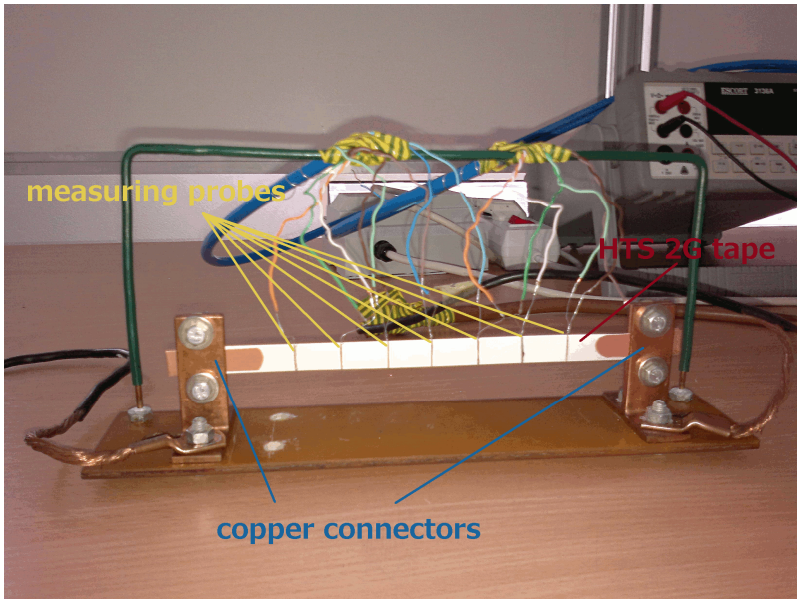

Fig. 4.23. SF12050 tape fitted for measuring with quench caused by current higher than critical value

The experiment relies on measuring the voltage on the probes soldered to the HTS tape when it is supplied with current greater than the critical current for short periods of time (60 ms or 80 ms). The voltages were measured differentially on each segment of the tape. The segments of the tape and voltages on the probes were numbered as shown in Fig. 4.24.

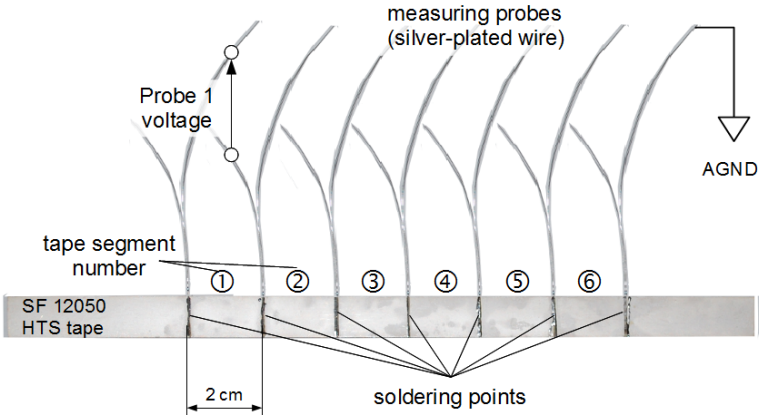

Fig. 4.24. Segments and probes voltages numbering in SF12050 tape measurements

Before the current increase, current of low value was flowing through the SF12050 wire for observation of waveforms in the steady state. The idea of supplying the wire is shown in Fig. 4.25.

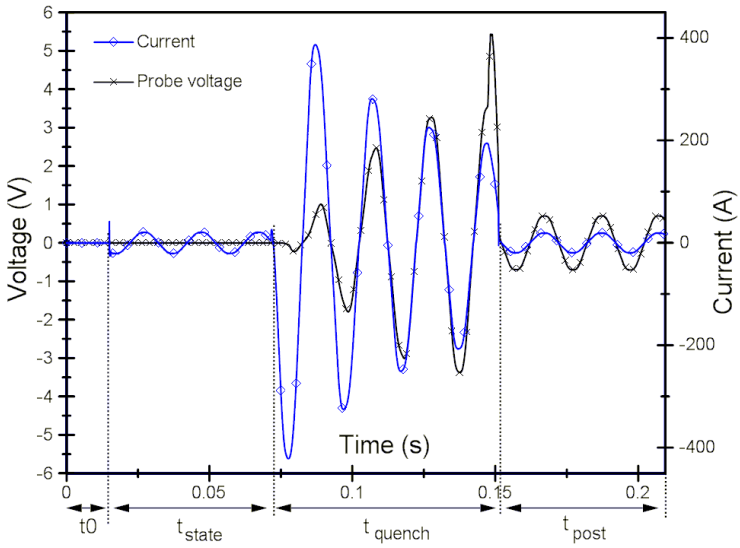

Fig. 4.25. Voltage on probe and supplying current in tape versus time with marked time intervals

A short period of time elapsed before the supplying current was switched on (time t_0 in Fig. 4.25). After that, the supply gets switched on and the current of value 20 A begins to flow (time t_{state}). Next, the quench is generated by

increasing the load and this lasts till the time is equal to t_{quench}. Lastly, the load is decreased and supplying current flows through the t_{post}. The summary of time interval values used in experiment is shown in Table 4.2.

Table 4.2 Summary of time intervals used in measuring experiment

Time interval indication	Value (ms)
t_0	10
t_{state}	60
t_{quench}	80
t_{post}	50

For such chosen time values, a number of measurements were carried out at currents exceeding the critical value. The initial value of the quench current was selected in such a way that it would be slightly lower than the value at which the bubbles of nitrogen appeared on the surfaces of the SF12050 wire (Fig. 4.26).

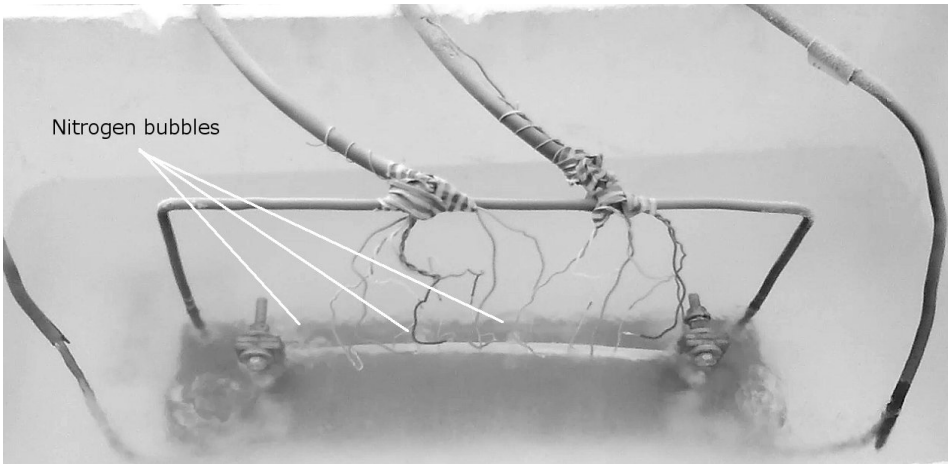

Fig. 4.26. Nitrogen bubbles appearing on the wire-liquid nitrogen surfaces (I_{peak}=380 A)

During the measurements, the current flowing through the tape and voltages were measured on all segments. Voltages described as Probe 1, Probe 2, Probe 3 etc. on following figures correspond to voltages on segment 1, segment 2, segment 3 and so on. The first superconductivity loss in the SF12050 wire can be observed on Fig. 4.27 and Fig. 4.28 (voltage peaks).

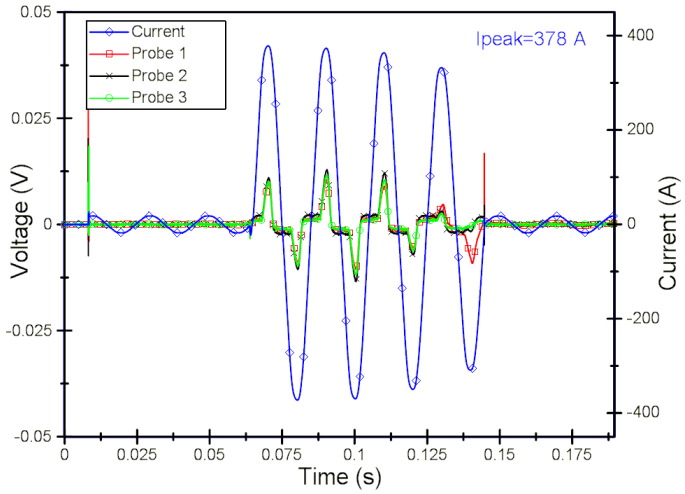

Fig. 4.27. Voltage on sensors No 1, 2, 3 and current in tape versus time (I_{peak}=378 A, I_{peak}/I_c=1.4)

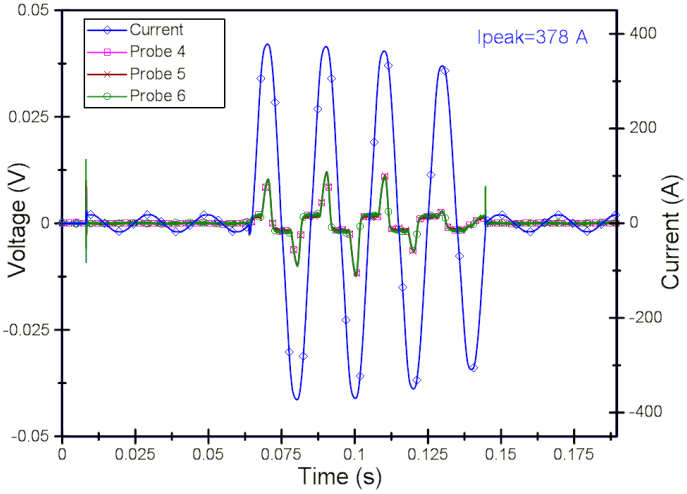

Fig. 4.28. Voltage on sensors No 4, 5, 6 and current in tape versus time (I_{peak}=378 A, I_{peak}/I_c=1.4)

All segments of tape lose their superconducting state for a while and go into the resistivity state, however – when the instantaneous current decreases, the tape returns to the superconducting state. During the following measurement, the current peak value was increased to 380 A and the recorded current and voltage waveforms are shown in Fig. 4.29 and Fig. 4.30.

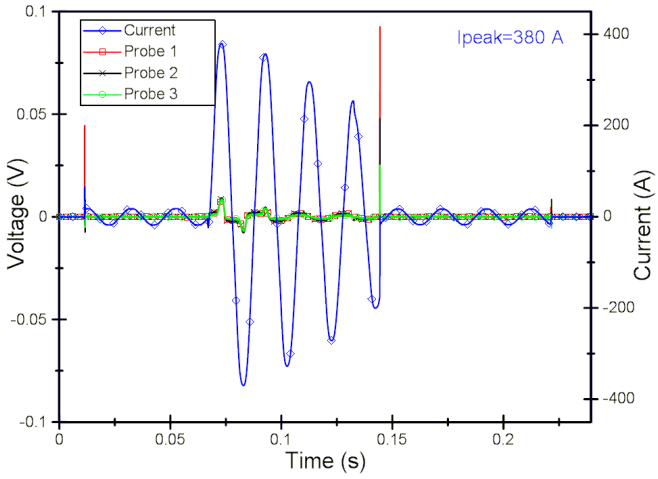

Fig. 4.29. Voltage on sensors No 1, 2, 3 and current in tape versus time (I_{peak}=380 A, I_{peak}/I_c=1.41)

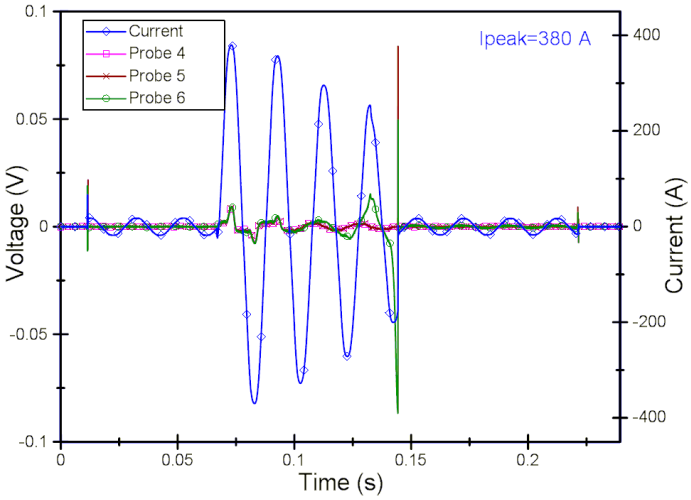

Fig. 4.30. Voltage on sensors No 4, 5, 6 and current in tape versus time (I_{peak}=380 A, I_{peak}/I_c=1.41)

Distinct loss of the superconducting state is observed on segment 6 (Probe 6 in Fig. 4.30). The other segments of tape go into the resistivity state for a while at the beginning of the quench, but they return to the superconducting state after the first period of current sine.

Current and voltage waveforms recorded when peak value of current was equal to 400 A, are shown in Fig. 4.31 and Fig. 4.32.

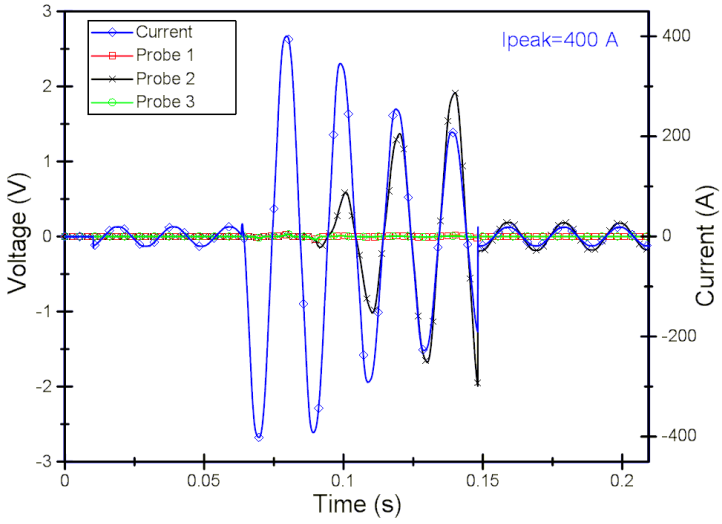

Fig. 4.31. Voltage on sensors No 1, 2, 3 and current in tape versus time (I_{peak}=400 A, I_{peak}/I_c=1.48)

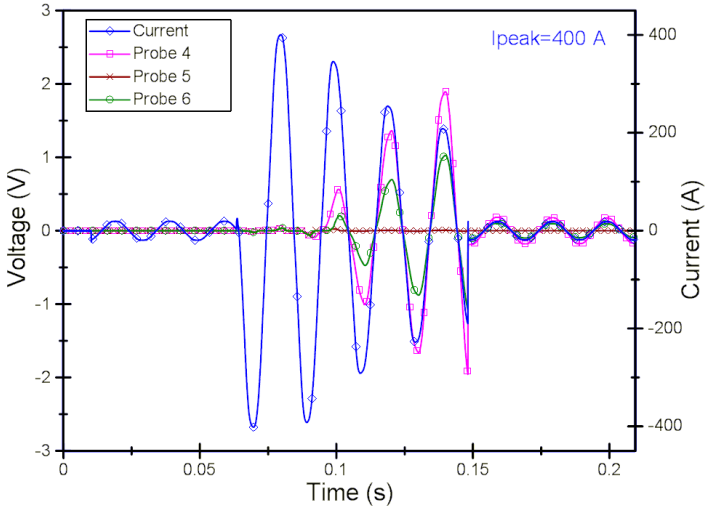

Fig. 4.32. Voltage on sensors No 4, 5, 6 and current in tape versus time (I_{peak}=400 A, I_{peak}/I_c=1.48)

Loss of the superconductivity can be observed in segments 2, 4 and 6. The peak value of the recorded voltage on one of the segments is about 2 V, while the current amplitude drops to 200 A.

Another measurement experiment was carried out when the quench was caused by the peak current equal to 422 A (Fig. 4.33 and Fig. 4.34).

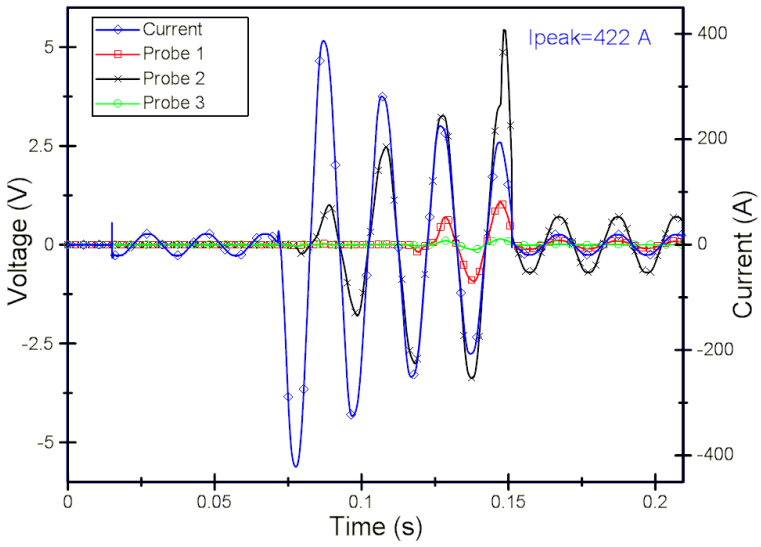

Fig. 4.33. Voltage on sensors No 1, 2, 3 and current in tape versus time (I_{peak}=422 A, I_{peak}/I_c=1.56)

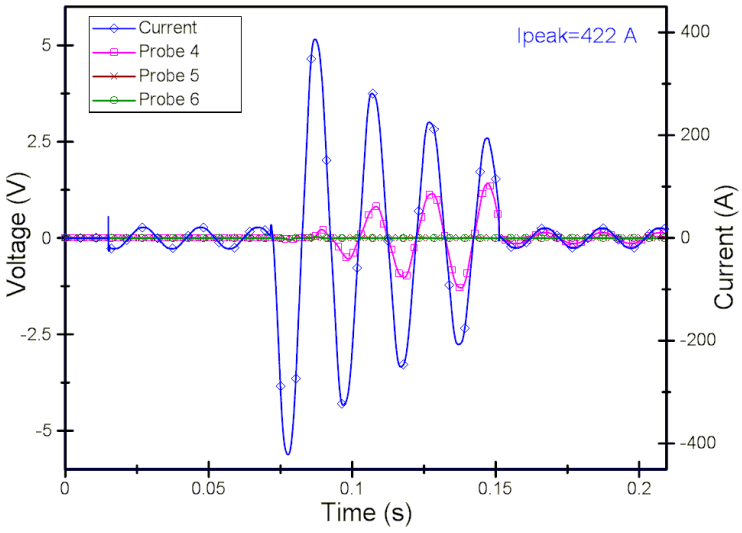

Fig. 4.34. Voltage on sensors No 4, 5, 6 and current in tape versus time (I_{peak}=422 A, I_{peak}/I_c=1.56)

During this experiment, segments 1,2,3 and 4 of the SF12050 tape lose their superconducting state (see probes 1,2,3,4 voltages in Fig. 4.33 and Fig. 4.34).

The instantaneous power were measured, as product of the voltage and current, to obtain the heat sources value in each segment of the tape. The results are shown in Fig. 4.35 to Fig. 4.37.

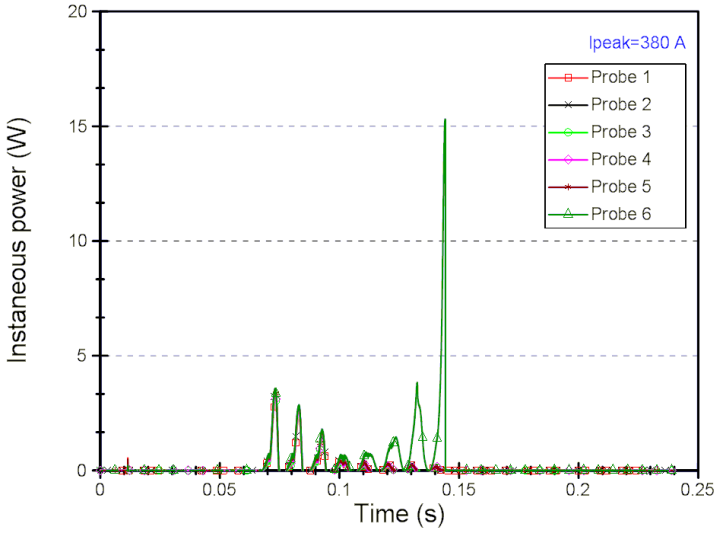

Fig. 4.35. Instantaneous power measured at segments of SF12050 wire (I_{peak}=380 A, I_{peak}/I_c=1.41)

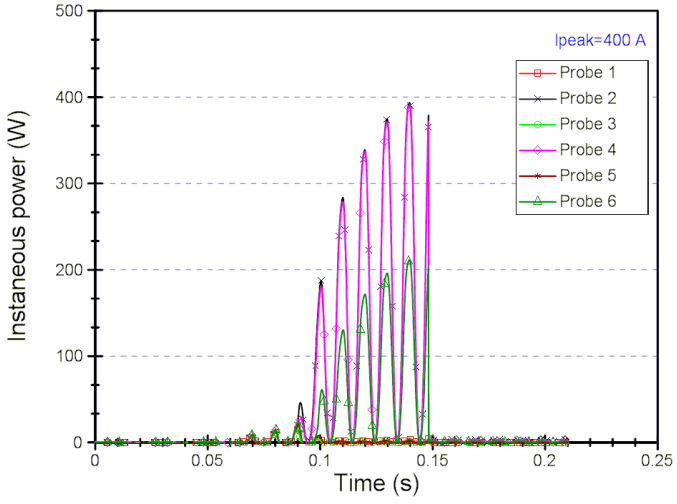

Fig. 4.36. Instantaneous power measured at segments of SF12050 wire (I_{peak}=400 A, I_{peak}/I_c=1.48)

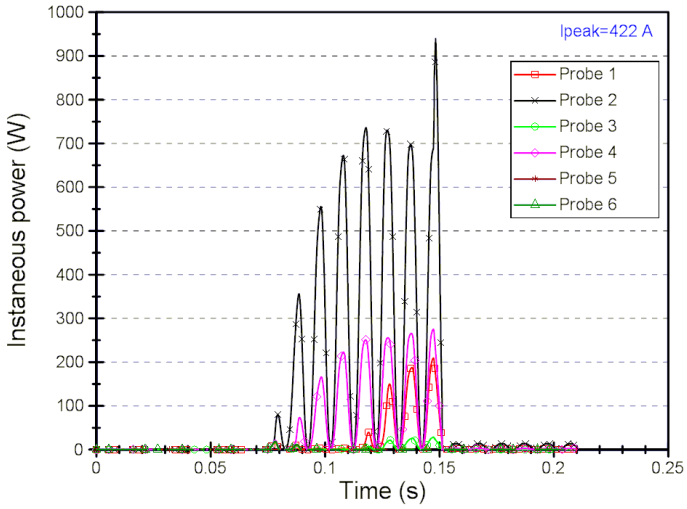

Fig. 4.37. Instantaneous power measured at segments of SF12050 wire (I_{peak}=422 A, I_{peak}/I_c=1.56)

From the current – voltage waveforms the resistance of each tape segment can be calculated. The results of the resistance change, for different quench current magnitudes, are shown in Fig. 4.38 to Fig. 4.40.

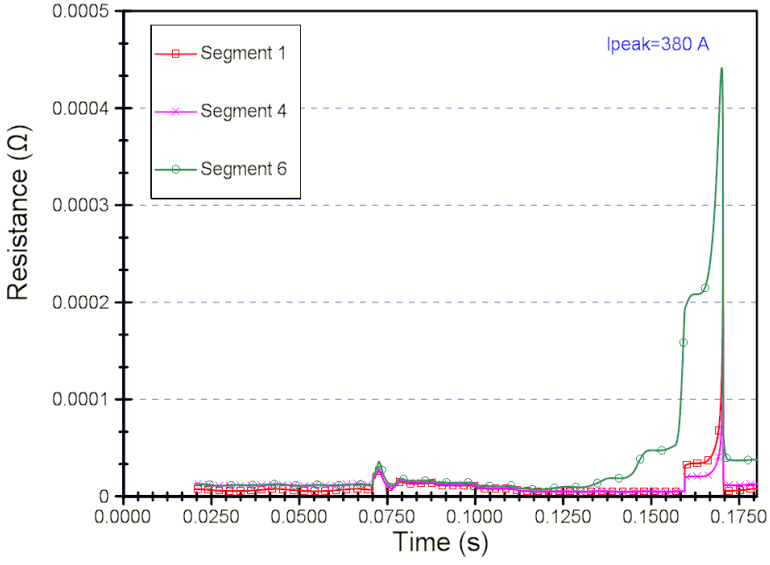

Fig. 4.38. Resistance versus time in chosen segments of SF12050 wire (I_{peak}=380 A, I_{peak}/I_c=1.41)

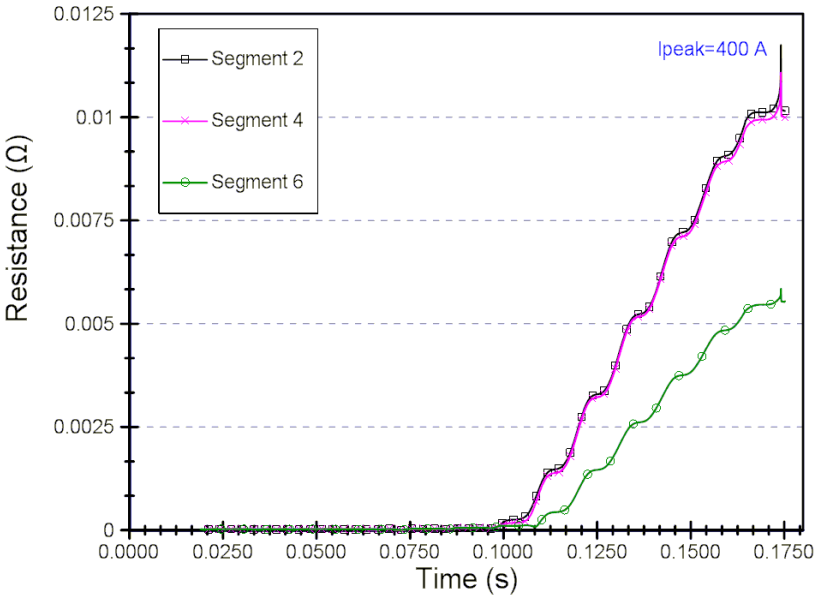

Fig. 4.39. Resistance versus time in chosen segments of SF12050 wire (I_{peak}=400 A, I_{peak}/I_c=1.48)

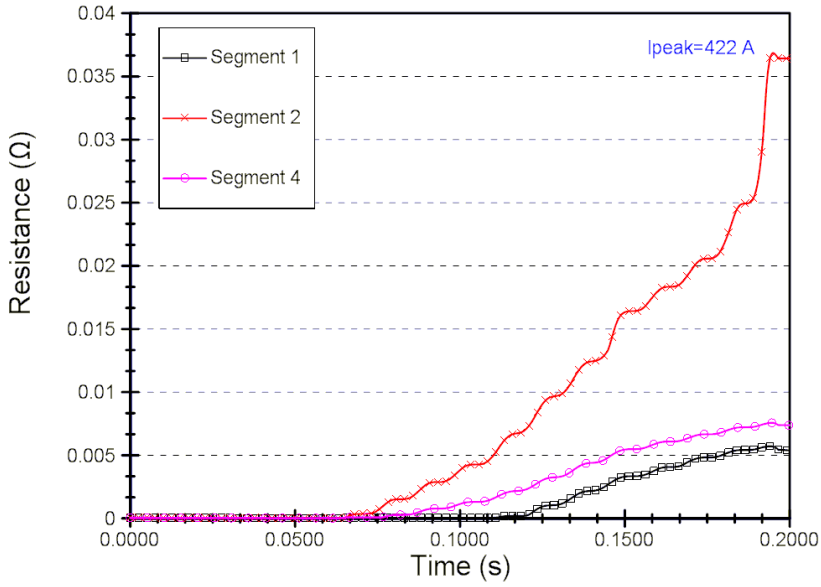

Fig. 4.40. Resistance versus time in chosen segments of SF12050 wire (I_{peak}=422 A, I_{peak}/I_c=1.56)

Having the instantaneous power distribution in the tape and acquiring the equation (4-3) it is possible to determine the temperature changes of each segment in time. The results are shown in Fig. 4.41 to Fig. 4.43.

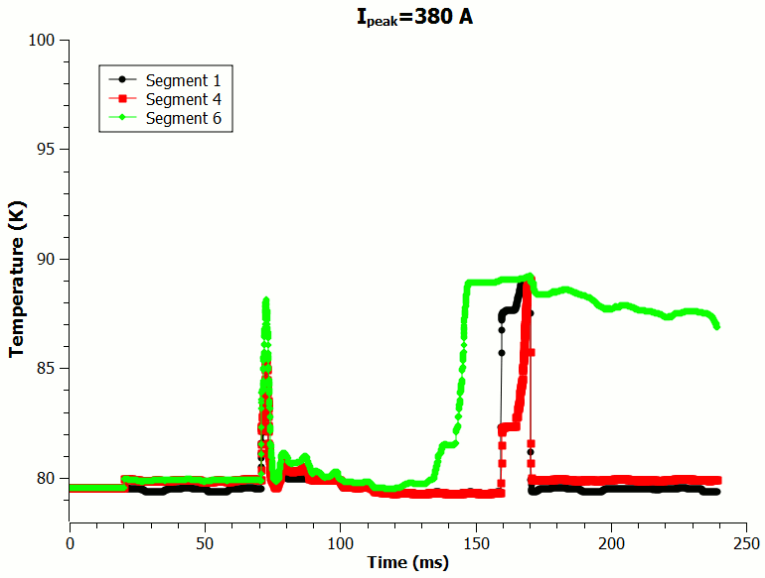

Fig. 4.41. Temperature changes in chosen segments of SF12050 wire (I_{peak}=380 A, I_{peak}/I_c=1.41)

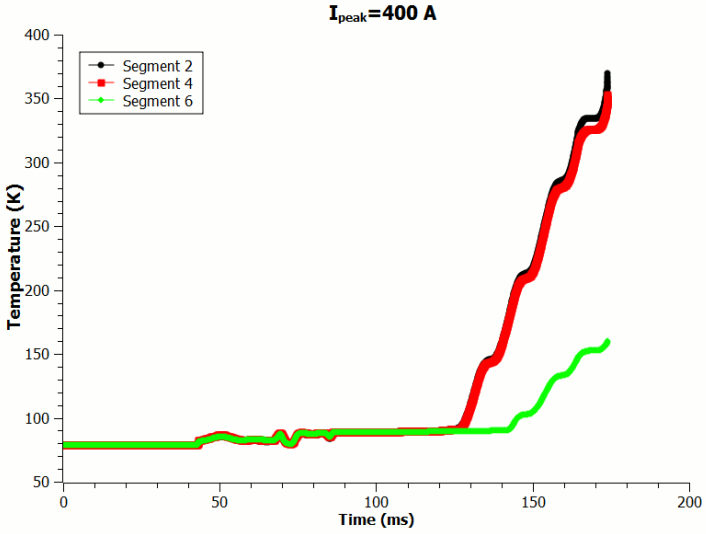

Fig. 4.42. Temperature changes in chosen segments of SF12050 wire (I_{peak}=400 A, I_{peak}/I_c=1.48)

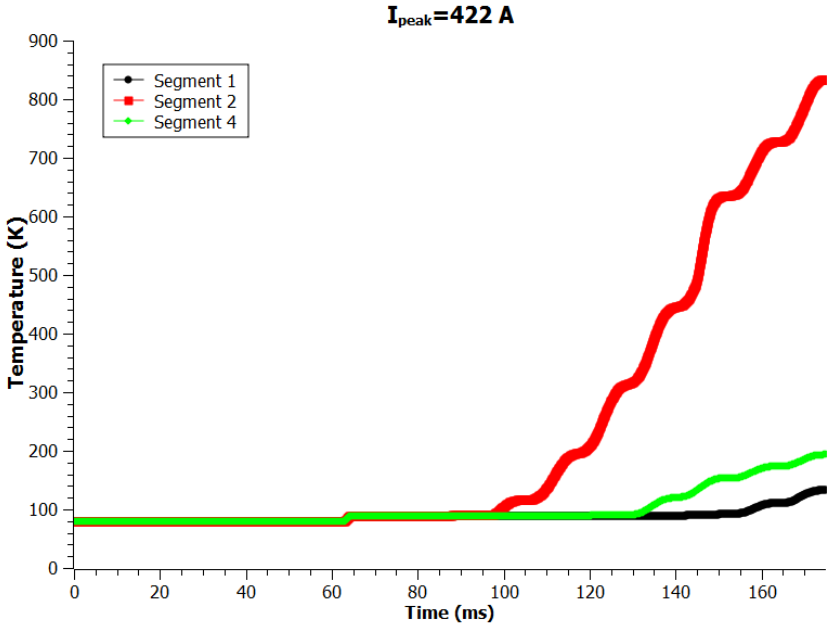

Fig. 4.43. Temperature changes in chosen segments of SF12050 wire (I_{peak}=422 A, I_{peak}/I_c=1.56)

4.3. Measurement results of SF12050 wire resistance

Another experiment conducted was measuring the SF12050 wire resistance depending on temperature changes. During that experiment, the critical temperature of the SF12050 wire can be determined. The idea of measurement experiment is shown in Fig. 4.44. The piece of HTS wire is placed between copper bars and supplied with a small current (0.2 A to 1 A) for voltage measuring. Distance between voltage terminals is 10 centimetres.

Copper bars provide homogenous distribution of temperature on the whole piece of wire, they also make sure that temperature changes in time are slower. One bar has a hole where the temperature sensor is placed. Terminals of the sensor are connected to LakeShore 218 Temperature Monitor. The wire mounted in copper bars is placed in liquid nitrogen bath. After the temperature drops to 77.4 K, the measurement set is placed in room temperature. The measurement set starts to heat and the temperature, current and voltage values are registered. The values are recorded by means of NI USB 6212 DAQ device and software written in National Instruments LabView system (Fig. 4.45).

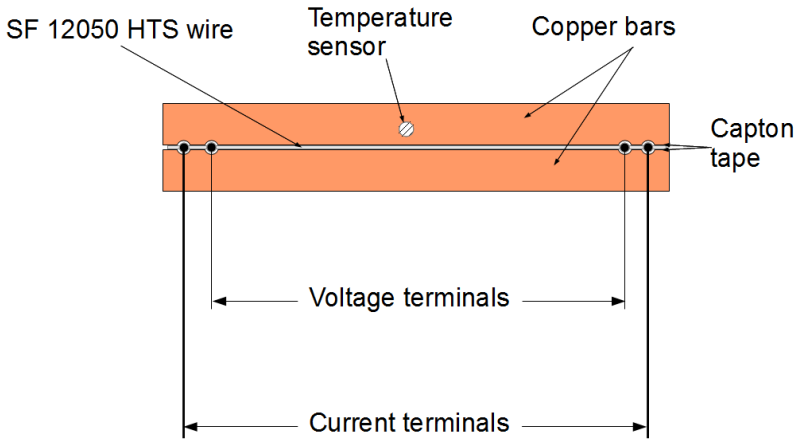

Fig. 4.44. Idea of resistance in the function of temperature measurements

Current flowing through the tape was only turned on for the time of 50 ms to measure the voltage. Time period between the measuring points was 500 ms. Due to the fact that temperature changes through the use of liquid nitrogen bath, and in order not to heat the tape throughout the measurement period (so as not to unsettle the temperature which changes naturally), the measuring current was only activated for a short period of time. The wire was insulated from copper bars by thin capton tape to obtain electrical insulation and allow heat transfer.

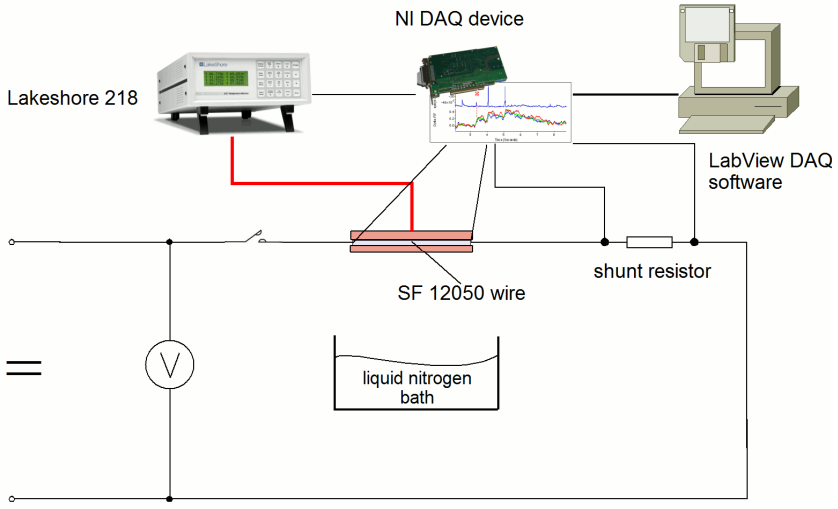

Fig. 4.45. The measuring system of resistance versus temperature changes in SF12050 wire

Measuring system allowed the estimation of the temperature critical value and resistance versus temperature curve of the SF12050 second generation superconducting wire (Fig. 4.46). The measured critical temperature value of examined 2G wire is about 89 K.

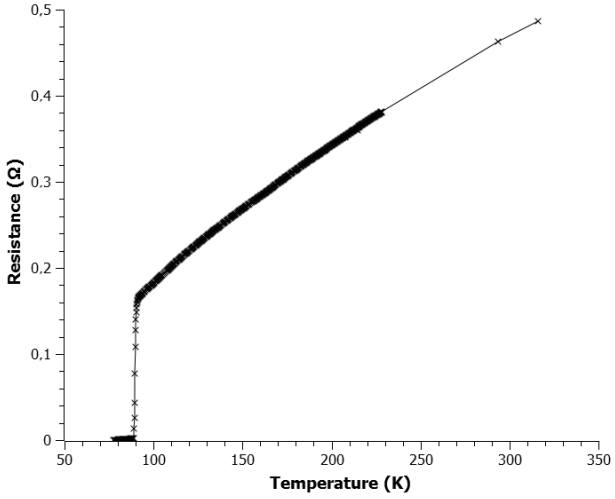

Fig. 4.46. Resistance of 1 m length SF12050 wire versus temperature

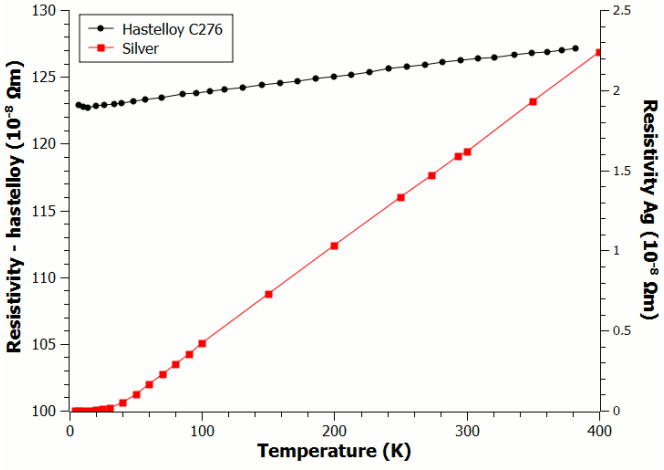

Fig. 4.47. Resistivity of silver and hastelloy versus temperature [91, 131, 150]

To obtain the resistivity versus temperature curve of YBCO layer in SF12050 tape it is need to know the curves of silver and hastelloy. The dependence of resistivity on the temperature of the silver and hastelloy is well described in

literature and presented in Fig. 4.47. From that it is possible to determine the resistivity versus temperature curve (Fig. 4.48).

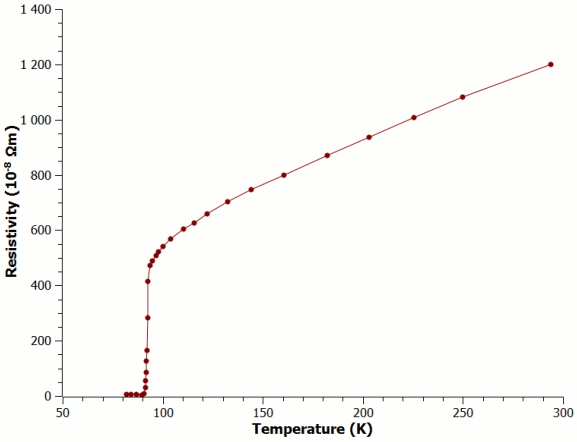

Fig. 4.48. Resistivity of YBCO layer in SF12050 wire

4.4. Temperature measurement in transient states with designed IR photodiodes setup

Another conducted experiment was performed to examine whether the designed IR photodiode system can record temperature changes in the 2G HTS tape. The idea of the experiment is based on the linear response (Fig. 4.49) of the silicon photodiode at low temperatures. The behaviour of the silicon photodiode at low temperature was the research subject of Pająkowski [113].

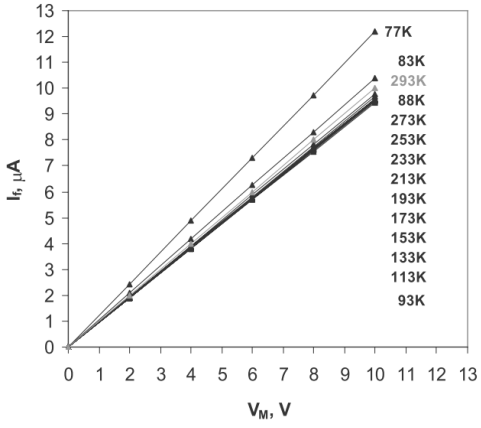

Fig. 4.49. Linear response of the silicon photodiode SFH 203 in low temperature [113]

The experiment was performed in the test stand shown in Fig. 4.2. The SF12050 tape was fitted in copper connectors. Seven measuring probes were soldered on the tape, like in the previous experiment, and – additionally – a set of eight infrared photodiodes was fitted.

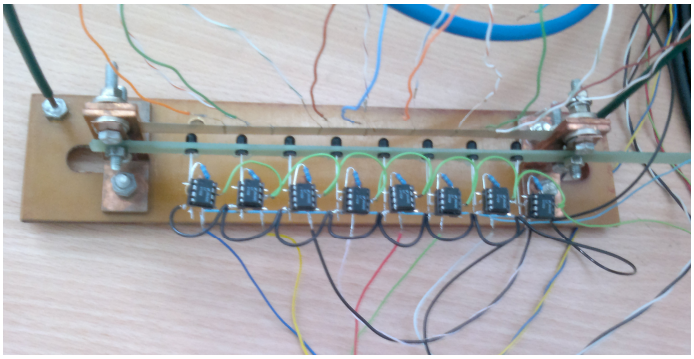

Fig. 4.50. HTS 2G tape and SFH203FA photodiodes set in for measuring

Measuring probes are soldered with the surfaces of the HTS tape and the IR photodiodes were set at the distance of 3 mm from the tape (Fig. 4.50). Quench was caused by the overcurrent. The signal from the photodiodes was measured through the light/voltage converter shown in Fig. 4.51.

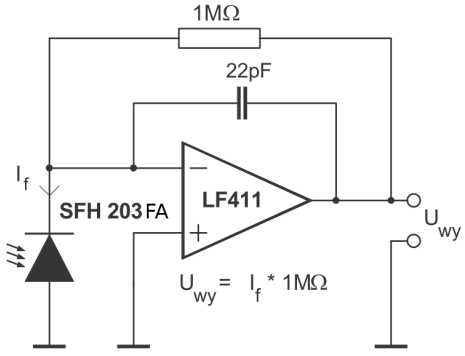

Fig. 4.51. The light/voltage converter circuit of the SFH 203 FA photodiode

The idea of measurement system is shown in Fig. 4.52. The system is using the NI DAQ 6251 PCI card and NI DAQ USB 6212 for data acquisition in transient states. The voltages from measuring probes, from shunt resistor, and from the light/voltage converter are collected by means of written software in LabView environment.

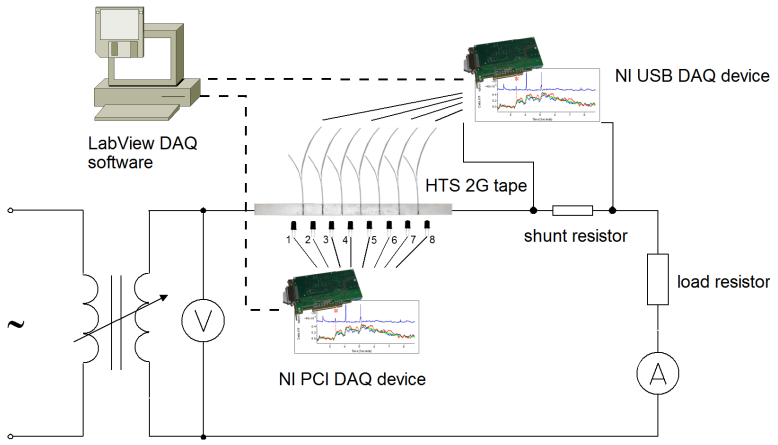

Fig. 4.52. The measurement system to determine the temperature changes of the HTS 2G tape

The first experiment to be conducted was to observe the signals recorded from the photodiode during transients induced by increasing the amplitude of the quench current. These measurements gave an answer to whether photodiodes are able to register a local rise in temperature. The results of measurements are shown in Fig. 4.53.

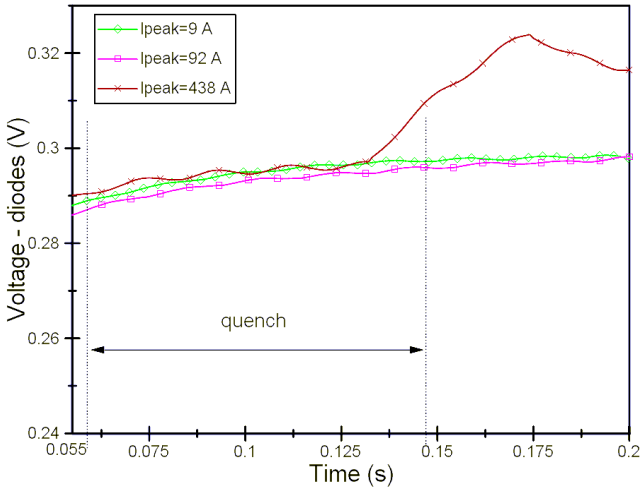

Fig. 4.53. Voltage on photodiode No 6 for different current peak values versus time

Segment number 5 of the SF12050 tape lost its superconductivity at the earliest stage during the experiments; therefore voltages present on photodiode No. 6 are presented in Fig. 4.53. It can be seen that local temperature rise above

the critical value of the current occurs in tape and is registered by the photodiode measuring system.

The ensuing measurements that were carried out record the data for peak current value greater than critical current value. Computer controlled supplying system was set to switch on at the times given in Table 4.3.

Table 4.3 Summary of time intervals used in measuring experiment with photodiodes

Time interval indication	Value (ms)
t_0	10
t_{state}	100
t_{quench}	60
t_{post}	100

In comparison to earlier experiments, the times t_{state} and t_{post} were increased in order to observe the phenomenon more fully. Several measurements were made with different amplitudes of supplying current. Chosen results are presented below. Only a few segments of tape lose their conductivity for the current peak value equal to 1.33 of the critical current value. The results of measurements are shown in Fig. 4.54.

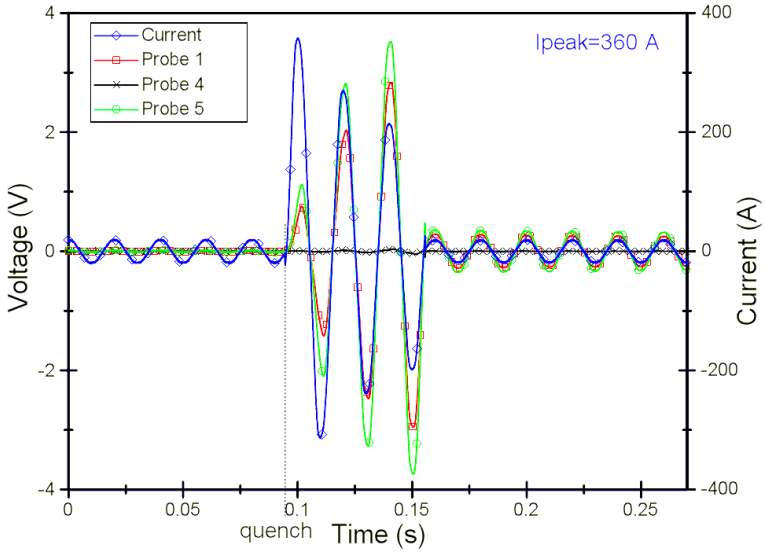

Fig. 4.54. Voltage on sensors No 1, 4, 5 and current in tape versus time (I_{peak}=360 A, I_{peak}/I_c=1.33)

Simultaneously, voltages coming from the photodiodes were recorded. Voltage increases were registered on photodiodes number 5, 6 and 7 (Fig. 4.55).

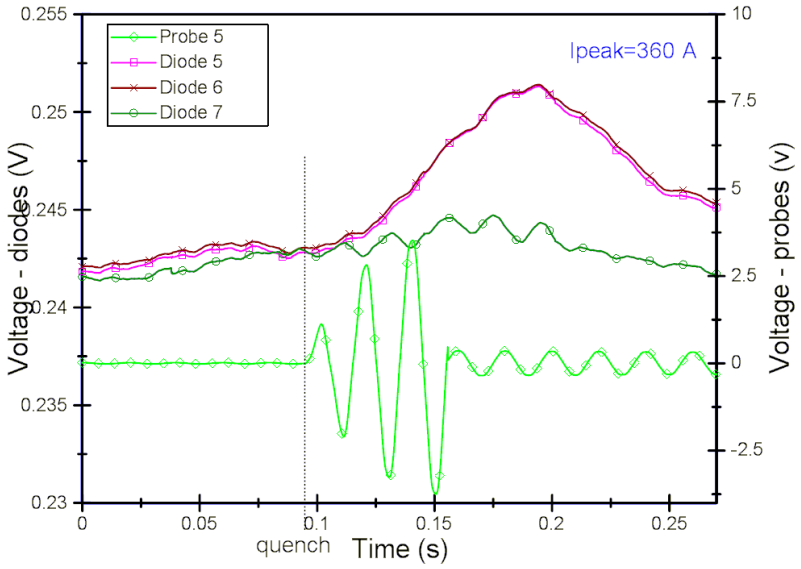

Fig. 4.55. Voltage on sensor No 5 and diodes 5,6,7 voltages versus time (I_{peak}=360 A, I_{peak}/I_c=1.33)

All segments of tape lost their conductivity for the current peak value equal to 1.57 of the critical current value. However, this occurs at different times after the quench (Fig. 4.56).

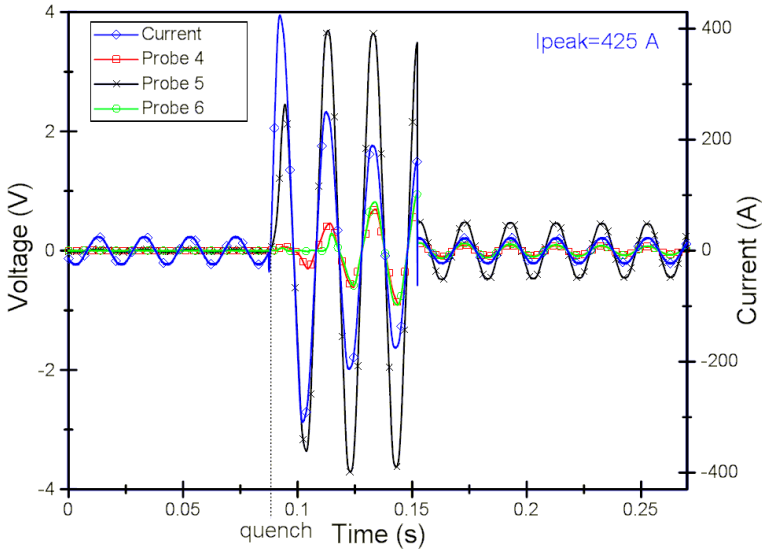

Fig. 4.56. Voltage on sensors No 4, 5, 6 and current in tape versus time (I_{peak}=425 A, I_{peak}/I_c=1.57)

Because the highest voltage value was recorded on probe 5 the voltages on the photodiodes 5,6,7 were shown in Fig. 4.57. It can be noticed that the voltages recorded on the photodiodes are lower than in the previous case (see Fig. 4.55 and Fig. 4.57). In next step the generated heat was calculated using formula (4-1) and the temperature of the tape segment was obtained as the final result (equation (4-3). The temperature curve and compared adequate voltage obtained from photodiode sensor are shown in Fig. 4.58 and Fig. 4.59.

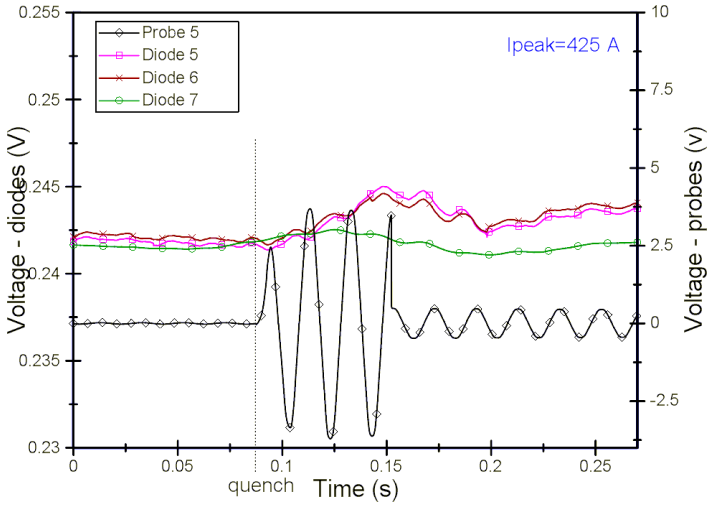

Fig. 4.57. Voltage on sensor No 5 and diodes 5,6,7 voltages versus time (I_{peak}=425 A, I_{peak}/I_c=1.57)

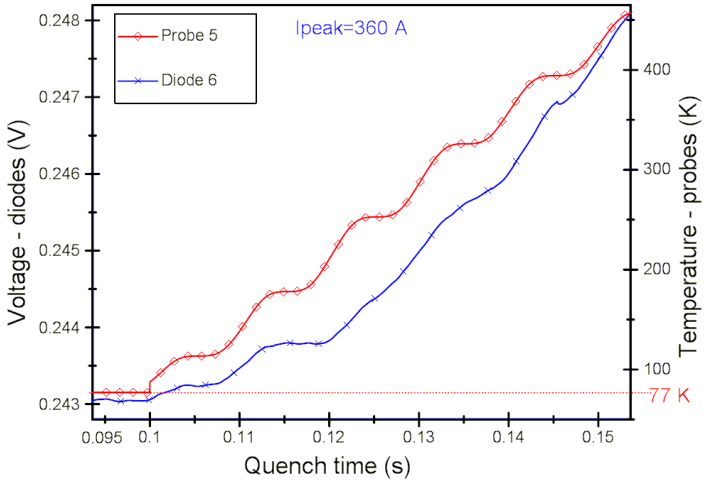

Fig. 4.58. Temperature of segment 5 and photodiode 6
voltage versus time during the quench (I_{peak}=360 A, I_{peak}/I_c=1.33)

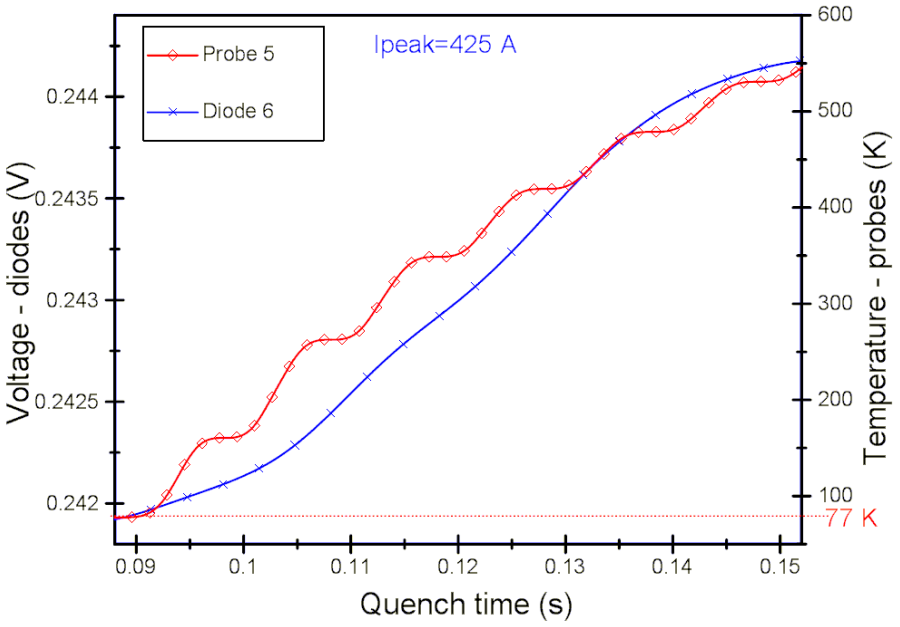

Fig. 4.59. Temperature of segment 5 and photodiode 6
voltage versus time during the quench (I_{peak}=425 A, I_{peak}/I_c=1.57)

It can be noticed that there is good agreement between the temperature curve obtained from probe and photodiode voltage. Further measurements were carried out with extended quench time. The computer controlled supplying system was set to switch on at the times given in Table 4.4.

Table 4.4 Summary of time intervals used in measuring experiment with photodiodes

Time interval indication	Value (ms)
t_0	10
t_{state}	100
t_{quench}	80
t_{post}	100

During the quench, segment number 6 of the tape was overheated and the tape materials were burned out. Current and voltages registered at the contiguous segments are shown in Fig. 4.60.

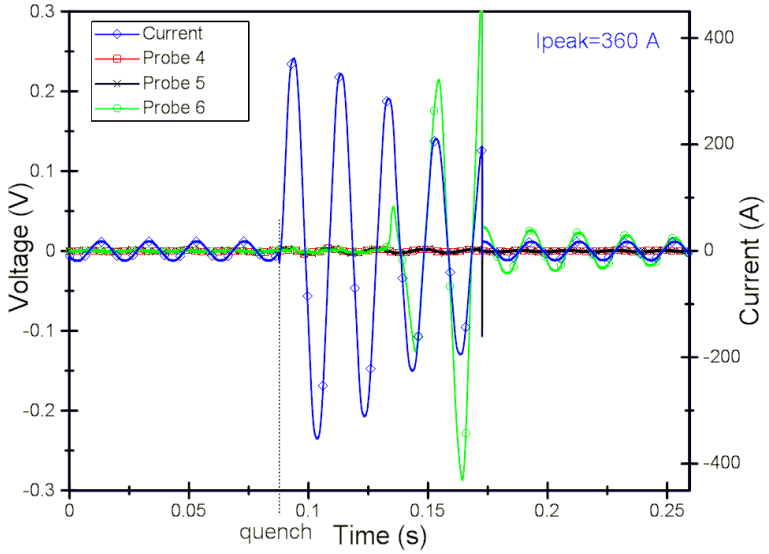

Fig. 4.60. Voltage on sensors No 4, 5, 6 and current in tape versus time (I_{peak}=360 A, I_{peak}/I_c=1.33)

Because the temperature of the segment 6 was the highest the photodiodes gave a clear signal and the registered voltage surmounted the limit of 5 V set in NI DAQ board (Fig. 4.61).

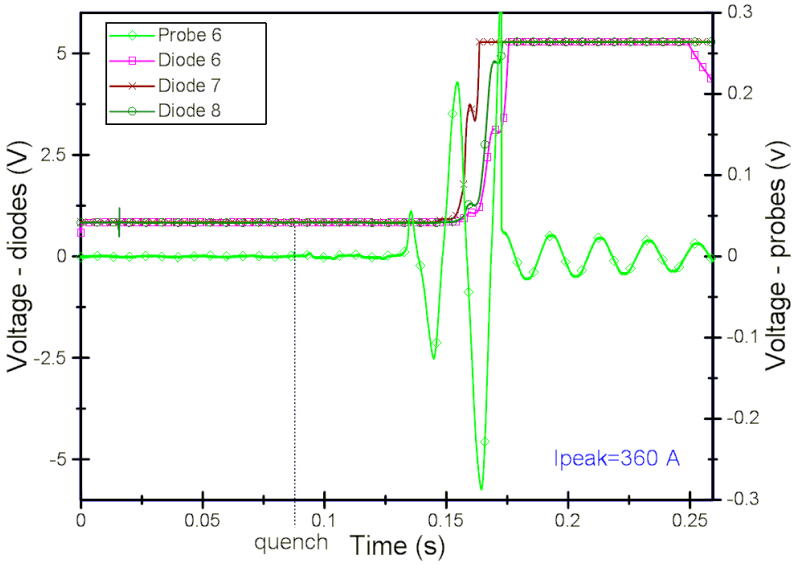

Fig. 4.61. Voltage on sensor No 6 and diodes 6,7,8 voltages versus time (I_{peak}=360 A, I_{peak}/I_c=1.33)

Another performed experiment was conducted to check the influence of photodiode viewing angle and surrounding source insulation on the measuring results. The measurements were made with SFH203FA photodiodes fitted in black plastic casings (Fig. 4.62).

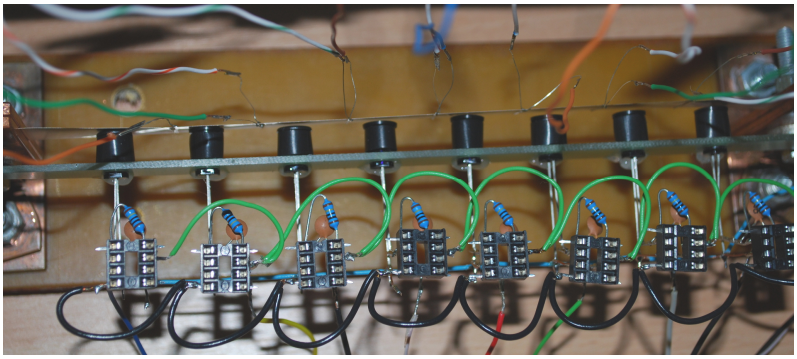

Fig. 4.62. HTS 2G tape and SFH203FA photodiodes in casings set in for measuring

According to the silicone photodiode manufacturer, the viewing angle of the SFH203FA photodiode is equal to 40 degrees (Table 4.5) [112].

Table 4.5 SFH203FA photodiodes parameters [112]

Datasheets	SFH 203(FA)
Product Photos	SFH203FA, SFH313FA
Catalog Drawings	SFH Opto Side SFH Opto Top
Standard Package	1,000
Category	Sensors, Transducers
Family	Optical - Photo Detectors - Photodiodes
Series	-
Wavelength	900nm
Color - Enhanced	-
Spectral Range	800nm ~ 1100nm
Diode Type	PIN
Responsivity @ nm	0.59 A/W @ 850nm
Response Time	5ns
Voltage - DC Reverse (Vr) (Max)	50V
Current - Dark (Typ)	1nA
Active Area	1mm²
Viewing Angle	40°
Operating Temperature	-40°C ~ 100°C
Package / Case	Radial
Dynamic Catalog	BP 104 FAS-Z and SFH
Other Names	475-1075 Q62702P0956 SFH 203 FA

Photodiode and HTS tape distance was equal to 3 mm. The measurement area of photodiode chip can be obtained by projecting the cone, which forms an angle of 40 degrees on the surface of the HTS tape (Fig. 4.63),). In this case, the diameter of the measurement area is equal to about 5.68 mm. It can thus be assumed that the photodiode has only recorded signals emitted from the measurement area of the tape surface when tape height was equal to 12 mm.

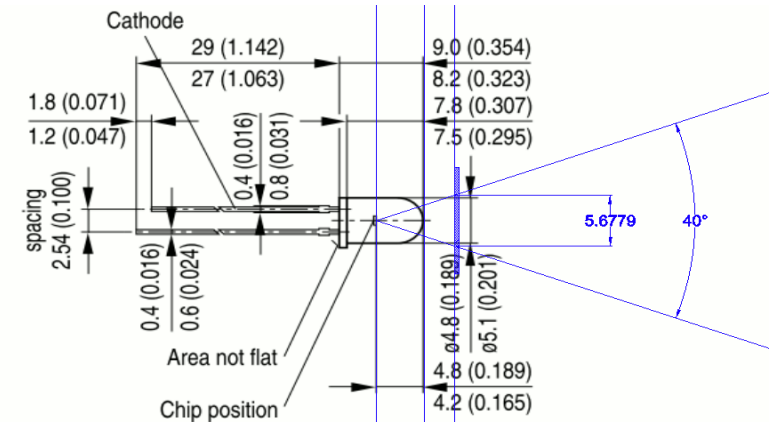

Fig. 4.63. Photodiode dimensions and measuring area marked as a circle with diameter equal to 5.6779 mm on the HTS tape marked as blue square

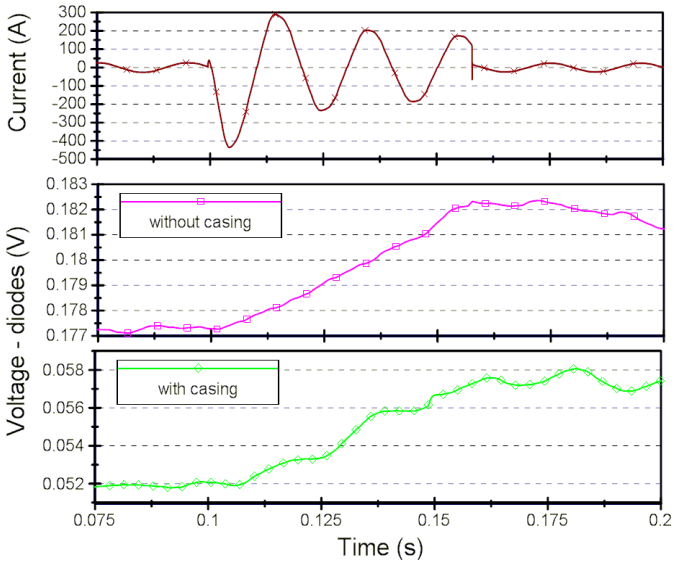

Fig. 4.64. Voltage versus time of photodiode No. 6 in casing and without casing, quench current amplitude I_{peak}=429 A

The results of measurements are presented in Fig. 4.64. Registered voltage has bigger value in the case of photodiodes set without the casing. The shape of the no casing photodiode voltage curve is smoother. However, difference between the maximum and the minimum voltage value is similarin both cases, and is equal to about 6 mV. Photodiodes without casing are a better choice for photodiode measuring systems due to the fact that they produce a higher level of voltage, as well as resulting in a smoother voltage curve.

Taking the above results into account, it can be concluded that it is possible to register changes of temperature in the HTS thin layer tape with IR photodiodes. However, further research in this area is required.

5. Conclusions

The dissertation presents transient state analysis of chosen superconducting devices with the use of FEM method and object oriented programming. It is important to investigate the transient behaviour of electrical superconducting devices since it may be subjected to various kinds of high voltage stresses caused by system disturbances, disconnecting operations or lightning strikes. Developed models allow for the designation of critical parameters of devices with high temperature superconductors. The researched group of devices has been limited to those which can be modelled using planar or axisymmetric geometry. The calculations have been performed for the following devices chosen: superconducting fault current limiter, current lead made of bulk BSCCO high temperature superconductor, current lead made of 2G HTS tape, second generation thin layer HTS wire.

The main problems encountered during the creation of numerical models of current flow, transient magnetic and heat transfer were presented. Particular emphasis is placed on modelling of the second generation thin-film tapes and their accurate energy representation in the scale factor models.

Algorithms of coupled problems of current flow, transient magnetic and heat flow for contact cooling and cryogenic liquid bath cooling were developed. On the basis of developed algorithms, hybrid numerical models have been elaborated. The hybrid models allow for determination of changes in the critical parameters in transient states of chosen superconducting devices.

The models take into account the non-linear dependency of the critical current and critical magnetic field on the temperature.

Calculation of transients in superconducting devices allows for better design that takes into account narrower margins of safety.

Numerical hybrid model has been developed for transient state consideration of HTS thin layer tapes. This model explores the real critical parameter characteristics of HTS material. Transport current dependency on time, temperature and intensity of electric field was taken into account in the model.

The developed model is used to analyze the stability of the HTS tape in liquid nitrogen cooling in short circuit current conditions. The results reveal that in some cases it is possible to maintain short term stable operation during overcurrents with peak values higher than the critical current and the temperature rise of several degrees.

Experimental results show that the hybrid model has provided accurate predictions of changes of critical parameters in transient states for the HTS wire, and a good prediction of transients in the current lead made of thin layer HTS tapes.

For the commercially available current lead made of Bi 2223 tube, impact of the location of the disorder and its energy on the nonstationary temperature distribution was studied. Transition temperature and density of the thermal

power were also explored. Influence of structural solutions and manner of cooling of the current lead on courses of maximum temperature was also examined; this allowed for an evaluation and determination of conditions necessary for stable operation of the device.

It is shown that the second generation thin layer HTS tapes can be analysed whilst treated as a factor scaled with anisotropic resistivity and heat conductivity. Power losses generated in transient states due to the transport current have the same values in real scale model and factor scale model.The temperature distribution along the tape is almost the same in both models; however, the maximum relative error achieved is about 4% in the factor scale model comparing to 3% in real scale model. The tape model was factor scaled to reduce the computational time. Both models were compared and a good agreement was found.

The agreement carried out for the measurement of changes of critical parameters of the HTS tape in transient states allowed for the registration of *V-I* characteristics of individual segments of the tape. Registered quantities enabled to appoint momentary (quick) changes of the power and temperature in the explored piece of the 2G superconducting tape. The tape isn't going over in the homogeneous way to the resistive state when the fluctuation of the current is not much greater than the critical current value. Based on the performed measurements, it is possible to state that it is only above the value of 1.5 of critical current value, that the whole tape loses its superconductive state, even though the loss of superconductivity does not take place all at the same time in the first sine period.

When the factor causing an exit from superconducting state is local temperature rise in the tape, the resistive zone extends to the adjacent parts. The speed of resistive zone propagation is dependent on the temperature of the local hot spot, and the amplitude of current flowing through the 2G HTS tape.

In course of the experimental measurements the electrical parameters of assembly were recorded and the results were used to verify the developed hybrid numerical models.

A measurement system using silicone photodiodes with infrared filter for registration of dynamic changes of temperature of thin-layer HTS tape was also developed. The study confirmed validity of the chosen concept of measurement system that meets the established requirements for temperature measurement. The system allows for recording of temperature changes in the HTS tape in cryogenic conditions and transient states.

The measuring system based on photodiodes is a prototype, so the solutions adopted and the experience gathered can be the basis for an industrial system elaboration.

Experimental studies carried out throughout the research period have shown the correctness of the numerical models developed to simulate the transient

states in superconducting devices with elements built of high-temperature superconductors.

Use of the developed hybrid computer models of dynamic disappearance of superconductivity has allowed for quantification of the influence of temperature, working current, and properties of the impulse disturbing superconductivity on the parameters of thermal stability of the relay tracts and superconductive winding.

Results of research on the developed hybrid numerical models validated by experimental studies allow for concluding that object-oriented programming in LUA linked to FEM solvers of FEMM and COMSOL environments makes it possible to reflect changes in the critical parameters during transient states of superconducting devices; this conclusion proves validity of the thesis.

The objectives of the thesis were achieved by improving the methods of calculation of superconducting device critical parameters in transient states and providing a system for measuring rapid changes in temperature in the HTS tape.

The most important achievements of the thesis may be classified as:

- development of algorithms for calculation of the coupled problems of current, and electromagnetic and thermal fields in superconducting devices cooled with cryogenic liquid or cryocooler,
- completion of numerical calculations of space-time distribution of temperature, current and thermal power density in YBCO thin film conductors of the second generation during transient states,
- investigation of the velocity of propagation of the resistive zone for different structural solutions of current leads made of HTS superconductor and various ways of cooling,
- examination of the rate of resistive zone decay for different solutions of current leads made of solid BSCCO 2223 superconductor and various ways of cooling,
- development of author's programs cooperating with COMSOL and FEMM utility applications (codes), which allowed for creating hybrid computational models coupling thermal, electromagnetic and flow fields with oneself,
- development of cluster computing platform for high-throughput calculations conducted in COMSOL environment,
- development of mathematical and numerical models for calculations of thin-film systems in transient states based on the second generation superconducting tapes using non-uniform scale factors,
- investigation of the influence of modelling with non-uniform scaling factor for the results and its verification with the results of measurements,

- development and implementation of author's acquisition system for measuring electrical parameters of HTS superconducting second generation tapes and measurement of transient states,
- examination of the influence of the amplitude value of the current flowing through the tape in transient states on the speed of propagation of the resistive zone and value of the maximum temperature reached,
- development and implementation of author's measurement system based on infrared silicon photodiodes for recording changes in temperature of 2G HTS tape during transient states,
- conducting measurements of temperature distribution and dynamics of changes in thin superconducting tapes in transient states using the designed measurement system and verification of the results.

Presented in this dissertation results provides a potential for further research, which can be done in modelling of critical parameters of high temperature superconducting devices in transient states. The future research topics can cover the applicatrions of hybrid models for devices modelling with 3D geometries.

The use of power law assumes the uniform changes of high temperature superconducting material resistivity (the power factor n is the same for given superconductor), however the measurement results show that in some conditions the change of HTS resistivity is non-uniform. Another research can be done on implementation of the heterogeneous changes of resistivity in models and random changes of power factor that depends on superconductor's material.

The developed measurement system with infra-red photodiodes can be further evolved and find industrial applications.

6. References

[1] Abrahamsen A.B., Mijatovic N., Seiler E, Zirngibl T., Træholt C., Nørgard P. B., Pedersen N. F., Andersen N. H., Ostergard J., "Superconducting wind turbine generators", Superconductor Science And Technology, vol. 23, 2010

[2] Alferov D., Budovsky A., Dul'kin I., Fisher L., Ivanov V., Sidorov V., Shul'ga R., Tshay E., Yevsin D., "Study of superconducting fault current limiter model with AC circuit-breaker", IEEE/CSC & ESAS European Superconductivity News Forum (ESNF), No. 11, pp. 1-8, January 2010

[3] Anderson P.W., "The resonating valence bond state in La_2CuO_4 and superconductivity", Science 235, pp. 1196–1198, 1987

[4] Baldan C.A., Shigue C.Y., Ruppert F.E., "Fault Current Test of a Bifilar Bi-2212 Bulk Coil", IEEE Transactions On Applied Superconductivity, vol. 18, issue 2, pp. 664-667, 2008

[5] Bardeen J.; Cooper L. N., Schrieffer J. R, "Microscopic Theory of Superconductivity", Physical Review 106, pp. 162–164, 1957

[6] Bauer P., "HTS technology leads the way", Superconductor Systems and Auxiliaries Section ITER, http://www.iter.org/newsline/169/652, 2011

[7] Bednorz J. G., Müller K. A., "Possible high Tc superconductivity in the Ba-La-Cu-O system", Zeitschrift für Physik B, Vol. 64, p. 189-193, 1986

[8] Benesty J., Chen J. Huang Y.A., "On the Importance of the Pearson Correlation Coefficient in Noise Reduction", IEEE Transactions on Audio, Speech and Language Processing, Vol. 16,I.4, pp. 757 – 765, 2008

[9] Bergallo, M. Neumana C., Sonzogni V., "Composite mesh concept based FEM error estimation and solution improvement", Computer Methods in Applied Mechanics and Engineering, vol. 188, issue 4, pp. 755-774, 2000

[10] Bluzer N., "Temporal relaxation of nonequilibrium in YBaCu-0 measured from transient photoimpedance response", Physical Review, vol. B44. pp. 10222-10333, 1991

[11] Bock J., "Nadprzewodnikowe ograniczniki prądu zwarciowego", Elektro-energetyka, No. 4, pp. 67-73, 2010

[12] Bock J., Breuer F., Walter H., Elschner S., Kleimaier M., Kreutz R., Noe M., "CURL10 : development and field test of a 10 kV / 10 MVA resistive current limiter based on bulk MCP BSCCO 2212", IEEE Transactions On Applied Superconductivity, Vol. 15, 1955-60, 2005

[13] Boehman L., Schauer J., Harold J., Stevenson T., „Cryogenic Liquid Heat Transfer Analysis", Aerospace Structures Information And Analysis Center, August 1987

[14] Bogdanov I., Kozub S., Myznikov K., Slabodchikov P., Sychev V., Sytnik V., Vassiliev L., Zubko V., Akimov I., Gryaznov N., Rakom D., Shikov

A., "Application of HTS Bi-2223 for current leads of superconducting magnets", Proceedings of EPAC 2000, Vienna, Austria

[15] Bohno T., Tomioka A., Imaizumi M., Sanuki Y., Yamamoto T., Yasukawa Y., Ono H., Yagi Y., Iwadate K., "Development of 66 kV/6.9 kV 2 MV A prototype HTS power transformer", Physica C: Superconductivity, Vol. 426–431, Part 2, pp. 1402–1407, 2005

[16] Bradji A., Holzbecher E., "On the convergence order of COMSOL Solutions", COMSOL Conference, Grenoble, France, 23.-24. Oct., 2007

[17] Bugoslavsky Y., Perkins G. K., Qi X., Cohen L. F., Caplin A.D., "Vortex dynamics in superconducting MgB_2 and prospects for applications", Nature 410, pp. 563-565, 2001

[18] Manufacturer information materials, Can Superconductors, 2002-2012

[19] CAN Superconductors s.r.o, CAN current leads, http://www.can-superconductors.com/products/current-leads, viewed 2012

[20] Cha Y.S., Evans D.J., Hull J.R., "Measurement of critical current and transient characteristics of a high-temperature superconductor tube with a pulsed current supply", IEEE Transactions on Applied Superconductivity, vol. 9, Issue.2, pp. 1320-1323, 1999

[21] Chang K.S., Jang J.Y., Choi S.J., Jo H.C., Kim Y.J., Ahn M.C., Kim H.M., Ko T.K., "A Structure Design of HTS Current Leads With Respect to the Structure of Coated Conductor and the Current Terminal", IEEE Transactions on Applied Superconductivity, vol. 21, Issue.3, pp. 3013, 2011

[22] Chen X. Jin J., "Development and Technology of HTS Transformers", Research Communication, Vol. 1, No. 1, pp 2.1-2.7, 2007

[23] Chen M., Paul W., Lakner M., Donzel L., Hoidis M., Unternaehrer P., Weder R., Mendik M., "6.4 MVA resistive fault current limiter based on Bi-2212 superconductor", Physica C vol. 372-376, pp. 1657-1663, 2002

[24] Chybczyńska K., Wróblewski M., Wawrzyniak M., Susła B., "Conductance Quantization in Nb-Ti/Cu Alloys and BiSrCaCuO/PbAg Superconducting Tapes", Przegląd Elektrotechniczny, R. 88, Vol. 10b, pp. 132-134, 2012

[25] Cieplak M., Adamus Z., Konczykowski M., Cheng X. M., Byczuk A., Abal'oshev A., Sang H., Chien C. L., "Superconducting pinning by magnetic domains in a ferromagnet-superconductor bilayer", Acta Physica Polonica A 106, pp. 693-698, 2004

[26] Cieśla A., "Use of the high temperature superconductors (HTS) to the magnetic separation", International Journal of Applied Electromagnetics And Mechanics, Vol. 25, I. 1-4, pp. 83-87, 2007

[27] Cieśla A., "Nadprzewodnictwo w stulecie odkrycia: wybrane przykłady zastosowań", Przegląd Elektrotechniczny, Vol. 87, I. 12a, pp. 1-6, 2011

[28] Cieśla A., "Use of the low (LTS) and high (HTS) termperature superconductors in the magnetic separation. Economic comparison", Przegląd Elektrotechniczny, Vol. 87, I. 3, pp. 21-24, 2011
[29] Citver G., Barzi E., Burov A., Feher S., Limon P., Peterson T., "Steady State and Transient Current Lead Analysis", IEEE Transactions on Applied Superconductivity, vol. 9, no. 2, 1999
[30] Comsol Group, "Running COMSOL in parallel on clusters", Comsol Knowledgebase, http://www.comsol.com/support/knowledgebase/1001/, 2013
[31] Cyrot M., Pavuna D., "Wstęp do nadprzewodnictwa. Nadprzewodniki wysokotemperaturowe", Wydawnictwo Naukowe PWN, Warszawa, 1996
[32] Czerwiński D., Goleman R., Giżewski T.: "Equivalent electromagnetic and circuit model for HTS current leads", 6th International Conference: Electromagnetic Devices and Processes in Environment Protection, Nałęczów, 24-27 June 2008
[33] Czerwiński D., Giżewski T., "Histereza magnetyczna w nadprzewodnikach wysokotemperaturowych", Przegląd Elektrotechniczny, pp. 619-622, nr 9, 2003
[34] Czerwiński D., Giżewski T., "Numerical Analysis of Magnetic Hysteresis Losses in High Temperature Superconductors", 4th International Conference: Electromagnetic Devices and Processes in Environment Protection - ELMECO-4, Nałęczów, Poland, September 21-24, 2003
[35] Czerwiński D., "Wykorzystanie modelu Preisacha do odwzorowania pętli histerezy w nadprzewodnikach HTS", VI Seminarium i Warsztaty: Zastosowania Nadprzewodników, Kazimierz Dolny, str. 15, 16 – 18 czerwca 2005
[36] Czerwiński D., Jaroszyński L., "Analiza numeryczna pola elektromagnetycznego w taśmach HTS z uwzględnieniem zjawiska histerezy", VII Seminarium i Warsztaty "Zastosowania Nadprzewodników", Kazimierz Dolny, str. 132 – 138, 1 – 3 czerwca 2006
[37] Czerwiński D., Jaroszyński L., "Modelowanie numeryczne elementów nadprzewodnikowych", VIII Seminarium i Warsztaty Zastosowania Nadprzewodników Nałęczów, str. 112-121, 2008
[38] Czerwiński D., Jaroszyński L. "Analiza numeryczna pola elektromagnetycznych w przepustach prądowych HTS z uwzględnieniem zjawiska histerezy", VIII Seminarium i Warsztaty Zastosowania Nadprzewodników Nałęczów, str. 122-128, 2008
[39] Czerwiński D., "Equivalent electromagnetic and circuit model for HTS current leads", Przegląd Elektrotechniczny, r. 88, nr 2, pp. 161-164, 2012
[40] Czerwiński D., "Numerical performance in the grid network relies on a Grid-Appliance", Springer Computer Networks CCIS series, 2011, Volume 160, pp. 214-223, 2011

[41] Czerwiński D., Przyłucki S., Sawicki D., "Wydajność systemów operacyjnych w środowiskach wykorzystujących wirtualizację", ang. „Operating systems efficiency in virtualization environments", Studia Informatica, Vol. 32, nr 3A, pp. 125-134, 2011
[42] Dirks J.A., "High-temperature superconducting transformer performance, cost, and market evaluation", Pacific Northwest Laboratory Report PNL-7318, 1993
[43] Fairweather G., Lin Q., Lin Y., Wang J., Zhang S., "Asymptotic Expansions and Richardson Extrapolation of Approximate Solutions for Second Order Elliptic Problems on Rectangular Domains by Mixed Finite Element Methods", SIAM Journal on Numerical Analysis, Vol. 44, No. 3, pp. 1122-1149, 2006
[44] Fieller E.C., Hartley H.O., Pearson E.S., "Tests for Rank Correlation Coefficients", Biometrika, Vol. 44, No. ¾, pp. 470-481, 1957
[45] Ford, P. J., "The Rise of the Superconductors.", CRC Press, 2005
[46] Gerber A., Li J. N., Tarnawski Z., Franse J. J. M., Menovsky A., "Magnetic instabilities in high-temperature superconductors under rapidly varying magnetic fields", Physical Review B (Condensed Matter), Vol. 47, Issue 10, pp.6047-6053, 1993
[47] Ginsberg D.M at all, "Physical Properties of High Temperature Superconductors", World Scientific, Technology & Engineering, 1994
[48] Glowacki B.A., "Niobium aluminide as a source of high-current superconductors", Intermetallics, 7, pp. 117-140, 1999
[49] Goddard K., Łukasik B., Rotaru M., Sykulski J., "Design study of a high temperature superconducting generator with YBCO windings", Przegląd Elektrotechniczny, 2010, nr 5
[50] Gömöry F., Šouc J., Fabbricatore P., Farinon S., Strýček F., Kováč P., Hušek I., "Magnetic hysteresis loss in Bi-2223/Ag tapes with different filament arrangement", Physica C, Volume 371, Issue 3, pp. 229-236, 2002
[51] Gouge M., Schwenterly S., Hazelton D., "Design, Fabrication and Testing of a Superconducting Fault Current Limiter (SFCL)", CRADA Final Report For CRADA Number ORNL-03-0683, 2011
[52] Goyal A., "Second-Generation HTS Conductors", Kluwer Academic Publishers, 2005
[53] Graja A., „Niskowymiarowe przewodniki organiczne", Warszawa WNT, 1989
[54] Gubser D., Miller M., Toth L., Rayne R., Lawrence S., "Superconducting current leads of YBCO and Pb-BSCCO", IEEE Transactions on Magnetics, vol. 27, pp. 1854-1857, 1991
[55] Hamrick J., "HTS power cable project update", Superconductivity News Update, November 2008

[56] Hazelton D. W., Selvamanickam V., "SuperPower's YBCO Coated High-Temperature Superconducting (HTS) Wire and Magnet Applications", Proceedings of The IEEE - PIEEE , vol. 97, no. 11, pp. 1831-1836, 2009

[57] Hegmann F., Hughes R., Preston J., "Picosecond photoresponse of epitaxial $YBa_2Cu_30_7$ thin films", Applied Physics Letters, vol. 64, pp. 3172-3174, 1994

[58] Heller R., Fietz W.H., Lietzow R., "Status of the High Temperature Superconductor Current Lead Development at the Research Centre Karlsruhe", IEEE/CSC & ESAS European Superconductivity News Forum, No. 3, pp. 1-7, 2008

[59] Hemmi T., Ninomiya A., Ishigohka T., Kurahashi K., Arai K., Yamaguchi H., Umeda M., Kaiho K., "Transient behavior of Bi2223/Ag HTS tape for sharp rising current", IEEE Transactions on Applied Superconductivity, vol. 12, no. 1, pp. 1422-1425, 2002

[60] Hillebrand J., "The Magnetic Levitation Train: A Technology Ahead of Its Time?", GRIN Verlag, 2008

[61] Holzbecher E., Si H., "Accuracy Tests for COMSOL - and Delaunay Meshes" European COMSOL Conference, Hannover, 2008

[62] Hutchcraft W.E., Gordon R.K., "Reduction of truncation error using Richardson extrapolation in the finite difference and finite element analysis of one dimensional electrostatics problems" Conference Proceedings - IEEE SOUTHEASTCON, Compendex, pp. 140-143, 1996

[63] Jänicke L., Kost A., "Convergence Properties of the Finite Element Method", IEEE Transactions on Magnetics, vol. 35 , pp. 1414-1417, 1999

[64] Janowski T., Stryczewska H. D., Kozak S., Malinowski H., Wojtasiewicz G., Surdacki P., Kondratowicz-Kucewicz B., Kozak J.: "Nadprzewodnikowe ograniczniki prądu", LIBER, Lublin, 2002

[65] Janowski T., Kozak S., Kondratowicz-Kucewicz B., Wojtasiewicz G., Kozak J., "Analysis of Transformer Type Superconducting Fault Current Limiters", IEEE Transactions on Applied Superconductivity, vol.17 i.2, pp. 1788-1790, 2007

[66] Jirsa M., P&Ust L., Dlouhý D., Koblischka M. R, "Fishtail shape in the magnetic hysteresis loop for superconductors: Interplay between different pinning mechanisms", Physical Review B, Vol. 55, Issue 5, pp.3276-3284, 1997

[67] Kajikawa K., Hayashi T., Yoshida R., Iwakuma M., Funaki K., "Numerical Evaluation of AC Losses in HTS Wires with 2D FEM Formulated by Self Magnetic Field", IEEE Transactions on Applied Superconductivity, vol.13 i.2, pp. 3630-3633, 2003

[68] Kalsi S., "Development Status of Superconducting Rotating Machines", IEEE PES Meeting, New York, 2002

[69] Kalsi S., "The State of Superconducting Technology", presented at US Naval Graduate School Monterey, California, March 2005

[70] Karasik B., Milostnaya I., Zorin M., Elantev A., Gol'tsman G., Gershenzon E., "High Speed Current Switching of Homogeneous YBaCuO Film Between Superconducting and Resistive States", IEEE Transacitons on Applied Superconducitvity, vol. 5, no. 2, 1995

[71] Kim S., Ishiyama A., "Transient stability analysis in Bi-2223/Ag superconducting tapes", IEEE Transacitons on Applied Superconducitvity, vol. 7, no. 2,pp. 203-206, 1997

[72] Kovalev L.K., Ilushin K.V., Penkin V.T., Kovalev K.L., Koneev S.M.-A., Modestov K.A., Larionoff S.A., Gawalek W., Oswald B., "Electrical machines with bulk HTS elements.: The achieved results and future development", Physica C, 357-360, pp. 860-865, 2001

[73] Kozak S.: „Numerical model of superconducting fault current limiter", Przegląd Elektrotechniczny, R. LXXX 11, str. 1101-1105, 2004.

[74] Kozak S., Janowski T., Wojtasiewicz G., Majka M., Kozak J., "The HTS winding of 15 kV class inductive SFCL", IEEE Transaction on Applied Superconductivity, Vol. 20, no 3, pp: 1203 – 1206, 2010

[75] Kozak S., Wojtasiewicz G., "Wybrane zastosowania nadprzewodnictwa w energetyce", XXIV-SPETO, pp. 131-134, 2001.

[76] Kozak S., Wojtasiewicz G.: „Pomiary charakterystyk statycznych modelu nadprzewodnikowego ogranicznika prądu typu indukcyjnego", III Seminarium Zastosowania Nadprzewodników Lublin-Nałęczów 2001

[77] Krabbes G., Fuchs G., Canders W.-R., May H., Palka R., "High Temperature Superconductor Bulk Materials", Wiley, New York, 2006

[78] Kreutz R., Bock J., Breuer F., Juengst K.P., Kleimaier M., Klein H.U., Krischel D., Noe M., Steingass R., Weck K.H., "System Technology and Test of CURL 10, a 10 kV, 10 MVA Resistive High Tc Superconducting Fault Current Limiter", IEEE Transactions On Applied Superconductivity, Vol. 15, No. 2, 2005

[79] Krosny S., Woźniak M., Hopkins S., Stępień M., Grzesik B., Glowacki B., "Modelling of transient state phenomena of composite superconducting conductors during pulse Ic(B) measurements", Journal of Physics: Conference Series, vol. 234, part 2, pp 1-8, 2010

[80] Kujur A., Behera D., "DC electrical resistivity and magnetic studies in Yttrium Barium Copper oxide/barium titanate composite thin films", Elsevier Thin Solid Films 520, pp. 2195–2199, 2012

[81] Łanczont M., Janowski T., "Analiza działania nadprzewodnikowych ograniczników prądu, Technologie nadprzewodnikowe i plazmowe w energetyce", Lubelskie Towarzystwo Naukowe, ISBN: 978-83-61391-76-9, Lublin 2009

[82] Larbalestier D., Blaugher R., Schwall R., Sokolowski R., Suenaga M., Willis J., "Power Applications of Superconductivity in Japan and Germany", WTEC Panel Report September 1997, http://www.wtec.org /loyola/scpa/toc.htm, last viewed 2012

[83] Larbalestier D, Gurevich A, Feldmann DM, Polyanskii A., "High-Tc superconducting materials for electric power applications", Nature 414(6861), pp. 368–377, 2001
[84] Lee C., Soek B., "Design of the 3 Phase 60 MVA HTS Transformer With YBCO Coated Conductor Windings" IEEE Transactions on Appl. Supercond., vol. 15, no. 2, pp. 1867–1870, 2005
[85] Lee S., Byun S., Kim W., Lee J., Choi K., "Design of a Single Phase 33 MVA HTS Transformer With OLTC", IEEE Transactions on Appl. Supercond., vol. 17, no. 2, pp. 1939–1942, 2007
[86] Leonard R.B., "Thermal Stability of Hastelloy Alloy C-276", Corrosion, Vol. 25, No. 5, pp. 222-232, 1969
[87] Leszczyński J., Korzeniowska E., "Model Beana a Krytyczna Gęstość Prądu w Masywnym Nadprzewodniku Ceramicznym", 3th Seminar and Workshop „Applications of Superconductors AoS-3", pp. 21-30, Lublin – Nałęczów, 22-23.11.2001
[88] Leszczyński J., "Zjawiska ekranowania i transformacji w nadprzewodnikach", 6th Seminar and Workshop „Applications of Superconductors AoS-6", Kazimierz Dolny, 16 – 18.06.2005
[89] Lindgren M., Trifonov V., Zorin M., Danerud M., Winkler D., Karasik B., Gol'tsman G., Gershenzon E., "Transient resistive photoresponse of YBa2Cu307 films using low power 0.8 and 10.6 mm laser radiation", Applied Physics Letters, vol. 64, pp. 3036- 3038, 1994
[90] Lombardo V., Barzi E., Turrioni D., Zlobin A. V., "Critical Currents of YBa2Cu3O7-δ Tapes and Bi2Sr2CaCu2Ox Wires at Different Temperatures and Magnetic Fields", IEEE Transactions On Applied Superconductivity, Vol. 21, No. 3, pp. 3247 - 3250, 2011
[91] Lu J., Choi E. S., Zhou H. D. " Physical properties of Hastelloy® C-276™ at cryogenic temperatures", Journal Of Applied Physics 103, 064908, pp. 064908.1–064908.6, 2008
[92] "Brookhaven Lab Retirees Win Benjamin Franklin Medal For Their Invention of Magnetically Levitated Trains", Brookhaven National Laboratory, 18 April 2000
[93] Majka M., Kozak S., "Zastosowanie taśm I i II generacji do budowy nadprzewodnikowych ograniczników prądu", Przegląd Elektrotechniczny, 2009, nr 5
[94] Majoros M., Tomov R., Glowacki B., Campbell A., Oberly C., "Hysteresis Losses in YBCO Coated Conductors on Textured Metallic Substrates", IEEE Transactions On Applied Superconductivity, Vol. 13, No. 2, pp. 3626-3629, 2003
[95] Makeer D., "Finite Element Method Magnetics Users Manual", 2010
[96] Malandrino G., Nigro R.L., Fragalà I.L., "MOCVD of Platinum (100) Films on Random Hastelloy C276", Chem. Vap. Deposition, vol. 5: pp. 59–61, 1999

[97] Mehairjan V., Popov M., Geschiere A., Kling W., "Transient analysis of a 150 kV fault current limiting high temperature superconducting cable", Proceedings of the International Conference on Power Systems Transients (IPST 2011), Delft, The Netherlands, 2011
[98] Metha S. P., Aversa N., Walker M. S., "Transforming Transformers", IEEE Spectrum-Superconductivity in Electric Power, pp.43–49, 1997
[99] Mikkonen R., "Highlights of S.C. Power Applications in Europe", IEEE Transactions on Applied Superconductivity, vol. 12, no. 1, pp. 782-787, 2002
[100] Minami M., Nagaya S., Kawashima H., "A trial manufacturing of lkWh flywheel with high temperature superconducting magnetic bearing for energy storage system", T. IEE Japan, Vol. 120-D, No. 10, pp 1220 – 1224, 2000
[101] Morawski A., Łada T., Presz A., Mazur T., Diduszko R., Zaleski A., Przybylski K., Bodoardo S., Dellaroca V., "Nano-SiC doped MgB_2 bulk superconductor with T_c over 42K by high gas pressure", Przegląd Elektrotechniczny 11, pp. 1125-1128, 2004
[102] Motowidlo L., Selvamanickam V., Galinski G. , Vo N., Haldar P., Sokolowski R., "Recent progress in high-temperature superconductors at Intermagnetics General Corporation", Physica C, vol 335 pp. 44-50, 2000
[103] Nakashima H., Isoura K., "The test results and plan of Maglev development in Japan", MAGLEV '2000, June 2000
[104] Narumi E., Song L., Yang F., Patel S., Kao Y., Shaw D., "Superconducting YBa2Cu3O6.8 films on metallic substrates using in situ laser deposition", Applied Physics Letters ,Vol. 56, I.26, pp. 2684-2686, 1990
[105] Navigant Consulting, Burlington, MA, United States of America http://www.navigantconsulting.com, viewed 2012
[106] "Nexans goes live on grid with world's first fault current limiter based on second-generation superconductors", Press release, Nexans 2012
[107] National Instruments: PCI Multifunction Data Acquisition, http://sine.ni.com/nips/cds/view/p/lang/en/nid/209158, viewed 2012
[108] Lab View Measurements Manual, National Instruments 2011
[109] Nguyen D.N., Sastry Pamidi V.P.S.S., Schwartz, J., "Numerical calculations of the total ac loss of Cu-stabilized $YBa_2Cu_3O_{7-\delta}$ coated conductor with a ferromagnetic substrate", Journal of Applied Physics, Vol. 101, I. 5, pp. 053905 - 053905-9, 2007
[110] Noe M., "Superconducting Fault Current limiters (SCFCLs)", Summer School on Materials and Applications on Superconcuctivity, Karlsruhe, Germany, Institute For Technical Physics, July 23-27, 2007
[111] Ogawa J., Shiokawa M., Ciszek M., Tsukamoto O., "AC losses in YBCO coated conductors carrying AC transport currents in perpendicular AC external magnetic field", IEEE Transactions On Applied Superconductivity, Vol. 13, No. 2, pp. 1735 – 1738, 2003

[112] SFH203FA Datasheet, Osram Semiconductors Inc, 2012
[113] Pająkowski J., „Zachowanie fotodiody w niskiej temperaturze", Elektronika nr 6, pp. 30-32, 2012
[114] Palka R., "Modelling of High Temperature Superconductors and Their Practical Applications", International Compumag Society Newsletter, Vol. 12, No. 3, pp. 3–12, Nov. 2005
[115] Pałka R., "Zastosowanie monolitycznych nadprzewodników wysokotemperaturowych w maszynach elektrycznych", Prace Naukowe Instytutu Maszyn, Napędów i Pomiarów Elektrycznych, pp. 118-123, 2008
[116] Patel A., Pałka R. Głowacki B., "New bulk – bulk superconducting bearing concept using additional permanent magnets", Przegląd Elektrotechniczny (Electrical Review), R. 88 NR 6, pp. 108-110, 2012
[117] Patel A., Palka R. Glowacki B.A., "New fully superconducting bearing concept using the difference in irreversibility field of two superconducting components", Superconductor Science and Technol., 24 (1) 015009, 2011
[118] Petranovic R., Miri A., "Modeling of the Transient Behavior of a Resistive Type High Tc Fault Current Limiter", IEEE Transactions on Applied Superconductivity, vol. 13, no. 2, 2003
[119] Plechacek V. Hejtmanek J., "Properties of superconducting Bi-2223 tubular current leads", Physica C: Superconductivity, pp. 2577–2578, 1997
[120] PN-IEC 60050-815:2002 – Międzynarodowy Słownik Terminologiczny Elektryki – Część 815: Nadprzewodnictwo
[121] Specyfikacja taśmy SF12050 produkcji SuperPower dostępna w Pracowni Technologii Nadprzewodnikowych w Lublinie, 2011
[122] Qin M. J.; Li G., Liu H. K., Dou S. X., Brandt E. H., "Calculation of the hysteretic force between a superconductor and a magnet", Physical Review B, vol. 66, Issue 2, pp. 024516-1 – 024516-11, 2007
[123] Rastogi A., Yamasaki H., Iijima Y., Kakimoto K., Takeda K., "Hysteresis losses in IBAD-PLD YBCO tapes in magnetic fields oriented nearly parallel to the surface", Physica C vol. 372-376, pp. 1739-1742, 2002
[124] Rose-Innes A.C., Rhoderick E.H., "Nadprzewodnictwo", PWN, Warszawa, 1973
[125] Roy F., Dutoit B., Sirois F., "Evaluation of the Applicability of Phenomenological HTS Models for Numerical Analysis of Quenches in Coated Conductors: Simulations Vs. Experiments", IEEE Transactions on Applied Superconductivity, Vol. 21(3), pp. 1190-1193, 2011
[126] Runde M., "Application of high-T_c superconductors in aluminum electrolysis plants", IEEE Transactions on Applied Superconductivity, vol.5 i.2, pp. 813-816, 1995
[127] Sakai S. Shiohara K., Ishii Y., Tachikawa K., Koizumi T., Aoki Y., Hasegawa T., Yamada Y., "Development of HTS Current Leads Prepared by the TFA-MOD Processed YBCO Tapes", IEEE Transactions on Applied Superconductivity, Volume.20, Issue.3, pp. 1714, 2010

[128] Schultz L., "SupraTrans II: Research facility for large scale HTS applications", European Conference on Applied Superconductivity 2011 (EUCAS-ISEC-ICMC), Den Haag/ Netherlands, 2011
[129] Seiler E., Frolek L., "AC loss of the YBCO coated conductor in high magnetic fields", Journal of Physics: Conference Series 97, pp.12-28, 2008
[130] Shi J., Tang Y., Xia Y., Ren L., Li J., Jiao F., "Energy Function Based SMES Controller for Transient Stability Enhancement", IEEE Transactions on Applied Superconductivity, vol. 22, no. 3, 2012
[131] Smith D.R, Fickett F. R., "Low-Temperature Properties of Silver", Journal of Research of the National Institute of Standards and Technology, Volume 100, Number 2, pp. 119–179, 1995
[132] Singh M., Fischman G., Hellmann J., Logan K., Coyle T, Hobbs L., Smith J., Sideridis C., Green M., Cook R., "Global Roadmap for Ceramic and Glass Technology", Wiley, 2007
[133] Smoliński S., "Nadprzewodnictwo zastosowania", WNT, Warszawa, 1983
[134] Sosnowski J.: Analysis of the electromagnetic losses generation in the high temperature superconductors. 22nd Seminar IC-SPETO'99, pp.129-132, 1999.
[135] Sosnowski J., Malinowski H., "Magnetic Characteristics Measurements In Htc Superconductors", Global Journal of Science Frontier Research Physics & Space Science, Vol. 12 Issue 3, pp. 1-4, 2012
[136] Sosnowski J., "Przewody nadprzewodnikowe: perspektywy zastosowań i ograniczenia", Nowa Elektrotechnika, nr 11 (75), pp. 28-32, 2010
[137] Sosnowski J., "Nadprzewodnictwo i zastosowania", Wydawnictwo Książkowe Instytutu Elektrotechniki, 2003
[138] Sosnowski J., "Kriokable nadprzewodnikowe", Wydawnictwo Książkowe Instytutu Elektrotechniki, 2012
[139] Staniszewski B., "Wymiana ciepła", Państwowe Wydawnictwo Naukowe, Warszawa 1979
[140] Stankowski J., Czyżak B., "Nadprzewodnictwo", WNT, Warszawa, 1999
[141] Steve N., Nassi M., Bechis M., Ladiè P., Kelley N., Wakefiel C., "High temperature superconducting cable field demonstration at Detroit Edison", Physica C, vol 354, pp. 49-54, 2001
[142] Sun E., Brindza P., Lassiter S., Fowler M., Xu E., "Convergence Studies of Thermal and Electromagnetic Transient Quench Analysis of 11 GeV Super High Momentum Spectrometer Superconducting Magnets in Jefferson Lab", IEEE Transactions on Applied Superconductivity, vol. 21, no. 3, pp. 2384-2387, 2011
[143] Sundling R., "First generation (1G) Bi-Sr-Ca-Cu-O wire", Advanced Energy Materials Group, 2010
[144] SuperPower wire specification SF12050

[145] SuperPower® 2G HTS Wire Specifications, http://www.superpower-inc.com, 2011
[146] Sutherland M., Hawthorn D.G., Hill R.W., Ronning F., Wakimoto S., Zhang H., Proust C., Boaknin E., Lupien C., Taillefer L., Liang R., Bonn D.A., Hardy W.N., Gagnon R., Hussey N.E., Kimura T., Nohara M., Takagi H., "Thermal Conductivity across the Phase Diagram of Cuprates: Low-Energy Quasiparticles and Doping Dependence of the Superconducting Gap", Phys. Rev. B 67, pp.174520 (11 pages), 2003
[147] Sykulski J.K., Beduz C., Stoll R.L., Harris M.R., Goddard K.F., Yang Y., "Prospects for large high-temperature superconducting power transformers: conclusions from a design study", IEEE Proceedings Electric on Power Applications, Vol.146 , I. 1, pp. 41-52, 1999
[148] Takahashi H., Igawa K., Arii K., Kamihara Y., Hirano M., Hosono H., "Superconductivity at 43 K in an iron-based layered compound LaO1-xFxFeAs", Nature 453, pp. 376-378, 2008
[149] Tanaka K., Okada M., Ohata K., Sato J., Kitaguchi H., Kumakura H., Togano K., "Fabrication of Bi-2212 ROSATwire with reduced silver content", Physica C, vol 357-360 pp. 1102-1106, 2001
[150] Tannert D. B., Larson D. C., "Electrical Resistivity of Silver Films", Physical Review, vol. 166, Issue 3, pp. 652-655, 1968
[151] Trott D., Gobbert M., "Conducting finite element convergence studies using COMSOL 4.0", COMSOL Conference Proceedings , Boston, 2010
[152] Tumański S., "Technika pomiarowa", WNT 2007
[153] Ubiquiti cable cat 6E TCL2 specification
[154] Waldram J.R.: "Superconductivity of metals and cuprates", IOP, 1996
[155] Wang J., Wang S., Zheng J., "Recent Development of High Temperature Superconducting Maglev System in China", IEEE Transactions On Applied Superconductivity, Vol. 13, No. 3, pp 2142 – 2147, 2009
[156] Waynert J. A. *et al*., "Restoration and Testing of an HTS Fault Current Controller", IEEE Trans, Appl. Superconduct., vol. 13, no. 2, pp. 1984-1987, 2003
[157] Wu M.K. *et al*., "Superconductivity at 93 K in a new mixed-phase Y-Ba-Cu-O compound system at ambient pressure", Phys. Rev. Lett. 58, pp. 908–910, 1987
[158] Yamada Y., Ishii Y., Sakai S., Shiohara K., Tachikawa K., Aoki Y., Kaneko A., Koizumi, T., Tamura H., Mito T., "HTS Current Leads Prepared by the TFA-MOD Processed YBCO Tapes", IEEE Transactions on Applied Superconductivity, vol. 21, Issue: 3, pp. 1054 – 1057, 2011
[159] Yazawa T. *et al*., "66 kV-Class High-Tc Superconducting Fault Current Limiter magnet Model Coil Experiment", IEEE Trans. Appl. Superconduct., vol. 13, no. 2, pp. 2040-2043, 2003
[160] Yildirim T., Gülseren O., "A simple theory of 40 K superconductivity in MgB_2 : first-principles calculations of Tc , its dependence on boron mass

and pressure", Journal of Physics and Chemistry of Solids 63, pp. 2201-2206, 2002

[161] Ynui Y., Tsytsumi Y., Miyashita T., Masuda S., Sakamoto T., Kakao Y., Okuyama K., "A feasibility Study and Experiments on Cryoresistive Transformer Cooled at –150°C with Fluorocarbon", IEEE Transactions on Power Apparatus and Systems, PAS-96, No 6, 1977

[162] Yumura H., Watanabe M., Ohya M., Ashibe Y., Ito H., Masuda T., Sato K., "30 m YBCO cable for the Albany HTS cable project", Journal of Physics, Conf. Ser. Vol. 97, 2008

[163] Zai Q.J., Jian X.J., "Critical current measurement and experimental comparison of 1 G and 2 G HTS tapes", International Conference on Applied Superconductivity and Electromagnetic Devices, pp. 145–149, 2011

[164] Zakrzewski K., "Kriotechnika i nadprzewodnictwo w zastosowaniu do transformatorów", Biuletyn Techniczno-Informacyjny SEP o. Łódź, Nr. 4, pp. 2-8, 2008

[165] Zaleski A., Kaczorowski D., "$ZrNi_2In$ - New Superconducting Heusler Alloy", E-MRS Fall Meeting, Symposium E, 2004

[166] Zhang G., Wang Z., Qiu M., "The Improved Magnetic Shield Type High Tc Superconducting Fault Current Limiter and the Transient Characteristic Simulation", IEEE Transactions on Applied Superconductivity, vol. 13, no. 2, 2003

[167] Zhu Y. *et al*., "Microstructure and structural defects in MgB2 superconductor", Physica C, 356, pp. 239-253, 2001

[168] Ziaja J., Mazurek B., "Physical - chemical properties of the superconductor ceramics YBa2Cu3O7-x with the dopant m-ZrO2", Przegląd Elektrotechniczny, Zastosowania Nadprzewodników ZN 5, Nałęczów, pp. 66-70, 2004

[169] Ziaja J., Mazurek, B., "Parametry krytyczne nadprzewodzącej ceramiki wysokotemperaturowej $YBa_2Cu_3O_{7-x}$ dotowanej ZrO_2", Przegląd Elektrotechniczny, R. 80, nr 11, pp. 1086-1088, 2004

[170] Zubko V., Nosov A., Polyakova N., Fetisov S., Vysotsky V., "Hysteresis Loss in Power Cables Made of 2G HTS Wires With NiW Alloy Substrate", IEEE Transactions on Applied Superconductivity, vol. 21, issue 3, pp. 988-990, 2011

7. Appendix A

SF12050ANISOTROPY.LUA

```
--define parameters for sf12050 lead in LN bath (in micrometers)
factorh=100;
tapelength=180000;
T_silverthick=2;
hastelloythick=50;
HTSthick=1;

T_silverthick_h=2*factorh;
hastelloythick_h=50*factorh;
HTSthick_h=1*factorh;


--define array of nonlinear thermal conductivity for silver
silver_thc={}
for n=1, 47 do
        silver_thc[n]={}
        for k=1,2 do
                silver_thc[n][k] = 0
        end
end

--read silver_thc array data from file
nlines=0
handle = openfile("silver_thermal_conductivity.dat", "r");

-- Process the first line
-- the "*n" tell LUA to read a whole line which contains two numbers separated by spaces
a,b = read(handle, "*n","*n");
while(a ~= nil) do
        -- do your own processing here
        -- print (a,b);
        nlines=nlines+1;
        silver_thc[nlines][1]=a;
        silver_thc[nlines][2]=b;
        --print(qln[n][1],qln[n][2]);
        a,b = read(handle, "*n","*n");
end
closefile(handle);

--silver - define function which will return thermal conductivity for given temperature
function silver_t(tempedge)
        silverTC=0;
        deltatemp=tempedge;
        if deltatemp <=0 then
                deltatemp=0
        end;
        np=47;
```

```
        for k=1,np-1 do
          a  = silver_thc[k][1];
          b  = silver_thc[k+1][1];
          at = silver_thc[k][2];
          bt = silver_thc[k+1][2];
          if deltatemp<=b then
                  break
          end;
        end
        silverTC=((deltatemp-a)*(bt-at)/(b-a))+at;
        return silverTC;
end;

--define array of nonlinear thermal conductivity for hastelloy
hastelloy_thc={}
 for n=1, 31 do
   hastelloy_thc[n]={}
   for k=1,2 do
        hastelloy_thc[n][k] = 0
   end
 end

--read hastelloy_thc array data from file
nlines=0
handle = openfile("hastelloy_thermalcond.dat", "r");

-- Process the first line
-- the "*n" tell LUA to read a whole line which contains two numbers separated by spaces
a,b = read(handle, "*n","*n");
while(a ~= nil) do
        -- do your own processing here
        -- print (a,b);
   nlines=nlines+1;
   --  print(n);
   hastelloy_thc[nlines][1]=a;
   hastelloy_thc[nlines][2]=b;
   --print(qln[n][1],qln[n][2]);
   a,b = read(handle, "*n","*n");

end
closefile(handle);

--hastelloy - define function which will return thermal conductivity for given temperature
function hastelloy_t(tempedge)
        hastelTC=0;
        deltatemp=tempedge;
        if deltatemp <=0 then
                deltatemp=0
        end;
        np=31;
        for k=1,np-1 do
          a  = hastelloy_thc[k][1];
          b  = hastelloy_thc[k+1][1];
          at = hastelloy_thc[k][2];
          bt = hastelloy_thc[k+1][2];
```

```
            if deltatemp<=b then
                        break
            end;
        end
        hastelTC=((deltatemp-a)*(bt-at)/(b-a))+at;
        return hastelTC;
end;

--define array of nonlinear thermal conductivity for HTS superconductor
HTS_thc={}
 for n=1, 48 do
   HTS_thc[n]={}
   for k=1,2 do
        HTS_thc[n][k] = 0
   end
 end

--read HTS_thc array data from file
nlines=0
handle = openfile("ReHTS_thermal_cond.dat", "r");

-- Process the first line
-- the "*n" tell LUA to read a whole line which contains two numbers separated by spaces
a,b = read(handle, "*n","*n");
while(a ~= nil) do
        -- do your own processing here
--      print (a,b);
   nlines=nlines+1;
--  print(n);
   HTS_thc[nlines][1]=a;
   HTS_thc[nlines][2]=b;
   --print(qln[n][1],qln[n][2]);
   a,b = read(handle, "*n","*n");

end
closefile(handle);

--hastelloy - define function which will return thermal conductivity for given temperature
function HTS_t(tempedge)
        superTC=0;
        deltatemp=tempedge;
        if deltatemp <=0 then
                deltatemp=0
        end;
        np=48;
        for k=1,np-1 do
          a  = HTS_thc[k][1];
          b  = HTS_thc[k+1][1];
          at = HTS_thc[k][2];
          bt = HTS_thc[k+1][2];
          if deltatemp<=b then
                break
          end;
        end
        superTC=((deltatemp-a)*(bt-at)/(b-a))+at;
```

```
        return superTC;
end;


-- example usage of nonlinear thermal conductivity functions to implement the materials anisotropy
--      hi_modifymaterial("Hastelloy"..n.."",1,hastelloy_t(tempLN)*(factorh*factorh));
--      hi_modifymaterial("Hastelloy"..n.."",2,hastelloy_t(tempLN));
--      hi_modifymaterial("ReHTS"..n.."",1,HTS_t(tempLN)*(factorh*factorh));
--      hi_modifymaterial("ReHTS"..n.."",2,HTS_t(tempLN));
--      hi_modifymaterial("T_Silver"..n.."",1,silver_t(tempLN)*(factorh*factorh));
--      hi_modifymaterial("T_Silver"..n.."",2,silver_t(tempLN));
```

LN2cooling.lua

```
--define parameters for sf12050 lead in LN2 bath
tempLN=77;
deltatemp=0;


--define arrays of temperature on the cooling edges D_ down T_ top
D_tedge={}
 for n=0, (numseg-1) do
   D_tedge[n] = tempLN
 end
T_tedge={}
 for n=0, (numseg-1) do
   T_tedge[n] = tempLN
 end


--define array of heat flux cooling in LN (delta T (k), delta Q W/m2)
qln={}
 for n=1, 49 do
   qln[n]={}
   for k=1,2 do
        qln[n][k] = 0
   end
 end

--read qln array data from file

nlines=0
handle = openfile("ln_qgen.dat", "r");

-- Process the first line
-- the "*n" tell LUA to read a whole line which contains two numbers separated by spaces
a,b = read(handle, "*n","*n");
while(a ~= nil) do
        -- do your own processing here
   nlines=nlines+1;
   qln[nlines][1]=a;
   qln[nlines][2]=b;
   a,b = read(handle, "*n","*n");
```

```
end

closefile(handle);

--define function which will return flux for LN cooling
function heatLN(tempedge)
        cooling=0;
        deltatemp=tempedge - tempLN;
        if deltatemp <=0 then
                deltatemp=0
        end;
        np=49;
        for k=1,np-1 do
         a  = qln[k][1];
         b  = qln[k+1][1];
         at = qln[k][2];
         bt = qln[k+1][2];
         if deltatemp<=b then
                break
         end;
        end
        cooling=((deltatemp-a)*(bt-at)/(b-a))+at;
        if cooling<0 then
                cooling=0
        end;
        return cooling;
end;

-- sample usage of defined functions
--                segcoolD=heatLN(D_tedge[k]);
--                segcoolT=heatLN(T_tedge[k]);
--                        hi_modifyboundprop("D_R"..k.."",3,segcoolD);
--                        hi_modifyboundprop("T_R"..k.."",3,segcoolT);
```

8. Summary

Knowledge of the behaviour of superconducting devices in transient states is very important to assess the stability of the unit. Disturbances of the superconducting state may be induced by mechanical, electromagnetic and heat reasons, but in effect, they finally reveal themselves as additional heat delivered to the superconducting element. These additional heat sources cause rapid local temperature rise which often leads to the superconducting element destruction.

Awareness of the superconducting device response during transients allows for designing more robust applications.

The first objective of the dissertation is to improve the methods for calculating the critical parameters of high temperature superconductor devices in transient states and to verify the elaborated models with measurements. The second objective is to develop a non-contact system for detecting quick temperature changes in thin second generation HTS tapes.

Algorithms developed by the author and computer models of the devices with HTS bulk components as well as the second generation HTS tapes have been used to achieve the first objective. The developed models can be used for numerical simulation of 2D and axisymmetrical geometries and are useful for such appliances as: superconducting fault current limiters, current leads and second generation HTS tapes.

Numerical models allow to examine and analyse the interaction between the parameters and physical quantities in superconducting device that would be difficult or even impossible to be measured.

Elaborated algorithms were implemented with object LUA language and allow for combining three problems during simulations: current flow, magnetic field and heat transfer.

Worked out hybrid models are based on the two dimensional diffusion equations for electromagnetic and thermal fields. The nonlinear superconductor temperature dependent characteristics of critical current, critical magnetic flux and thermal conductivity were taken into account. The models also includes the time and space variation in thermal power density, guiding the generation of heat in the superconducting element during the superconductivity decay.

Developed models were mostly verified with measurements with good agreement. During measurements for the 2G HTS tapes the impact of the quench pulse on the propagation of the resistive zone was examined.

The second objective of the dissertation is the construction of the measurement system for detecting temperature changes in HTS 2G tapes during quench in a non-contact manner. The system uses infrared silicon photodiodes as sensors. The signal from the photodiode is amplified and converted to voltage signal registered by data acquisition computer system.

Short response time (5 ns) photodiodes were used to obtain the changes of temperature at the appropriate time. The measuring system based on photodiodes is a prototype, so the solutions adopted and the experience accumulated can be the basis for an industrial system.

Acquired research results represent a contribution to cryogenic measurement techniques and theory of the stability of superconducting devices. These elements are essential in the design of superconducting devices.

9. Streszczenie

Wiedza na temat zachowania się urządzeń nadprzewodnikowych w stanach przejściowych jest bardzo istotna z punktu widzenia stabilności pracy i niezbędna zarówno przy ich projektowaniu, jak i eksploatacji. Zaburzenia stanu nadprzewodnictwa mogą być wywołane przez różne przyczyny (mechaniczne, elektromagnetyczne, cieplne), ale w efekcie końcowym ujawniają się jako dodatkowe źródła ciepła w elemencie nadprzewodzącym. Źródła te powodują bardzo szybki wzrost lokalnej temperatury, co prowadzi często do zniszczenia elementu nadprzewodnikowego. Odpowiedź urządzenia nadprzewodzącego na zmiany jego parametrów krytycznych w stanach przejściowych pozwala na projektowanie bardziej niezawodnych aplikacji.

Monografia posiada dwa cele – poznawczy i aplikacyjny. Pierwszym jest udoskonalenie metod obliczania zmian parametrów krytycznych urządzeń nadprzewodnikowych wykonanych z nadprzewodników wysokotemperaturowych w stanach nieustalonych, drugim celem jest opracowanie układu pomiarowego do bezkontaktowego pomiaru temperatury w cienkowarstwowych taśmach nadprzewodnikowych HTS.

Do osiągnięcia pierwszego celu posłużyły opracowane algorytmy oraz komputerowe modele urządzeń nadprzewodnikowych z masywnymi elementami HTS oraz taśmami nadprzewodzącymi drugiej generacji. Opracowane hybrydowe modele mogą być stosowane do symulacji numerycznych urządzeń w geometrii dwuwymiarowej i z symetrią osiową.

Zaproponowane modele są przydatne do analizy takich urządzeń jak: nadprzewodzące ograniczniki prądu, przepusty prądowe oraz taśmy HTS drugiej generacji. Opracowane algorytmy pozwalają na sprzężenie trzech zagadnień podczas obliczeń numerycznych. Są to zagadnienia: przepływu prądu, rozkładu pola magnetycznego oraz rozpływu ciepła.

Modele hybrydowe oparte są na dwuwymiarowych równaniach dyfuzji dla pól elektromagnetycznych i cieplnych, uwzględniających nieliniowe zmiany parametrów materiałów nadprzewodnikowych od temperatury, indukcji magnetycznej i natężenia prądu. Algorytmy obliczeniowe sprzęgają ze sobą zagadnienia przepływu prądu, pola elektromagnetycznego i pola temperatur poprzez zastosowanie programowania obiektowego w języku LUA. Wyniki przeprowadzonych obliczeń porównane zostały z wynikami eksperymentów pomiarowych w celach weryfikacji opracowanych modeli i algorytmów. Podczas przeprowadzanych eksperymentów dla taśm HTS 2G zbadany został wpływ charakteru impulsu zaburzającego na sposób i prędkość rozchodzenia się strefy rezystywnej.

Porównanie wyników pomiarów oraz obliczeń numerycznych potwierdziło poprawność opracowanych algorytmów i modeli hybrydowych

Drugi cel badawczy został osiągnięty poprzez skonstruowanie układu pomiarowego do detekcji zmian temperatury cienkowarstwowej taśmy HTS w stanach przejściowych. Układ pomiarowy zawiera fotodiody podczerwone jako sensory oraz sondy napięciowe do weryfikacji otrzymanych wyników pomiarowych. Sygnał z fotodiod został wzmocniony i zarejestrowany przez skomputeryzowany system akwizycji danych. Do pomiaru zostały użyte diody z czasem odpowiedzi równym 5 ns co pozwoliło rejestrować zmiany temperatury taśmy w stanach nieustalonych.

Układ pomiarowy oparty o fotodiody ma charakter prototypowy, a przyjęte w nim rozwiązania i zgromadzone doświadczenia mogą stanowić podstawę budowy takich układów do zastosowań przemysłowych.

Uzyskane wyniki badań stanowią wkład w kriogeniczne techniki pomiarowe oraz teorię stabilności urządzeń nadprzewodnikowych. Elementy te są niezbędne w procesie projektowania urządzeń nadprzewodnikowych oraz przy ich eksploatacji.